

SITE-SPECIFIC INCORPORATION OF POST-TRANSLATIONAL MODIFICATIONS IN ALPHA-SYNUCLEIN: INSIGHTS INTO AGGREGATION, STRUCTURE, AND FUNCTION

Marie Shimogawa

A DISSERTATION

in

Chemistry

Presented to the Faculties of the University of Pennsylvania

in

Partial Fulfillment of the Requirements for the

Degree of Doctor of Philosophy

2025

Supervisor of Dissertation

E. James Petersson, Ph.D.

Professor of Chemistry

Graduate Group Chairperson

E. James Petersson, Ph.D

Professor of Chemistry

Dissertation Committee

David M Chenoweth, Ph.D. Professor of Chemistry

Ronen Marmorstein, Ph.D. George W. Raiziss Professor

George Burslem, Ph.D. Assistant Professor of Biochemistry, Biophysics and Chemical Biology

ACKNOWLEDGMENT

James – I cannot emphasize how wonderful of a mentor you are and my appreciation for all your guidance and support more. I will never forget the first day we met, when you visited us at UTokyo. I still have the business card you gave me that day. Thank you for encouraging my ambition to do a PhD in the US, allowing me to do research and earn skills of my interest, and being very supportive and helpful when I had difficulty in science or in personal life. I know very well how lucky I am to have you as an advisor. Hontouni osewani narimashita.

The EJPLab – It was fortunate to have spent my PhD in such a supportive and respectful environment with talented colleagues, and I miss you all a lot. Buyan, I really appreciate your talents and mentorship, as well as for making my transition much easier. Jenny, you were such an amazing scientist and buddy (no one beats you with pipetting skills!), it meant so much to always have you around. Venky, thank you for all the random, joyful and sometimes serious conversations. Kristen, my longest desk mate, you were an incredibly supportive peer, providing inspirations both in science and personal aspects. Kohei, it was so nice to have you around for a year - I got so much help, both in peptide chemistry and in life. Younger generations, thank you all for inheriting the good lab culture and for including me in a lot of fun activities. My mentees, Evan, Ibrahim and Bernard – I appreciate your generosity, I enjoyed all the collaborations and discussions. I need to thank those of you that helped me move for work, it was such a sweet gesture, and it really showcases the lab culture that I am proud of: Denver, Evan, Kyle, and Ibrahim, for a full service all the way and Jason and Bernard, for doing the loading in Philly. Yanan, my recent desk mate, and Grace, I have enjoyed all the chit-chats we have had over years. Xinning, thanks for all the fantastic outings, it was nice to speak some Japanese with you too.

Liz and the Rhoades Lab, thanks for tons of collaborations and for always welcoming me around. The joint lab events were a lot of fun. Props to my mentee Taylor – it was always so delightful to talk to you, a lot of good science and personal life discussions.

Department friends – Brandon, I miss the nights of calligraphy and sushi, and I cannot appreciate all your support more. Dan, thanks for all the nomikai nights and for always being a great listener. Karthik and Emily, it was so awesome to see you guys around all the time and cheer for each other as cohorts. Japanese folks and Japanese speakers, thanks for bringing joy and making me feel like home.

Non-chemistry Philly friends – Seoyoung and Sungya, thank you for being great friends of mine since the beginning of our PhD. I can recall so many memories, our random discussions have always been entertaining.

My middle/high school friends and undergrad friends in Tokyo, thank you for being in touch despite how long it has been and how rarely I am around. I truly enjoy how we get to talk both about good-old memories as well as recently developed topics.

To my family – my parents and my sister, thank you for supporting my adventure to start and continue my career abroad and far away, for all the caring messages, support packages and for making sure I get best out of the stays whenever I am home.

Lastly, Alexis – you're the sweetest person in the world - thank you very much for always being there for me and so understanding, both as an in-field peer and a partner. I would not have been able to go through this without your help and support.

ABSTRACT

SITE-SPECIFIC INCORPORATION OF POST-TRANSLATIONAL MODIFICATIONS IN ALPHA-SYNUCLEIN: INSIGHTS INTO AGGREGATION, STRUCTURE, AND FUNCTION

Marie Shimogawa

E. James Petersson

The misfolding and aggregation of alpha-synuclein (α S) are central to synucleinopathies, including Parkinson's disease. Post-translational modifications (PTMs) regulate α S aggregation and interactions, yet their site-specific effects remain unclear. This dissertation employs genetic code expansion (GCE), enzymatic modification, and protein semi-synthesis to incorporate PTMs and investigate their influence on α S function and pathology. To study lysine acetylation, GCE was used to incorporate acetyl lysine (^{Ac}K) at twelve sites, revealing that $^{Ac}K_{12}$, $^{Ac}K_{43}$, and $^{Ac}K_{80}$ slow aggregation *in vitro* and in neurons, with $^{Ac}K_{80}$ emerging as a promising therapeutic target due to its minimal impact on membrane interactions. While HDAC8 exhibited high deacetylation activity toward $^{Ac}K_{80}$, its lack of specificity over $^{Ac}K_{43}$ suggests that better Lys acetyltransferases or deacetylase targets must be identified. Structural analysis suggests $^{Ac}K_{80}$ -mediated aggregation suppression extends beyond simple monomer conformational changes or fibril morphology alterations. Given the frequent use of glutamine as an ^{Ac}K mimic, its validity was tested, revealing that Gln43 and Gln80 mutants replicated ^{Ac}K 's effects on aggregation, while Gln12 did not, emphasizing the need to validate mimics on a site-by-site basis. Alternative chemical strategies, including thioether acetylation mimic and thioamide acetyl lysine analog, were explored to enhance PTM stability and analytical utility. The effects of phosphorylation were examined using GCE (phosphorylation at Ser87, pS₈₇) and enzymatic modification (phosphorylation at Tyr39, pY₃₉) - pS₈₇ had minimal impact on vesicle binding and pY₃₉ does not dramatically influence fibril structure at physiological stoichiometry (10-25%), unlike when it is present at 100%, as detected by changes in

binding of site-specific radioligands. Preliminary work suggests a combinatorial effect between pY₃₉ and AcK₄₃ in aggregation, though future synthetic efforts are needed to efficiently generate doubly modified α S and elucidate this effect. These findings establish methodologies for precise PTM incorporation and highlight site-specific PTM effects on α S aggregation, fibril structure, and function, providing a foundation for future studies on PTM crosstalk and therapeutic targeting.

TABLE OF CONTENTS

ACKNOWLEDGMENT	II
ABSTRACT	IV
LIST OF TABLES.....	XI
LIST OF FIGURES	XII
LIST OF SCHEMES	XV
CHAPTER 1: INTRODUCTION	1
§1.1 Alpha-synuclein (α S) and synucleinopathies	1
§1.2 Alpha-synuclein aggregation and morphology	3
§1.3 Alpha-synuclein post-translational modifications (PTMs)	5
§1.4 Challenges for studying PTMs	7
§1.5 Strategies for site-specifically incorporating authentic PTMs	8
CHAPTER 2: INVESTIGATION OF ALL DISEASE-RELEVANT LYSINE ACETYLATION SITES IN ALPHA-SYNUCLEIN ENABLED BY NON-CANONICAL AMINO ACID MUTAGENESIS.....	12

§2.1 Introduction	12
§2.2 Results	16
§2.3 Conclusion.....	34
CHAPTER 3: GLUTAMINE IN PART MIMICS NEUROPROTECTIVE EFFECTS OF THE AUTHENTIC LYSINE ACETYLATION ON ALPHA-SYNUCLEIN	37
§3.1 Introduction	37
§3.2 Results	38
§3.3 Conclusion.....	48
CHAPTER 4: ADDITIONAL TOOLS TO STUDY LYSINE ACETYLATION OF ALPHA-SYNUCLEIN	50
§4.1 Introduction	50
§4.2 Results	51
§4.3 Conclusion.....	58
CHAPTER 5: GENETIC CODE EXPANSION AND ENZYMATIC MODIFICATIONS AS ACCESIBLE METHODS FOR STUDYING SITE-SPECIFIC POST-TRANSLATIONAL MODIFICATIONS OF ALPHA- SYNUCLEIN	60
§5.1 Introduction	60
§5.2 Results	61

§5.3 Conclusion.....	73
CHAPTER 6: CONCLUSION AND PERSPECTIVES.....	75
CHAPTER 7: MATERIALS AND METHODS.....	82
§7.1 General information.....	82
§7.2 Protein semi-synthesis for generation of α S ^{-Ac} K ₈₀	83
§7.3 Construction of expression plasmids.....	84
§7.4 Production of recombinant α S constructs – Lys acetylation and Gln mutational mimic work.....	86
§7.5 Production of recombinant α S constructs – Ser phosphorylation work.....	88
§7.6 Production of α S-pY ₃₉	89
§7.7 Synthesis of thioether acetylation mimics (Thiol-ene addition).....	91
§7.8 Synthesis of AcLys thioamide analog (^{AcS} K).....	91
§7.9 Fluorescent labeling.....	92
§7.10 Circular Dichroism (CD).....	92
§7.11 Protein aggregation kinetics and percentage incorporation into fibrils.....	93
§7.12 Preparation of synthetic vesicles.....	95
§7.13 Fluorescence correlation spectroscopy (FCS).....	95

§7.14 Vesicle binding affinity	97
§7.15 Transmission electron microscopy (TEM)	98
§7.16 HDAC8 deacetylation assay	98
APPENDIX A: THE EFFECTS OF GLUTAMATE ARGINYLATION ON ALPHA-SYNUCLEIN: STUDYING AN UNUSUAL POST-TRANSLATIONAL MODIFICATION THROUGH SEMI-SYNTHESIS	100
§A.1 Summary	100
§A.2 Relevant Methods	101
§A.3 Results	103
APPENDIX B: CYSTEINE-BASED MIMIC OF ARGINYLATION REPRODUCES NEUROPROTECTIVE EFFECTS OF THE AUTHENTIC POST-TRANSLATIONAL MODIFICATION ON ALPHA-SYNUCLEIN ...	105
§B.1 Summary	105
§B.2 Relevant Methods.....	106
§B.3 Results	109
APPENDIX C: SYNTHESIS OF PEPTIDES AND PROTEINS WITH SITE-SPECIFIC GLUTAMATE ARGINYLATION	114
§C.1 Summary.....	114
§C.2 Relevant Methods.....	115

§C.3 Results 117

APPENDIX D: SEMI-SYNTHETIC COA-ALPHA-SYNUCLEIN CONSTRUCTS TRAP N-TERMINAL

ACETYLTRANSFERASE NATB FOR BINDING MECHANISM STUDIES 120

§D.1 Summary 120

§D.2 Relevant methods..... 121

§D.3 Results 122

BIBLIOGRAPHY..... 123

LIST OF TABLES

Table 1. Yield for production of α S thioether Lys acetylation mimic at each acetylation site.53

Table 2. Components of isokinetic mixture.....117

LIST OF FIGURES

Figure 1. Aggregation of α S.	2
Figure 2. Aggregation phases tracked by ThT.....	4
Figure 3. α S PTMs in human.....	6
Figure 4. Example schematics of GCE and chemical protein synthesis for incorporating PTMs. 9	
Figure 5. Neurodegeneration-relevant Lys acetylation sites in α S.....	15
Figure 6. Semi-synthesis of α S with acetylation at Lys80.....	17
Figure 7. Expression of α S with acetylation at Lys80 through ncAA mutagenesis.	19
Figure 8. Effects of lysine acetylation on micelle-bound α S.....	21
Figure 9. Effects of lysine acetylation on in vitro aggregation.	22
Figure 10. Effects on aggregation seeding in primary neuron cells.....	24
Figure 11. Effects of lysine acetylation on vesicle binding affinity.	27
Figure 12. Structural impact of Lys80 acetylation on fibril morphology.	32
Figure 13. Site-specificity of HDAC activity.	34
Figure 14. Evaluation of α S-Gln mutants as Lys acetylation mimic in α S aggregation.....	39
Figure 15. Effects of glutamine mutation on aggregation seeding in HEK cells.	40
Figure 16. Effects of Gln mimics on α S conformation.	42

Figure 17. Transmission Electron Microscopy images of α S Lys acetylation constructs and α S Gln mutants.	44
Figure 18. Effects of Gln mimics on helicity of SDS micelle-bound α S.	45
Figure 19. Effects of Gln mimics on vesicle binding.....	47
Figure 20. Synthesis of thioether Lys acetylation mimic via thiol-ene reaction.....	52
Figure 21. Aggregation kinetics of thioether Lys acetylation mimics.	55
Figure 22. Monomer conformation of authentic Lys80 acetylation and thioether mimic.	57
Figure 23. Affinity purification of α S with phosphorylation at S87, produced by genetic code expansion.	63
Figure 24. HPLC chromatogram collected for affinity-purified phosphoserine GCE products. ...	64
Figure 25. MALDI-MS characterization of affinity-purified or HPLC-purified α S - pS87 constructs.	65
Figure 26. Phos-tag SDS-PAGE gels ran with α S phosphorylated at different sites.	67
Figure 27. Analysis of α S phosphorylated by Tyr kinase c-Abl.	68
Figure 28. Radioligand competition binding to fibrils containing pTyr at physiological stoichiometry.....	70
Figure 29. Effects of pSer87 on vesicle binding, investigated by NMR.	72
Figure 30. Effects of pSer87 on vesicle binding, investigated by FCS.	73

Figure 31. Preliminary combinatorial PTM study with pTyr39 and acetylation at nearby Lys.	80
Figure 32. Aggregation kinetics and total monomer incorporation for mimic arginylated α S. ...	111
Figure 33. Aggregation kinetics and total monomer incorporation for seeded aggregation assays.	112
Figure 34. Proteinase K digestion of PFFs with 5% arginylation mimic.	113
Figure 35. MALDI-MS of product peptide library XXXXXE ^{Arg} XXXXXC.....	119

LIST OF SCHEMES

Scheme 1. Reaction scheme for the synthesis of thioamide analog of acetyl Lys..... 58

Scheme 2. Semi-synthesis of α S bearing both Lys acetylation and pY₃₉. (X = 21, 32, 34 or 43) 81

CHAPTER 1: INTRODUCTION

§1.1 Alpha-synuclein (α S) and synucleinopathies

Alpha-synuclein (α S) is a small, 140-amino acid protein highly expressed in the brain, particularly in presynaptic terminals, where it is involved in synaptic vesicle trafficking and neurotransmitter release^{1,2}. Although α S is thought to play roles in maintaining synaptic plasticity, membrane interactions, and neuronal homeostasis, its precise physiological function remains incompletely understood. Structurally, α S is classified as an intrinsically disordered protein (IDP), meaning it lacks a stable tertiary structure in solution³⁻⁵.

The aggregation of α S is a defining feature of synucleinopathies, a family of neurodegenerative disorders that includes Parkinson's disease (PD), Parkinson's disease with dementia (PDD), multiple system atrophy (MSA), and dementia with Lewy bodies (DLB)^{6,7}. Among these, PD is the second most common neurodegenerative disease after Alzheimer's disease, affecting an estimated 0.3% of the global population (2-3% of people with age 65 or more) and accounting for about 15% of all dementia cases^{6,7}. Clinically, PD is characterized by motor impairments such as shaking while at rest, muscle stiffness, and slowness of movement, alongside non-motor symptoms including sleep disturbances, cognitive impairment, and mood disorders⁶⁻⁸. Pathologically, PD diagnosis is confirmed by dopaminergic neuron loss in the substantia nigra and intracellular inclusions of aggregated α S in Lewy bodies (LBs) and Lewy neurites (Figure 1)⁹⁻¹¹. In MSA, α S aggregates manifest as glial cytoplasmic inclusions (GCIs).

α S consists of three distinct regions with functional and pathological relevance. The N-terminal region (residues 1–60) is amphipathic, contains seven imperfect 11-amino acid repeats, and is responsible for membrane binding, which is driven by conserved KTKEGV motifs³. Adjacent to this is the non-

amyloid- β component (NAC) region (residues 61–95), a hydrophobic sequence necessary for α S fibril formation and amyloid aggregation. The C-terminal domain (residues 96–140) is negatively charged and remains disordered under most conditions but plays roles in protein-protein interactions and chaperone binding^{3,4}. Upon membrane binding, the N-terminal and NAC regions adopt an α -helical conformation, where the membrane curvature affects whether it forms a single, long helix or a pair of antiparallel helices¹²⁻¹⁴. It is noted that while the prevailing hypothesis suggests that α S exists as an intrinsically disordered monomer, another model proposes that α S physiologically exists as an aggregation-resistant tetramer, with its disruption leading to the release of monomers that are prone to misfolding and aggregation^{15,16}.

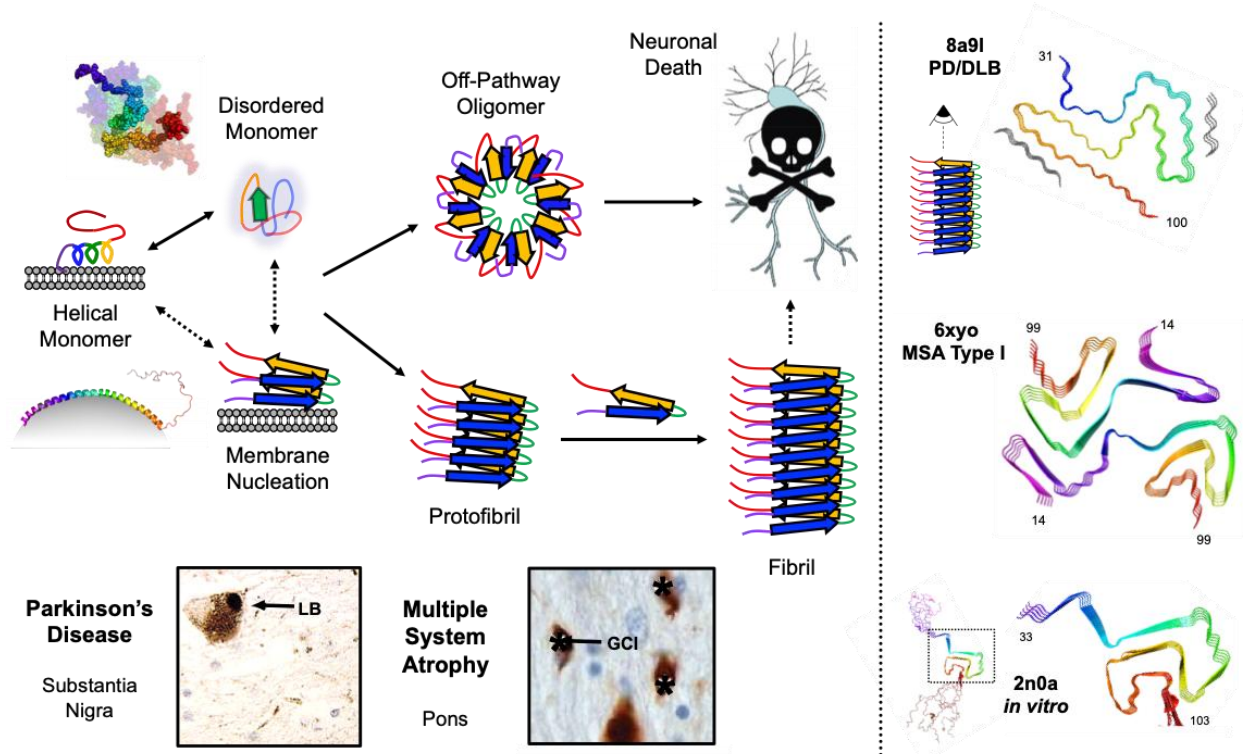


Figure 1. Aggregation of α S.

(Left) Conformational states and aggregation pathways of α S. (Right) Structural insights to fibrils formed in pathological or in vitro environments, viewed down on helical axis.

§1.2 Alpha-synuclein aggregation and morphology

In PD, α S transitions from its monomeric form into oligomers and subsequently into amyloid fibrils, which are the major components of LBs and GCIs^{11,17}. The toxicity of LBs is thought to be from α S aggregation and its interactions with membranous organelles, such as mitochondria, autophagosomes, or lysosomes¹⁸. α S fibrils can fragment and act as seeds, recruiting monomeric α S to form new oligomers and fibrils (Figure 1)¹⁹. This seeding mechanism facilitates the spread of pathology between neurons, leading to progressive neurodegeneration in PD²⁰⁻²³. While mature fibrils dominate the LB inclusions, oligomeric intermediates have also been implicated in cytotoxicity, although their exact role in disease remains unclear due to their structural and molecular diversity¹⁷.

At the molecular scale, α S aggregation pathway consists of multiple steps: primary nucleation, elongation, and secondary nucleation (Figure 2). In primary nucleation, monomeric α S undergoes conformational changes to form small oligomeric nuclei, which serve as precursors for fibril formation²⁴. During elongation, additional α S monomers add to the growing fibrils, templated by existing aggregates. Secondary nucleation, which contributes to disease progression, occurs when fibrils act as templates for new oligomer formation either at specific fibril surfaces²⁵ or via fibril fragmentation²⁶. This process is often tracked using fluorescent dyes such as thioflavin T (ThT).

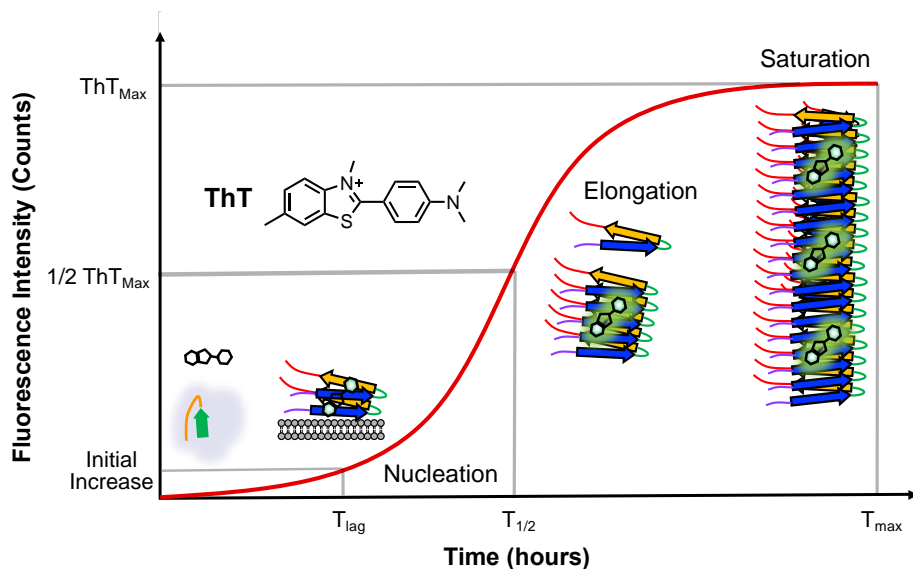


Figure 2. Aggregation phases tracked by ThT.

ThT fluorescence intensity changes are shown with major α S conformational states in each phase. The timepoints of half maximal ThT fluorescence ($T_{1/2}$) are used to determine the effects of post-translational modifications (PTMs) on α S aggregation.

α S fibrils formed in different environments can vary in morphology, toxicity, and seeding capacity (“strains”). So is the case between synucleinopathies, as patient-derived fibrils from different diseases exhibit distinct biochemical and structural properties^{27,28}. Oligomers formed under different conditions exhibit variations in morphology, calcium dysregulation, seeding efficiency, and membrane permeability²⁹. Moreover, some fibril strains maintain their structural identity during seeding, but recent evidence suggests that cellular and solution conditions influence fibril morphology. For example, when LB extracts were injected into oligodendrocytes in mice, the resulting inclusions resembled GCIs of

MSA rather than LBs, indicating that strains may not always propagate faithfully under different cellular conditions²⁸.

Advances in solid-state nuclear magnetic resonance (ssNMR) and cryo-electron microscopy (cryo-EM) have significantly improved our understanding of α S fibril structures (Figure 1). The first atomic-resolution α S fibril structure was solved using ssNMR (PDB: 2N0A), which revealed the Greek key motif (residues 36–100) that appears in many subsequent fibril structures³⁰. Cryo-EM has since provided structures of various α S fibril strains, including wild-type (WT) fibrils^{31,32} and even patient-derived fibrils from PD (PDB: 8A9L) or MSA (PDB: 6XYO)^{33,34}. All α S fibril structures share a core β -sheet-rich conformation and a steric zipper interface between protofilaments, but they differ in helical twist, protofilament interfaces, electrostatic interactions, and sidechain orientations, all of which contribute to their strain-specific properties. It is notable that both PD and MSA fibrils had unknown electron density surrounded by positively charged residues, indicating the presence of an unknown molecule interacting with these positively charged side-chains.

Understanding α S aggregation, fibril strain diversity, and the structural differences between pathological fibrils is crucial for developing targeted therapeutic strategies for synucleinopathies.

§1.3 Alpha-synuclein post-translational modifications (PTMs)

The exact mechanism for the distinct strain properties between synucleinopathies has not yet been understood. Our collaborative mass spectrometry work led to the finding that different post-translational modifications (PTMs) were identified from patients with different synucleinopathies (Figure 3).³⁵ This suggests that understanding the role of PTMs in regulating α S structure, aggregation, and interactions

with cellular components could help elucidate differential disease mechanisms, identify a novel biomarker and implicate therapeutic targets.

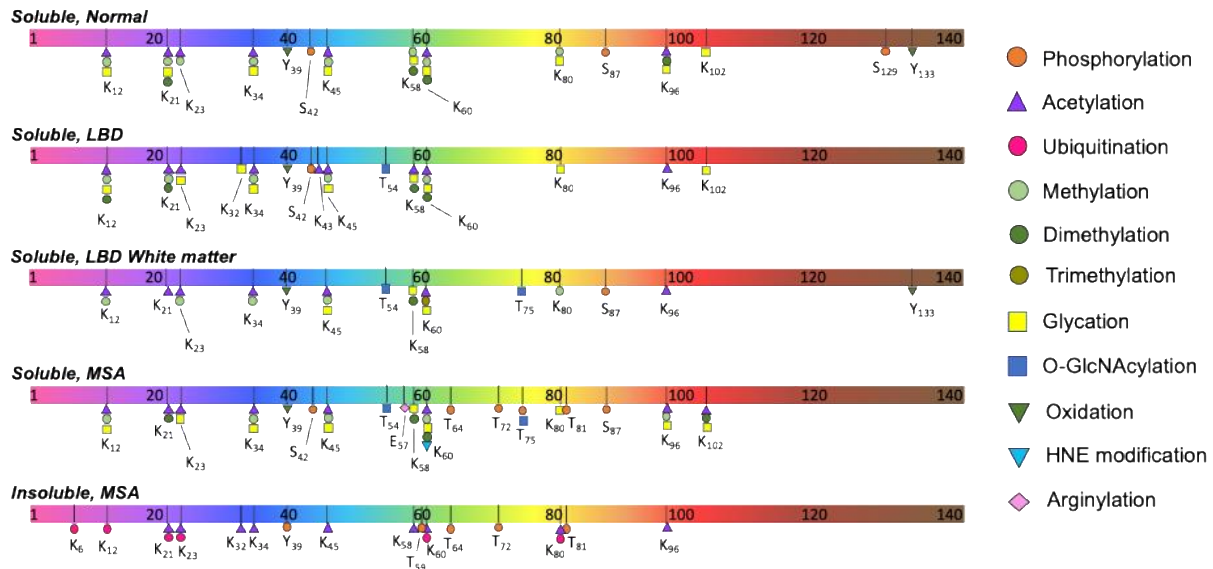


Figure 3. α S PTMs in human.

Post-translational modifications identified from human samples, including patients of Lewy body diseases (LBD, including PD and DLB) and MSA^{33,35}.

Phosphorylation is one of the most extensively studied PTMs in α S, with Ser129 phosphorylation (pS₁₂₉) being the most prominent modification in Lewy body pathology. While pS₁₂₉ is present in only ~4% of α S in healthy brains, it is detected in over 90% of α S within Lewy bodies and glial cytoplasmic inclusions (GCI) in MSA^{36,37}. However, its functional significance remains debated. Some studies suggest that pS₁₂₉ enhances α S aggregation, while others indicate that it may play a role in fibril structural diversity or protein degradation^{38,39}. Other phosphorylation sites, such as Y₃₉ (pY₃₉) and S₈₇ (pS₈₇), have been shown to alter α S aggregation kinetics, fibril structure, and membrane interactions, suggesting site-specific effects of phosphorylation in α S biology^{40,41}.

Ubiquitination of α S is associated with its degradation via the ubiquitin-proteasome system and autophagy-lysosomal pathways. Several Lys residues, including K₆, K₁₂, K₂₁, K₂₃, and K₉₆, have been identified as ubiquitination sites in Lewy bodies⁴². Mono-ubiquitination was found to serve a regulatory function between two degradation pathways⁴³. In contrast, SUMOylation, a related modification, appears to reduce α S aggregation and promote its solubility, suggesting a protective effect⁴⁴.

Non-enzymatic glycation, particularly methylglyoxal (MGO)-induced glycation, has been linked to increased α S aggregation and toxicity. Glycation may alter α S's membrane binding and clearance, potentially contributing to disease progression⁴⁵. On the other hand, O-GlcNAcylation, where an N-acetylglucosamine moiety is enzymatically added to Ser/Thr residues, has been shown to inhibit α S aggregation. O-GlcNAcylation at T₇₂ and S₈₇ has been demonstrated to stabilize soluble α S, highlighting the potential for modulating this PTM as a therapeutic strategy^{46,47}.

The effects of PTMs on α S can be highly context-dependent and site-specific. By systematically studying PTMs using precise incorporation methods, researchers can dissect their individual contributions to α S pathology and uncover potential therapeutic targets for synucleinopathies.

§1.4 Challenges for studying PTMs

One consideration needed for studying PTMs is that they are usually present as a fraction of proteins, to varied extents. This is also very dependent on PTM and its site: the level of N-terminal acetylation is very high in mammalian α S⁴⁸, while pY₃₉ was found to be present at ~25% and pS₈₇ at ~10% stoichiometry in human³⁵. With pY₃₉, our group observed bidirectional effects on aggregation kinetics as we increased the level of the PTM, which showcased the importance of considering the stoichiometry factor⁴⁹. It is

important that one carefully determines at what ratio you run experiments, or one performs experiments at multiple PTM ratios.

The effects of PTMs can be highly site dependent. To have the best control over experiments, it is desirable to obtain homogenous, site-specifically modified proteins of interest. However, traditional methods of studying PTMs, such as mutational mimics (e.g., Ser/Thr/Tyr-to-Glu/Asp for phosphorylation, Lys-to-Gln for acetylation), do not always accurately replicate the structural and functional consequences of authentic PTMs⁵⁰. This is particularly important for IDPs, which are so sensitive to any changes in structure⁵⁰. Therefore, it is crucial to develop site-specific incorporation methods to introduce authentic PTMs and evaluate each mimic in a systematic matter before you confidently interpret results with these mimics.

§1.5 Strategies for site-specifically incorporating authentic PTMs

The ability to study PTMs in α S at a site-specific and homogeneous level is essential for understanding their effects on aggregation, biomolecule interactions, and toxicity. However, bacterially expressed α S lacks PTMs, including N-terminal acetylation unless co-expressed with the NatB acetyltransferase complex⁵¹. Since PTMs are installed enzymatically in cells through complex regulatory pathways, producing homogeneously modified α S *in vitro* remains challenging in most other cases. Several methods have been developed to incorporate PTMs at specific sites, including genetic code expansion (GCE), enzymatic modification, and chemical protein synthesis. These approaches allow researchers to directly compare modified and unmodified α S, in a highly controlled manner.

Genetic code expansion (GCE) enables the incorporation of non-canonical amino acids (ncAAs) bearing PTMs directly into α S during bacterial or eukaryotic protein expression⁵². This method relies on orthogonal tRNA/aminoacyl-tRNA synthetase (aaRS) pairs, which allow for the site-specific

incorporation of phosphoserine, phosphorylated tyrosine, and acetyllysine at designated sites through suppression of stop codons (typically TAG) or nonstandard codons (Figure 4). GCE is particularly advantageous because it allows for PTM incorporation during recombinant expression, eliminating the need for laborious steps besides protein expression. Compared to chemical protein synthesis, GCE offers a more accessible and scalable way to produce site-specifically modified proteins for *in vitro* and *in vivo* studies. However, GCE has limitations, including the removal of PTMs during expression or purification, potential misincorporation, low incorporation efficiency, and depending on the ncAA, the requirement for specialized bacterial strains. Despite these challenges, GCE remains one of the most widely used methods for site-specific PTM incorporation.

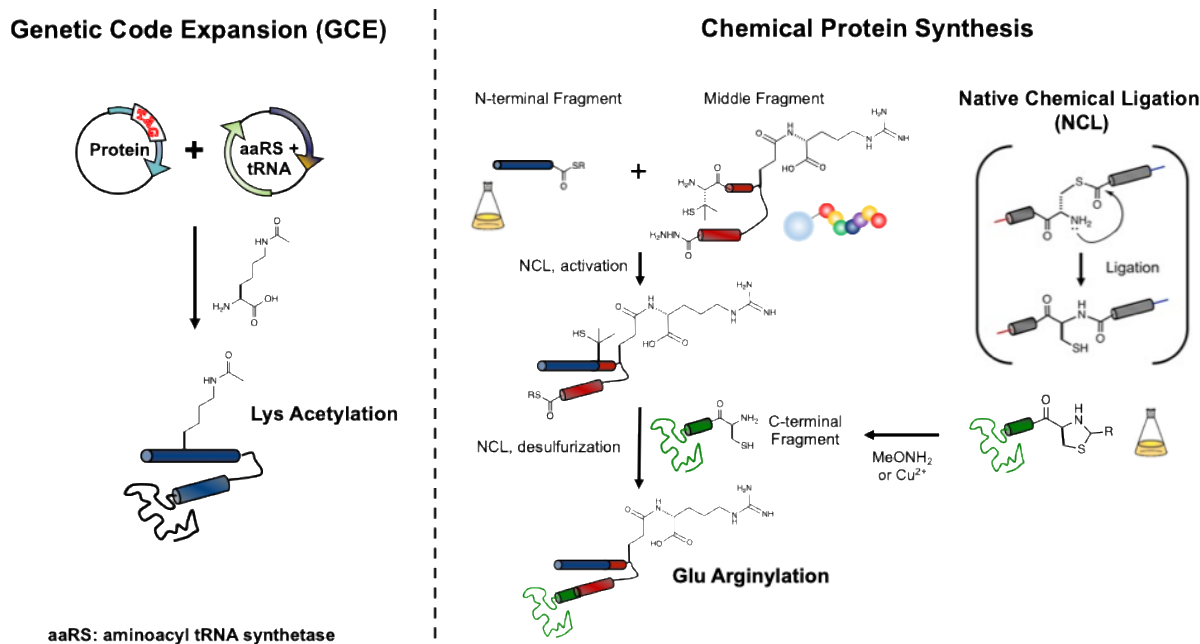


Figure 4. Example schematics of GCE and chemical protein synthesis for incorporating PTMs.

GCE is powerful for incorporating PTM ncAAs with an established system, usually at a single site.

Chemical protein synthesis is able to incorporate virtually any PTM and any numbers of modifications.

Chemical protein synthesis or semi-synthesis allows for precise incorporation of PTMs by assembling α S from synthetic peptide fragments and/or recombinantly expressed protein segments. This is typically achieved through native chemical ligation (NCL) or expressed protein ligation (EPL), in which synthetic peptides containing PTMs are ligated to larger protein domains (Figure 4)⁵³. One of the main advantages of chemical synthesis is the ability to achieve absolute control over modification type and modification sites, making it possible to introduce multiple PTMs simultaneously. However, NCL and related methods require extensive synthetic expertise, making them technically demanding and labor-intensive. One must also give extra considerations when determining ligation sites – as much as it is important to choose sites that make NCL efficient, one needs to be careful to avoid aggregation-prone peptide fragments, especially in the NAC region. Additionally, due to the challenges of producing full-length α S through chemical synthesis, this approach is mostly limited to *in vitro* biochemical and structural studies rather than cellular applications, with some possible exceptions^{54,55}.

Enzymatic modification provides a biologically relevant way to install PTMs *in vitro* or in cells. Kinases, acetyltransferases, and other modifying enzymes catalyze PTM addition at specific sites, maintaining the native cellular context of these modifications. For example, phosphorylation at S₁₂₉ has been achieved by co-expressing α S with PLK2 kinase in *Escherichia coli*, resulting in high-yield, site-specific modification⁵⁶. Similarly, phosphorylation at Tyr39 has been introduced using recombinant c-Abl kinase *in vitro*, although it had to be combined with NCL for absolute site-specificity⁴⁹. The advantage of enzymatic modification is that it mimics natural modification pathways and does not require genetic modifications or chemical synthesis. However, it often suffers from low reaction efficiency, lack of strict site specificity, and the potential for off-target modifications. Since many enzymes may recognize multiple sites on α S, researchers must run test reactions and optimize reaction conditions to ensure selective modification of the desired residue.

Each of these methods for site-specific, authentic PTM incorporation has distinct advantages and limitations, and the choice of approach depends on the research question being addressed. GCE provides a convenient way to incorporate PTMs in living cells but is restricted by efficiency and system compatibility. Chemical protein synthesis offers the highest level of precision but is technically demanding and mainly applicable to *in vitro* studies. Enzymatic modification provides a natural and scalable approach but requires careful optimization to achieve site specificity. By employing a combination of these methods, researchers can generate homogeneously modified α S and investigate the precise effects of PTMs, ultimately providing deeper insights into the role of PTMs in α S-related neurodegeneration.

The following chapters will explore site-specific PTMs in α S, focusing particularly on lysine acetylation and phosphorylation using GCE, enzymatic modification, and protein semi-synthesis. Chapter 2 systematically evaluates disease-relevant lysine acetylation sites in α S, examining their effects on aggregation, fibril structure, and membrane interactions. Chapter 3 investigates the extent to which glutamine substitution mimics authentic lysine acetylation, revealing site-dependent differences. Chapter 4 introduces additional chemical tools for studying Lys acetylation, including thioether acetylation mimics and thioamide analog of acetyl Lys. Chapter 5 highlights GCE and enzymatic modifications as accessible methods for site-specific incorporation of phosphorylation. The appendices provide studies on glutamate arginylation, synthesis of a peptide library, and semi-synthetic tools for PTM characterization. Together, this work advances methodologies for precise PTM incorporation while also evaluating the effectiveness of PTM mimics. These findings provide deeper insights into how authentic and mimicked modifications influence α S structure, aggregation, and function, contributing to a more nuanced understanding of PTM regulation in synucleinopathies.

CHAPTER 2: INVESTIGATION OF ALL DISEASE-RELEVANT LYSINE ACETYLATION SITES IN ALPHA-SYNUCLEIN ENABLED BY NON-CANONICAL AMINO ACID MUTAGENESIS

This chapter was adapted by the manuscript “Investigation of All Disease-Relevant Lysine Acetylation Sites in α -Synuclein Enabled by Non-canonical Amino Acid Mutagenesis,” which was submitted to bioRxiv.

Ming-Hao Lee performed cryo-EM studies and Hudson Lee performed HSQC NMR studies (David Eliezer’s group). Grace Park experimented aggregation seeding in neurons. Jennifer Ramirez assisted with FCS and production of isotopically labeled proteins. Paris Watson and Swati Sharma produced HDAC8 (David Christianson’s group). Zongtao Lin (Benjamin Garcia’s group) and Chao Peng performed MS analysis of patient samples.

Relevant methods: §7.1, §7.2, §7.3, §7.4, §7.9, §7.10, §7.11, §7.12, §7.13, §7.14, §7.15, §7.16

§2.1 Introduction

Alpha-synuclein (α S) is a 14 kDa protein that typically exists at presynaptic terminals in healthy neurons, where its primary function is believed to be in synaptic vesicle trafficking and regulating neurotransmission^{57,58}. Aggregates of α S commonly characterize several neurodegenerative diseases such as Parkinson’s Disease (PD), Dementia with Lewy Bodies (DLB) and Multiple System Atrophy (MSA), which are referred to as synucleinopathies. Evidence indicates that distinct pathology is caused by α S fibrils formed in different disease environments, or α S “strains.” Aggregation seeding experiments showed that α S strains have distinct abilities to propagate pathology, where α S fibrils from MSA patients are much more potent in seeding aggregation than those from DLB²⁸. In addition to this, recent cryo-electron microscopy (cryo-EM) experiments showed that structures of α S fibrils vary between different pathological contexts in PD/DLB³⁴ and MSA³³. Despite these findings, the mechanism underlying these

differences remains to be understood. It has been suggested that post-translational modifications (PTMs) may contribute to these differences⁵⁹. Among the PTMs that have been studied on α S thus far are *N*-terminal acetylation, phosphorylation, O-GlcNAcylation, lysine acetylation, lysine ubiquitination, tyrosine nitration and glutamate arginylation^{50,59-61}.

We have recently published a comprehensive study of the relative levels of PTMs in the soluble α S monomer pool between MSA, PD, and DLB patients vs. healthy controls³⁵. While many of the PTMs identified have been previously studied in chemical detail by our laboratory and others,^{50,62} lysine acetylation stood out as a PTM that is very common and highly physiologically relevant in other proteins, but had received relatively little attention to date in the context of α S. Given that other α S PTMs have found great significance as biomarkers (e.g. pS₁₂₉ – a hallmark of PD³⁶) and drug targets (e.g. kinase inhibitors⁶³), we wished to investigate these acetyl lysine (^{Ac}K) sites more thoroughly.

Lysine acetylation is a reversible PTM that can be introduced at specific sites by lysine acetyltransferases (KATs) or non-enzymatically added by reaction with abundant cytosolic acetyl coenzyme A. Lysine deacetylation is catalyzed by lysine deacetylases (KDACs), which include Zn²⁺-dependent histone deacetylases (HDACs) and NAD⁺-dependent sirtuins^{64,65}. In addition to our comprehensive PTM study in patient samples, there has been some previous evidence for the role of lysine acetylation in synucleinopathies. It has been suggested that activity imbalances between KATs and KDACs on histone or non-histone proteins are pathologically relevant to PD. In fact, activators of some sirtuins and inhibitors of specific KDACs/KATs have shown potential as therapeutics⁶⁶. Identified as a substrate of these enzymes, α S was found acetylated on Lys6 and Lys10 in mouse brain. Sirtuin-2 was found to deacetylate those sites and enhance the toxicity of α S⁶⁷. It is notable that in this work, semi-synthetic, acetylated α S was used for the deacetylation assay, however for other experiments glutamine was used to

mimic lysine acetylation, which is a common strategy of choice in the field of biochemistry or biophysics, due to easier access to the site-specifically, homogenously modified construct.

Recently, many more disease-relevant lysine acetylation sites have been identified in patient tissue. Eight ^{Ac}K sites were identified by Goedert and Scheres in mass spectrometry (MS) studies accompanying a cryo-EM structure of α S fibrils from MSA patients (Lys21/23/32/45/58/60/80/96, Figure 5)³³. Ten ^{Ac}K sites, many overlapping those found by Goedert and Scheres, were identified by MS in our previously noted studies of soluble α S from patients (Lys12/21/23/34/43/45/58/60/96/102, Figure 5)³⁵. In our accompanying mechanistic studies of the PTMs, authentic constructs of phosphorylated α S were produced through semi-synthesis because phosphorylation occurred at a few key sites with established semi-synthetic routes, but lysine acetylation was investigated only through glutamine mimics due to challenges in systematically investigating a large number of PTM sites where there was less literature to identify key targets.³⁵ Thus, there have not been studies of the effect of authentic lysine acetylation in α S at the sites identified from patient tissue.

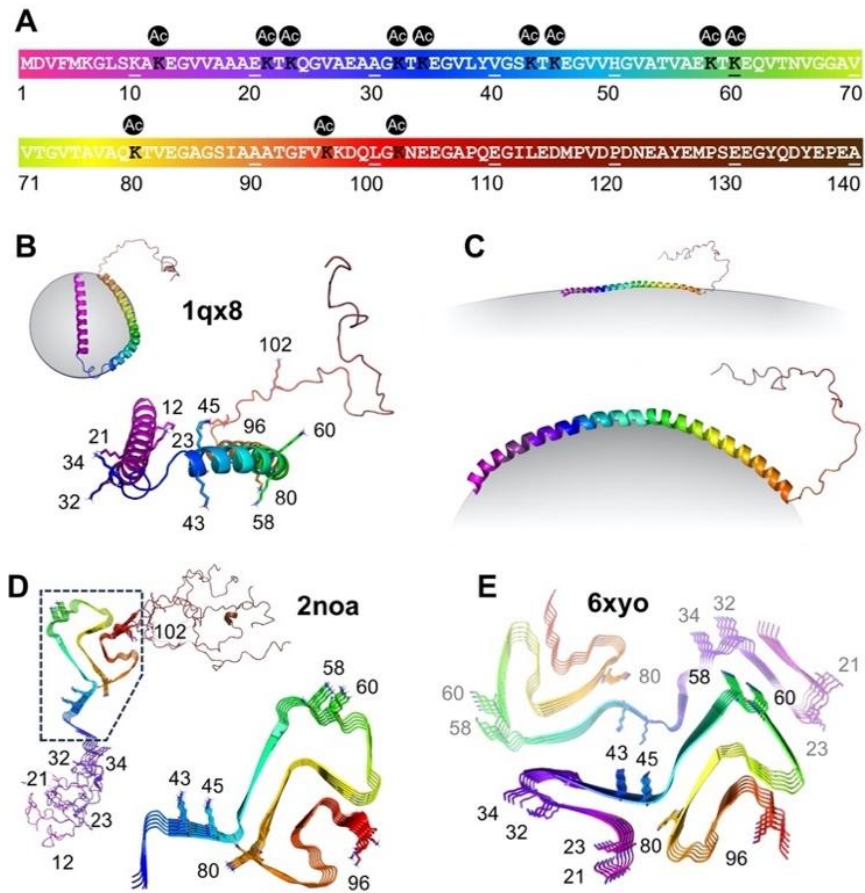


Figure 5. Neurodegeneration-relevant Lys acetylation sites in α S.

(A) α S sequence with positions 12, 21, 23, 32, 43, 45, 58, 60, 80, 96 and 102 marked. (B) Solution NMR structure of micelle-bound α S (PDB: 1qx8). (C) Proposed structure of vesicle-bound α S. (D) Solid-state NMR structure of recombinant α S fibrils (PDB: 2noa). (E) Cryo-EM structure of MSA patient α S fibrils (PDB: 6xyo).

In this work, we set out to study lysine acetylation at all 12 disease-relevant sites of α S (Figure 5A). We began by comparing the efficiency of producing acetylated α S through either native chemical ligation

(NCL) or non-canonical amino acid mutagenesis (ncAA mutagenesis). We found that ncAA mutagenesis provided comparable yields, and was therefore superior for scanning many acetylation sites due to the ease of generating new constructs. Once the 12 α S^{AcK} variants were expressed and purified, we studied their binding to membranes as well as their aggregation propensities. We performed NMR, fluorescence correlation spectroscopy (FCS), and transmission electron microscopy (TEM) experiments on acetylated variants that showed perturbed membrane binding or aggregation. NMR and FCS experiments were enabled by our ncAA mutagenesis approach which made it facile to produce isotopically or fluorescently labeled α S. We went on to characterize the seeding ability of select α S^{AcK} constructs in neurons and to test HDAC selectivity in deacetylating these sites. The combination of the site-specific incorporation approach and a variety of biological characterization methods provides a systematic understanding of lysine acetylation, identifying a few key α S^{AcK} sites as significant for further investigation and potential therapeutic intervention.

§2.2 Results

Comparison of ncAA Mutagenesis and NCL

Protein semi-synthesis is a powerful approach to site-specifically incorporate modifications of interest into a protein sequence⁶⁸ and it has been a method of choice for many α S PTM studies⁶², including Lys acetylation⁶⁷. To test this approach to synthesizing acetylated α S, we chose α S^{AcK₈₀} as an example, and combined solid-phase peptide synthesis (SPPS),⁶⁹ by which ϵ -acetyllysine is incorporated, with the expression of protein fragments and a three-part NCL sequence using acyl hydrazides⁷⁰ (Figure 6A).

N-terminal thioester fragment α S₁₋₇₆-MES (**1a**) and C-terminal fragment α S₈₅₋₁₄₀-C₈₅ (**4**) were each recombinantly expressed as a fusion with Mxe GyrA intein. The *N*-terminal thioester was generated by adding excess sodium 2-mercaptoethane sulfonate (MESNa) to cleave the intein by N,S-acyl shift.⁷¹ (reported yield 24.1 mg/L⁷²). Endogenous methionyl aminopeptidase in *E. coli* processes the *N*-terminus

of the 85-140 peptide to expose the *N*-terminal cysteine,⁷³ which further reacts with aldehydes or ketones *in vivo* to form thiazolidine derivatives.⁷⁴ The thiazolidine derivatives were deprotected with methoxyamine to give a free *N*-terminal cysteine (4.40 mg/L). The middle acyl hydrazide peptide αS_{77-84} -Pen₇₇^{Ac}K₈₀-NHNH₂ (**2**, Pen: penicillamine⁷⁵) was synthesized through SPPS (Yield: 12.4 mg, 12 μ mol, 48%).

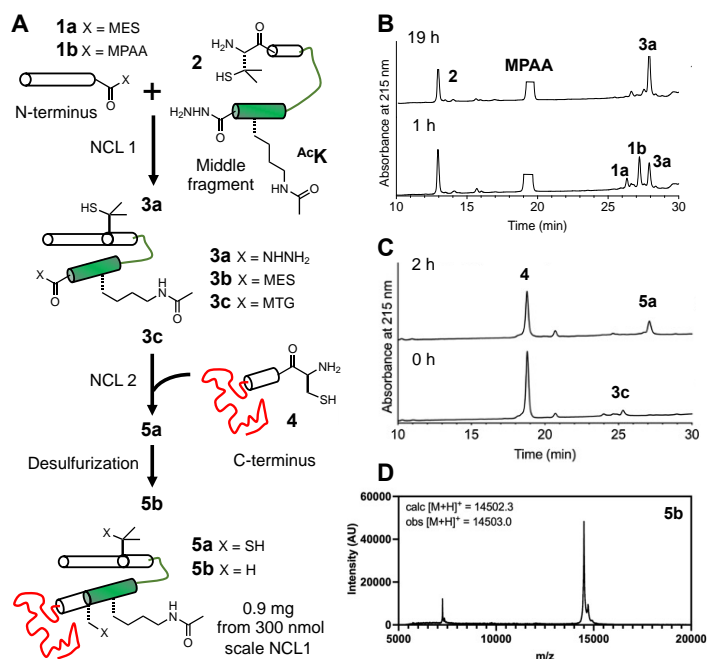


Figure 6. Semi-synthesis of αS with acetylation at Lys80.

(A) Acetylation is introduced through peptide synthesis, and the peptide is combined with expressed peptide fragments using NCL. (B) Analytical HPLC trace for the first ligation. **1a**: αS_{1-76} -MES, **1b**: αS_{1-76} -MPAA, **2**: αS_{77-84} -Pen₇₇^{Ac}K₈₀-NHNH₂, **3a**: αS_{1-84} -Pen₇₇^{Ac}K₈₀-NHNH₂. (C) Analytical HPLC trace for the second ligation. **3b**: αS_{1-84} -Pen₇₇^{Ac}K₈₀-MES, **3c**: αS_{1-84} -Pen₇₇^{Ac}K₈₀-MTG, **4**: αS_{85-140} -C₈₅, **5a**: αS -Pen₇₇C₈₅^{Ac}K₈₀. (D) MALDI MS of HPLC-purified αS -AcK₈₀ (**5b**).

α S₁₋₇₆-MES (**1a**) and α S₇₇₋₈₄-Pen₇₇^{Ac}K₈₀-NHNH₂ (**2**) were ligated overnight under routine NCL conditions (NCL1) in the presence of 4-mercaptophenylacetic acid (MPAA). (Yield: 1.46 mg, 172 nmol, 57%, Figure 6B). The purified product (**3a**) was activated by oxidation to form a MES thioester (**3b**) (Yield: 1.29 mg, 126 nmol, 73%). The second ligation (NCL2) between α S₁₋₈₄-Pen₇₇^{Ac}K₈₀-MES (**3b**) and α S₈₅₋₁₄₀-C₈₅ (**4**) to form α S-Pen₇₇C₈₅^{Ac}K₈₀ (**5a**) as performed in the presence of methyl thioglycolate to allow for desulfurization without intermediate purification (Figure 6C).⁷⁶ The product, α S-^{Ac}K₈₀ (**5b**), was obtained in 43% yield (0.90 mg, 62 nmol, Figure 6D). Although we successfully completed this synthesis, it is notable that we encountered solubility issues of the intermediate fragments (**3b**, **5a**) and the product (**5b**), after lyophilization.

Experiencing difficulties in sample handling and considering the inefficiency of applying NCL to scan 12 lysine acetylation sites distributed throughout the protein, we then sought to access site-specifically acetylated α S through ncAA mutagenesis (Figure 7A). We recombinantly expressed α S with lysine acetylation at site 80 in *E. coli* through amber codon suppression. We used a previously reported pair of aminoacyl tRNA synthetase (chAcK3RS with IPYE mutations) and cognate tRNA to incorporate ϵ -acetyllysine at a position dictated by an amber stop (TAG) codon⁷⁷. In addition to 10 mM ϵ -acetyllysine, 50 mM nicotinamide, an inhibitor to endogenous deacetylases, was added to the media before inducing α S expression. The protein was expressed as an intein fusion as reported before for easy removal of truncated protein through affinity purification.⁷⁸ After intein cleavage with 2-mercaptoethanol, the ^{Ac}K-containing protein was purified by reverse phase high performance liquid chromatography (RP-HPLC) and exchanged into appropriate buffers for biophysical assays (Figure 7B).

We obtained 0.65 mg of pure α S-^{Ac}K₈₀ per L of bacterial culture (Figure 7C, 7D), a yield comparable to that obtained by NCL, but because no lyophilization or handling of ligation intermediates is required, we did not encounter the solubility problems observed in the NCL process. Therefore, we deemed the

ncAA mutagenesis approach at least comparable to NCL for producing a specific construct. Since we wished to study 12 sites distributed throughout the α S sequence, ncAA mutagenesis was also advantageous because we avoided having to generate constructs for several different ligation sites and could simply perform site-directed mutagenesis to insert TAG codons for each new α S-^{Ac}K_n variant.

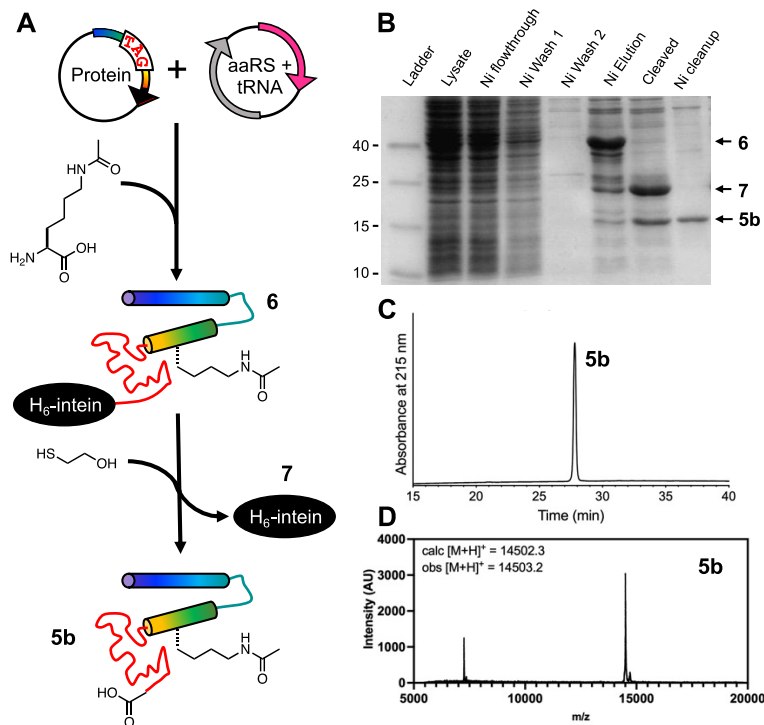


Figure 7. Expression of α S with acetylation at Lys80 through ncAA mutagenesis.

(A) An orthogonal aminoacyl tRNA synthetase (aaRS)/tRNA pair site-specifically incorporates acetyllysine in recombinant α S. Intein tagging at the C-terminus allows for traceless purification of the full-length product. (B) SDS-PAGE gel (Coomassie stain) showing Ni-affinity purification of recombinant α S-^{Ac}K₈₀. Purified α S-^{Ac}K₈₀ (**5b**) characterized with (C) analytical HPLC and (D) MALDI MS.

Bolstered by our success with $^{Ac}K_{80}$, we generated TAG mutants at sites 12, 21, 23, 32, 34, 43, 45, 58, 60, 96, or 102. We expressed and purified these proteins, observing successful ncAA mutagenesis at each site, however, the yield varied significantly between different sites (0.11-1.5 mg). This is an interesting result in light of the large number of sites that were tested in the same protein and the fact that αS is an intrinsically disordered protein, so protein folding should not affect incorporation. Examination of the local RNA sequence context of the amber (TAG) codon did not explain the varied suppression efficiency, based either on previously identified sequence impacts⁷⁹ or by comparing the sites within αS . Given the pseudo-repeat nature of the αS sequence, many sites feature similar sequences, and a comparison of 21 and 58 is particularly striking with a 10-fold difference in expression levels despite near identity in the flanking sequences. While these observations are notable for users of ncAA technology, in the context of this study, our approach allowed us to acquire sufficient amounts of the 12 different authentically modified αS constructs for biophysical experiments.

Thus, in spite of low expression yields for some sites, ncAA mutagenesis was a preferred method for this work, due to the better efficiency in scanning 12 different modification sites and the ease of handling aggregation-prone protein fragments. The expression-based strategy also allows for low-cost access to isotopically labeled, PTM-modified αS constructs, as we have demonstrated previously.⁸⁰

Effects on αS Helicity on Micelles and Aggregation

αS is known to bind to lipid surfaces and form helical structures, part of its physiological role in modulating neurotransmitter vesicle trafficking⁸¹. More specifically, on micelles, an NMR structure showed that micelle-bound αS forms a broken helix, where two helical strands are connected with a loop region (Figure 5B, PDB: 1xq8)⁸². A helical wheel model, created based on this structure, shows that lysine residues are aligned on the membrane surface, and that they are likely involved in enhancing binding by interactions with negatively charged lipid head groups⁷.

With each acetylated α S variant, we first examined the effects of Lys acetylation on the secondary structure of α S in the presence of micelles by wavelength scan circular dichroism (CD) spectroscopy. Each acetylated α S was compared to unmodified wild type (WT) α S in phosphate-based buffer, pH 7.4, with a large excess of sodium dodecyl sulfate (SDS). We normalized the molar ellipticity at 222 nm of each acetylated construct to that of WT to compare the effect on helicity at each site. We found that significant reduction of helicity was caused only by acetylation at site 43 and that acetylation at other sites had only minor effects on helicity (Figure 8). This study implies that only this site could potentially perturb α S function in neurotransmitter trafficking.

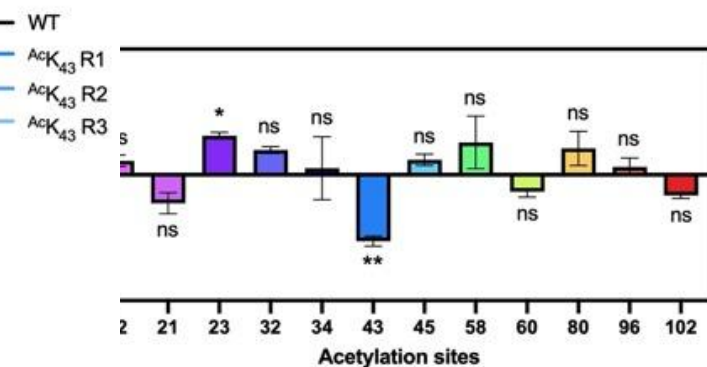


Figure 8. Effects of lysine acetylation on micelle-bound α S.

Molar ellipticity at 222 nm was normalized to WT value to quantify helicity on SDS micelles. Mean with SD, R=3

We then investigated whether lysine acetylation at different sites has impacts on α S in pathological contexts. To do this, we first performed *in vitro* aggregation experiments and assessed site-specific effects. A plate-based approach was taken to efficiently perform the assay, and each aggregation reaction was seeded by mixing with α S WT pre-formed fibrils (PFFs) that constituted 10% of the total monomer

concentration. The monomer samples were prepared by mixing α S WT with acetylated α S at either 10% or 25% of the total monomer concentration. These concentrations were chosen because our quantitative studies of other PTMs in patient samples indicated that most were present in this range, rather than stoichiometrically^{35,83} (see additional discussion in Conclusions). Aggregation was carried out at 37 °C with shaking and kinetics and thermodynamics (final fibril amounts) were monitored.

To examine the effects on aggregation kinetics, we took advantage of the change in fluorescence of the amyloid binding dye, thioflavin T (ThT), during aggregation to monitor the process *in situ*. We found that the effects differ between different modification sites (Figure 9). For Lys acetylation at 12, 23, 43, 80 and 102 we observed differential slowing effects – the effects were particularly significant at sites 12, 43 and 80, and the effects at 12, 23 and 43 were dose dependent. While we observed acceleration of aggregation for site 32 both at 10% and 25%, the effects were similar between the different dosages.

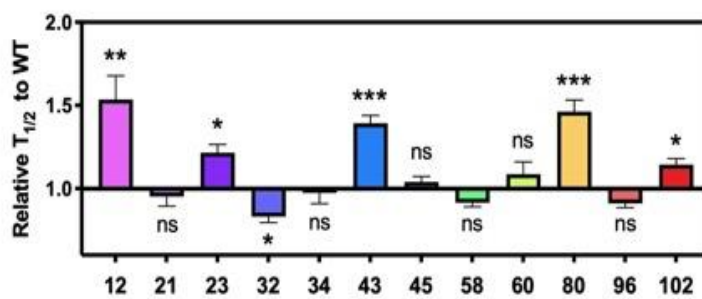


Figure 9. Effects of lysine acetylation on *in vitro* aggregation.

Aggregation kinetics were monitored by fluorescence intensity change of ThT. Time it takes to reach 50% fibrilization ($T_{1/2}$) for each condition was normalized to that of WT. Seeded aggregation was performed with α S monomers where acetylated α S was mixed with α S WT at 25%:75% ratio. SEM, R=6

To confirm that these effects were not the result of reduced monomer incorporation, we isolated fibrils at the endpoint of 10% or 25% aggregations and SDS-PAGE gels were run and stained with the Coomassie Brilliant Blue dye to quantify total monomer incorporation into the fibrils. We found that there were no consistent reductions in monomer incorporation, and in fact there were some moderate apparent enhancements of incorporation. However, these were generally not consistent between the 10% and 25% aggregation experiments, except in the case of ^{Ac}K₃₄. Taking all of the aggregation kinetics and monomer incorporation data into account, we chose to investigate the kinetically perturbed sites 12, 43, and 80 further, since the cellular process will be unlikely to reach equilibrium and our previous study had shown that the Gln mimic mutation at position 34 did not alter aggregation in cells.³⁵

Fibril Seeding in Neurons

To investigate the impact of Lys acetylation on aggregation in more physiologically relevant contexts – in cultured neurons – we followed the approach that we have done previously with arginylated α S.^{83,84} We prepared PFFs with the following compositions: α S WT or α S WT mixed with 25% acetylated α S, ^{Ac}K₁₂, ^{Ac}K₄₃ or ^{Ac}K₈₀. Mouse primary hippocampal neurons were grown for 8 days on a coated plate, to which 50 ng/ μ L PFFs were added, following established protocols.^{21,85,86} After 2 weeks, intracellular α S aggregates were quantified by staining with an antibody that recognizes phosphoserine 129 (pS₁₂₉), a commonly used pathological marker (Figure 10). Compared to the WT PFFs, all the acetylated PFFs tested resulted in significantly reduced aggregation seeding: the pS₁₂₉ signal (AU \pm SEM (arbitrary units, standard error of the mean)) of PFF-seeded α S aggregates was 2347 \pm 107.1 (WT), 1730 \pm 83.67 (^{Ac}K₁₂), 1854 \pm 70.79 (^{Ac}K₄₃), 1698 \pm 54.41 (^{Ac}K₈₀) with respect to DAPI. Notably, acetylation at these sites also slowed seeded aggregation in the *in vitro* fibrilization experiment, but did not reduce aggregates quantified at the endpoint. This supports the idea that aggregation in a cellular context is unlikely to reach saturation.

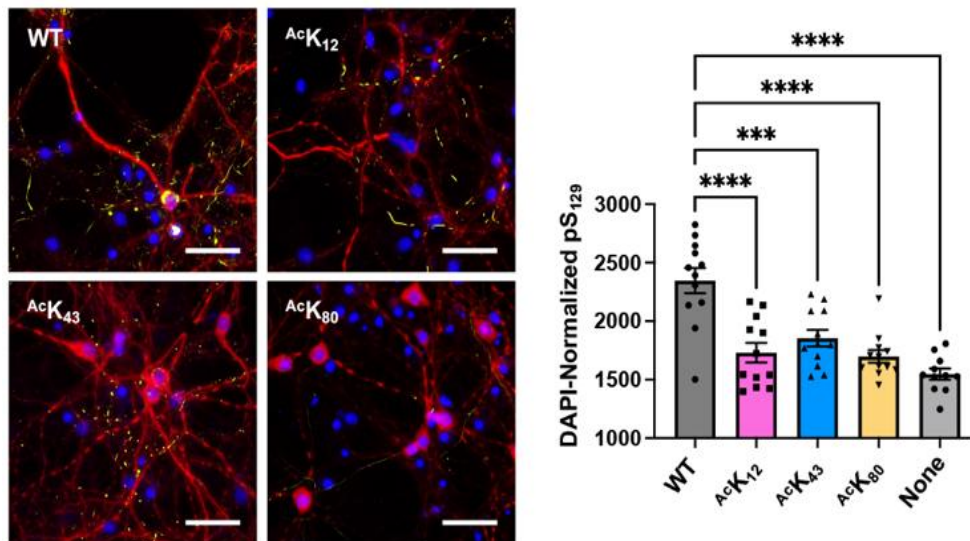


Figure 10. Effects on aggregation seeding in primary neuron cells.

Left: representative images of neuron cultures treated with unmodified or 25% acetylated α S PFFs, stained with an anti-pS₁₂₉ antibody (yellow), DAPI (blue), and an anti-MAP2 antibody (red). Scale bar = 50 μ m. Right: quantification of DAPI-normalized anti-pS₁₂₉ area of intracellular aggregates seeded by different α S PFFs. Mean with SE, R= 11-12. *** = 0.001 < p-value < 0.0001; **** = 0.00001 < p-value < 0.0001

Structural Characterization of α S Monomers

Having demonstrated that acetylation at K₁₂, K₄₃ or K₈₀ significantly reduced α S aggregation *in vitro* and in cells, we wished to gain information on the structural impact of acetylation at these sites. First, to give insights into the effects on monomer conformation, we acquired proton-nitrogen correlation spectra (¹H,¹⁵N – HSQC) for ^{Ac}K₁₂, ^{Ac}K₄₃, or ^{Ac}K₈₀, an experiment that is facile with nCAA mutagenesis, but challenging to perform via NCL due to the high cost of isotopically-labeled amino acids for SPPS. To access ¹⁵N-labeled α S, we expressed the acetylated α S and α S WT in M9 minimal media containing ¹⁵N-labeled ammonium chloride. This afforded comparable protein yields to expressions in LB media. It is

notable, however, that sub-stoichiometric isotopic labeling was observed at some Lys sites, depending on batches of expression, which could be due to deacetylation in *E. coli* cells followed by incorporation at Lys codons. Overlaying the HSQC spectra for α S-WT and α S-^{Ac}K₁₂, ^{Ac}K₄₃ or ^{Ac}K₈₀, peak shifts were observed only in signals from surrounding residues, suggesting that the structural change was local and there is no major impact of lysine acetylation on monomer structure.

Biophysical Characterization of Lipid Binding

We next wished to learn the effects of Lys acetylation at K₁₂, K₄₃ or K₈₀ on the native function of α S by investigating its lipid binding mode. To quantify conformational changes of α S upon vesicle binding, we acquired ¹H, ¹⁵N – HSQC spectra for WT, ^{Ac}K₁₂, ^{Ac}K₄₃ or ^{Ac}K₈₀ in the presence of small, unilamellar vesicles (SUVs) that are composed of 60:25:15 1,2-dioleoyl-sn-glycero-3-phosphocholine/1,2-dioleoyl-sn-glycero-3-phosphatidylethanolamine/1,2-dioleoyl-sn-glycero-3-phospho-L-serine (DOPC/DOPE/DOPS). The NMR peak chemical shifts were similar for all constructs and consistent with spectra previously reported for WT α S⁸⁷. There was no notable chemical shift perturbation at the surrounding residues of each acetylation site.

In the presence of vesicles, a reduction of intensity for residues 1-100 was observed for all the constructs, which is caused by binding of this portion of α S to the slowly tumbling lipid vesicles and is again consistent with previous observations^{88,89}. α S-^{Ac}K₈₀ had a similar intensity change to WT (~40%, Figure 11A), whereas α S-^{Ac}K₄₃ had a smaller intensity change, suggesting weaker vesicle binding (~20%, Figure 11A). This is consistent with the acetylation effects observed with SDS micelles (Figure 8). α S-^{Ac}K₁₂ had an intermediate intensity reduction (~30%, Figure 11A), a more significant effect of K₁₂ acetylation on vesicle binding than what was observed with SDS micelles (Figure 8). It is possible that this is due to the differences in curvature and headgroup between the micelles and the vesicles, which is

known to result in different α S binding modes^{12,14,90-92}. It is also possible that this is due to the increased sensitivity of NMR to subtle differences in binding.

While NMR is a very valuable technique for characterizing vesicle binding with a non-perturbing label, to measure affinity, we turned to FCS, a well-established method for rigorously determining vesicle apparent dissociation constants ($K_{d,app}$)⁹⁰. To enable this experiment, we expressed the acetylated α S constructs at site 12, 43, or 80 or a non-acetylated construct (“WT”), bearing a Cys mutation at site 114 (**8**, α S^{-Ac}K₁₂C₁₁₄, α S^{-Ac}K₄₃C₁₁₄, α S^{-Ac}K₈₀C₁₁₄, and α S-C₁₁₄) to allow for fluorescent labeling (Figure 11B). The fluorophore Atto488-maleimide was reacted with purified Cys mutants overnight at 4 °C or for a few hours at room temperature to yield labeled constructs (**9**, α S^{-Ac}K₁₂C^{Atto488}₁₁₄, α S^{-Ac}K₄₃C^{Atto488}₁₁₄, α S^{-Ac}K₈₀C^{Atto488}₁₁₄, and α S-C^{Atto488}₁₁₄), and the conversion was almost quantitative. We prepared synthetic lipid vesicles containing 50:50 1-palmitoyl-2-oleoyl-sn-glycero-3-phospho-L-serine/1-palmitoyl-2-oleoyl-glycero-3-phosphocholine (POPS/POPC). The diffusion times of free α S and of the vesicles were obtained first, and in assessing the α S-vesicle binding, we added the same quantity of α S to varied concentrations of vesicles and then determined the protein fractions bound by fitting a two-component autocorrelation function. The fraction bound values at each vesicle concentration were used to fit a binding curve for each α S construct. We found that acetylation at site 43 leads to two-fold weaker binding and acetylation at site 12 or 80 did not significantly affect binding (Figure 11C, $K_{d,app}^{WT} = 3.2 \pm 0.5 \mu\text{M}$, $K_{d,app}^{AcK12} = 3.9 \pm 0.3 \mu\text{M}$, $K_{d,app}^{AcK43} = 6.3 \pm 1.3 \mu\text{M}$, $K_{d,app}^{AcK80} = 4.0 \pm 1.0 \mu\text{M}$).

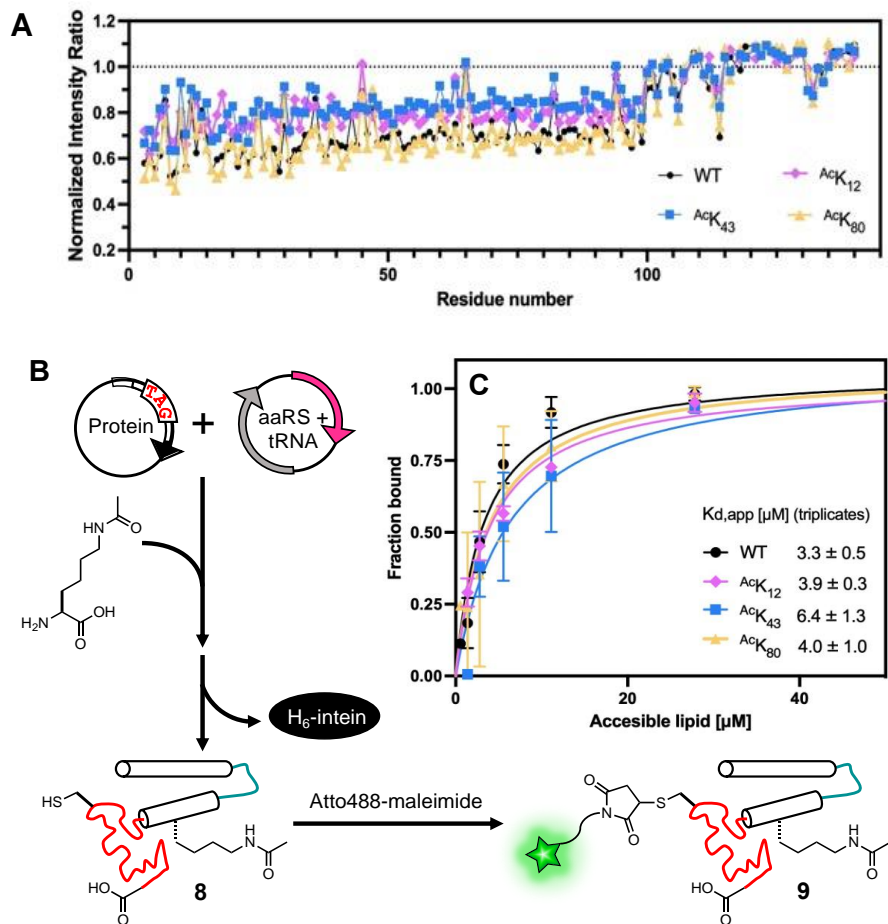


Figure 11. Effects of lysine acetylation on vesicle binding affinity.

(A) NMR intensity ratio for each residue calculated from ^1H - ^{15}N HSQC spectra collected with ^{15}N -labeled αS variants in the presence or absence of SUVs, normalized by the average ratio for residues 101-140. (B) αS with a TAG codon at the acetylation site of interest and a Cys mutation at a labeling site (**8**) was co-expressed with an aaRS/tRNA plasmid for acetyllysine incorporation. After intein cleavage, labeling with an Atto488 dye was performed through Cys-maleimide chemistry to give an acetylated, labeled protein (**9**) for FCS. (C) Vesicle binding affinity determined by fluorescent correlation spectroscopy measurements. For each construct, measurements were performed on three separate days. Mean with SD, R=3

Slightly reduced binding due to acetylation at site 43 correlates with the reduced helicity we observed in the CD wavelength scan and the differences in NMR peak intensities in the presence of vesicles. The NMR experiments showed that ^{Ac}K₄₃ reduced vesicle binding more significantly than ^{Ac}K₁₂ (moderate) or ^{Ac}K₈₀ (little to none). The FCS experiments supported this, showing that ^{Ac}K₄₃ led to weaker binding than ^{Ac}K₁₂ or ^{Ac}K₈₀, which were similar to WT. Previous NMR experiments suggested that the *N*-terminal helix of α S (residues 6-25) drives association with lipid membranes and the 26-97 region modulates the affinity, depending on lipid composition⁹³. The different effect between ^{Ac}K₄₃ and ^{Ac}K₁₂ or ^{Ac}K₈₀ suggests that K₄₃ is more important in modulating the binding affinity.

Taken together, our results show that among all the disease-relevant acetylation sites, ^{Ac}K₁₂, ^{Ac}K₄₃, and ^{Ac}K₈₀ each inhibit aggregation, but that ^{Ac}K₄₃ also inhibits membrane binding (as does ^{Ac}K₁₂, to a lesser degree). Thus, in the case of ^{Ac}K₄₃, the potential benefits of reduced amyloidogenicity may be offset by compromising function in neurotransmitter release.

Structural Characterization of α S Fibrils

To get preliminary insights into fibril structure effects, we performed TEM imaging on fibrils formed from acetylated α S (α S-^{Ac}K₁₂, ^{Ac}K₄₃ or ^{Ac}K₈₀), mixed with α S WT, at 25% of the total monomer concentration. Interestingly, we observed mixed morphology for PFFs prepared with α S-^{Ac}K₁₂, with some very narrow fibrils. Both 25% ^{Ac}K₁₂ and 25% ^{Ac}K₄₃ PFFs have minimal helical twist, making them difficult to characterize by cryo-EM. On the other hand, for PFFs prepared with 25% α S-^{Ac}K₈₀, we observed a slightly more twisted fibril morphology, so we attempted to solve a structure by single particle cryo-EM methods. Although the resolution is not sufficient to build an atomic model, comparison to previously published α S WT fibril structures (Figure 12) shows that the backbone fold is identical. This indicates that the effect of lysine acetylation on aggregation rates is not due to a dramatic change in fibril conformation. While further structural analysis will be performed on the ^{Ac}K₈₀ PFFs, when taken together

with the similarity of the $^{Ac}K_{80}$ and WT NMR data, this initial fibril structure analysis implies that a more subtle process is affecting aggregation rates, perhaps by altering the populations of early oligomers or protofibrils.

In order to more clearly observe the structural impact of K_{80} acetylation, we prepared fibrils with 100% $^{Ac}K_{80}$ α S in Tri-buffered saline (TBS) for cryo-EM studies. For these fibrils, we were able to solve structures of two different polymorphs, both composed of two strands (Figure 12, $^{Ac}K_{80}$ -A and $^{Ac}K_{80}$ -B). The protein fold is essentially the same in both polymorphs, but they differ in strand-strand packing. Since it is well-documented that differences in buffer composition and aggregation methods can lead to differences in fibril morphology, we also prepared $^{Ac}K_{80}$ α S fibrils in phosphate-buffered saline (PBS), the same conditions used in our aggregation kinetics studies. Gratifyingly, the $^{Ac}K_{80}$ α S fibrils prepared in PBS exhibited the same two polymorphs seen for TBS $^{Ac}K_{80}$ α S fibrils, with identical protein folds and two different strand-strand packings (Figure 12, PBS inset). We were also able to solve cryo-EM structures of WT α S fibrils generated under the same conditions in TBS. We observed two WT polymorphs (Figure 12, WT-A and WT-B) which exhibited similar folds and strand-strand packings to the $^{Ac}K_{80}$ polymorphs, but with a notable change in morphology around K_{80} . Acetylation of K_{80} disrupts a salt-bridge interaction with E_{83} that can be clearly seen in the WT-B polymorph (Figure 12, WT Fold) and neutralizes the sidechain charge, allowing it to pack in a hydrophobic pocket formed by Ala_{69} and Val_{71} (Figure 12, $^{Ac}K_{80}$ Fold). This leads to a twist of the backbone in the T_{75} - A_{90} segment, generating a modest change in the protein fold. Given that the $^{Ac}K_{80}$ protein fold is fairly similar to the WT protein fold, it is not surprising that they exhibit similar strand-strand packings and that K_{80} acetylation has a moderate impact on aggregation rates. We can use these structures to consider $^{Ac}K_{80}$ effects in the context of other structural studies of α S fibrils.

Our WT-A and WT-B structures resemble those first reported under PDB IDs 6rtb (Figure 12, inset) and 6rto.⁹⁴ These polymorphs have been observed by several investigators for WT α S fibrils formed at near-neutral pH, along with the commonly observed two-stranded polymorph typified by PDB ID 6a6b (Figure 12, inset),⁹⁵ which has the “Greek key” protein fold first reported in solid state NMR studies of single stranded fibrils under PDB ID 2n0a.⁹⁶ Our ^{Ac}K₈₀ α S fibril structures, ^{Ac}K₈₀-A and ^{Ac}K₈₀-B, resemble those recently reported for WT α S fibrils formed at pH \leq 6.5 under PDB IDs 8pix (Figure 12, inset) and 8pic.⁹⁷ In the two fibril polymorphs commonly populated at pH 7, K₈₀ makes key stabilizing salt bridge interactions. For the 6a6b/2n0a polymorph, K₈₀ makes a salt bridge with E₄₆; for the 6rtb/6rto polymorph, it makes a salt bridge with E₈₃. Disruption of these salt bridges by acetylation would destabilize either fold, favoring the ^{Ac}K₈₀ fold that we observe. The fact that a similar fold (8pix/8pic) has been seen at lower pHs can be rationalized by assuming that acidification leads to protonation of the E₄₆ or E₈₃ sidechains, weakening their interactions with K₈₀ just as acetylation does to drive a change fibril polymorph. While pH 6.5 is significantly above the pK_a of a typical glutamate sidechain, it is possible that the pK_as are perturbed in the local environment of the fibril, and full deprotonation would not be required to destabilize interactions with K₈₀. Thus, one can rationalize our observation of a polymorph like 8pix/8pic for our ^{Ac}K₈₀ at pH 7, when it had only been previously observed at lower pHs.

Finally, it is worth comparing the effects that we observe for ^{Ac}K₈₀ acetylation to the structural and biophysical effects observed with other α S PTMs which have been structurally characterized, such as Y₃₉ phosphorylation (pY₃₉) or S₈₇ phosphorylation (pS₈₇) and *N*-Acetyl glucosamine glycosylation (gS₈₇). For pY₃₉ α S, a 4-fold increase in aggregation rate has been observed for α S 100% phosphorylation, with nuanced effects at lower phosphorylation percentages. We have shown that pY₃₉ leads to only modest changes in monomer conformation, based on NMR and single molecule FRET studies.^{80,98} In contrast, Zhao *et al*'s cryo-EM structure shows a dramatic rearrangement of the fibril polymorph.⁹⁹ This indicates that the effect of Y₃₉ phosphorylation is primarily at the fibril level, similar to our findings here for ^{Ac}K₈₀

acetylation. Both pS₈₇ and gS₈₇ modifications inhibit aggregation much more drastically than pY₃₉. Two different structures of gS₈₇ α S fibrils have been reported, both showing a significant deviation from reported WT α S polymorphs.^{41,47} Despite their differences, the structures both provide a clear rationale for the effects of S₈₇ glycosylation. Intriguingly, Hu *et al.* highlight the way in which gS₈₇ changes the structure of the 80-89 region of α S to disrupt the E₄₆-K₈₀, destabilizing the 6a6b fold.⁴¹ The pS₈₇ structure is different from either gS₈₇ structure, and although the residue cannot be observed in the structure, it again demonstrates that a PTM can dramatically alter fibril morphology. Thus, like A^eK₈₀ studied here, these PTMs seem to primarily exert their influence on α S aggregation through changes in fibril structure, which is sensible given the disordered nature of the α S monomer.

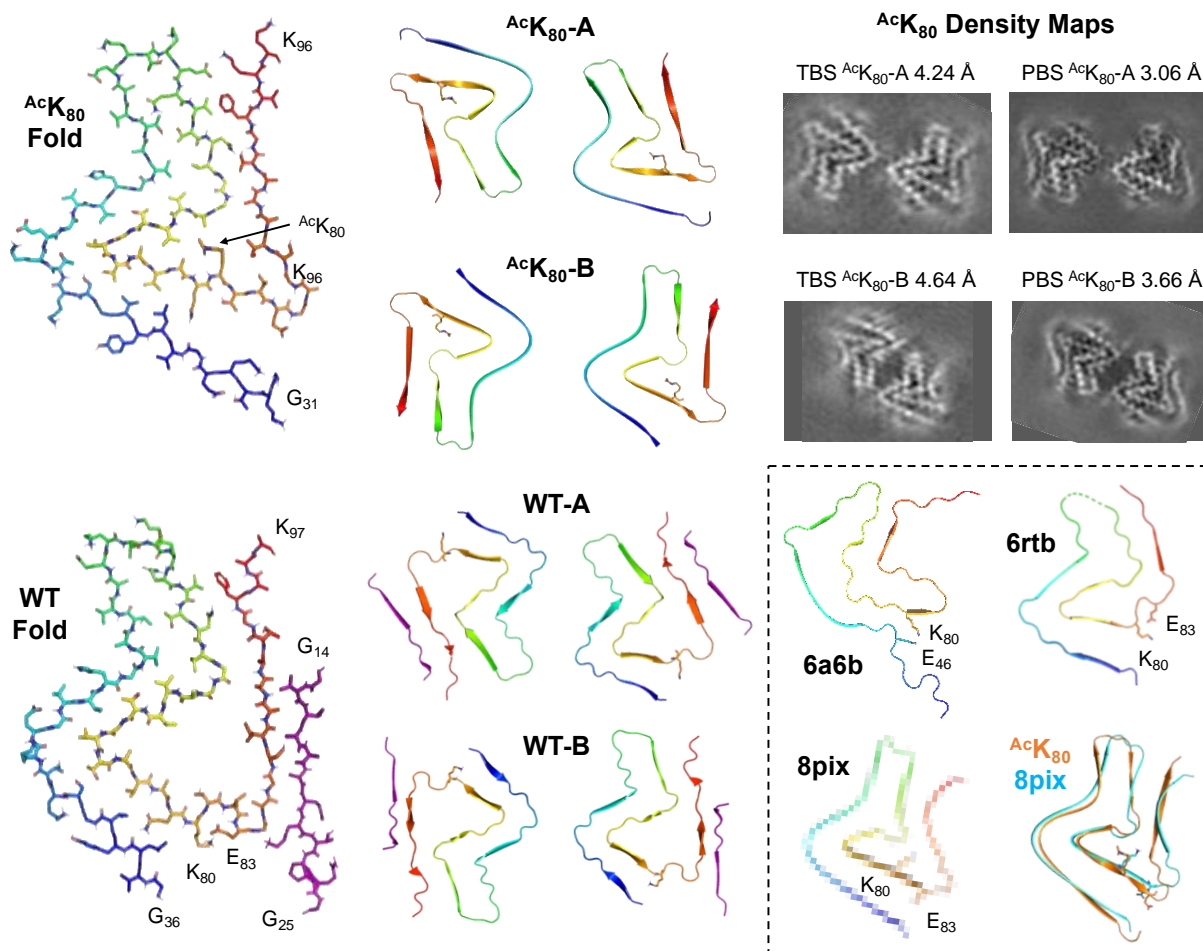


Figure 12. Structural impact of Lys80 acetylation on fibril morphology.

$^{Ac}K_{80}$ Fold and WT Fold show the fold of a single αS molecule in the fibrils, viewed down the fibril axis (from $^{Ac}K_{80}$ -A PBS and WT-A TBS structures). $^{Ac}K_{80}$ -A and $^{Ac}K_{80}$ -B show the two fibril polymorphs, with similar protein folds, but different strand-strand packing (from PBS structures). WT-A and WT-B show the two fibril polymorphs, with similar protein folds, but different strand-strand packing (from TBS structures). $^{Ac}K_{80}$ -A Density Maps show that the same fibril polymorphs were obtained for fibrils made in TBS and PBS. Inset: The interactions of K_{80} are shown in three previously αS fibril polymorphs designated by their PDB IDs.^{95,97,100} The overlay shows the similarity of the $^{Ac}K_{80}$ fold to the 8pix fold.

Deacetylase Site Specificity

Since acetylation of K₁₂, K₄₃ and K₈₀ can reduce α S aggregation, we considered the potential of increasing acetylation at these sites by inhibiting a KDAC. Doing so would require that the KDAC had some specificity for these residues. Using previously published methods,¹⁰¹⁻¹⁰³ we expressed and purified recombinant human HDAC8, a Zn-dependent HDAC known to act on non-histone proteins, including cytosolic targets like tubulin in HeLa cells¹⁰⁴. We treated samples of each of the acetylated α S variants with HDAC8 and monitored deacetylation through a matrix assisted laser desorption ionization (MALDI) MS assay using ¹⁵N-labeled α S as a standard. After 24 h, all of the constructs showed significant levels of deacetylation, but ^{Ac}K₃₄, ^{Ac}K₄₃, ^{Ac}K₄₅, and ^{Ac}K₈₀ retained an average of 44% acetylation, 3-fold greater levels than all other sites (Figure 13). These preliminary results indicate that inhibition of HDAC8 could increase acetylation levels of α S at specific lysine residues shown to retard aggregation *in vitro* and in PFF-seeded neurons.

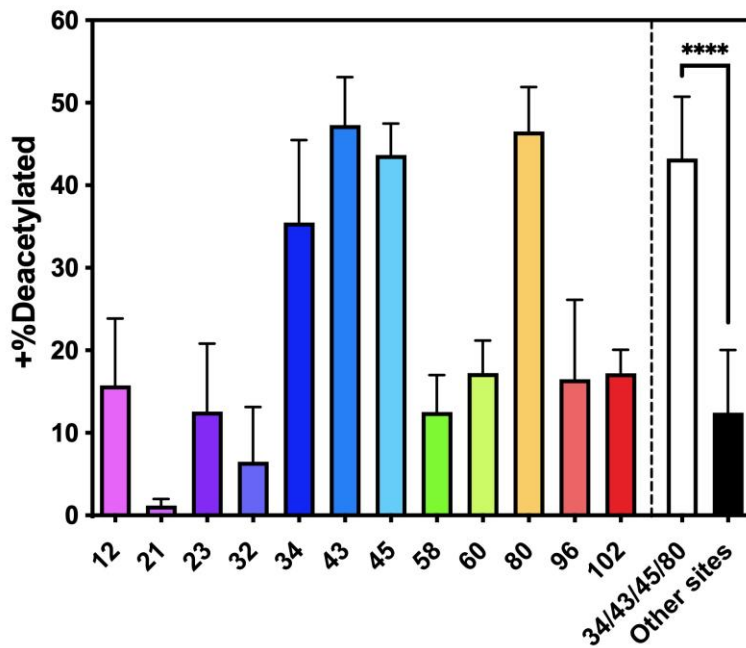


Figure 13. Site-specificity of HDAC activity.

Samples of each of the acetylated α S variants were mixed with HDAC8 and after 24 h, acetylation levels were checked with a MALDI MS assay using ^{15}N -labeled α S as a standard. Mean with SD, R=3

§2.3 Conclusion

In this study, we incorporated ^{13}C site-specifically at all 12 disease-relevant sites through ncAA mutagenesis and characterized the effects of this PTM on the physiological and pathological roles of α S using a variety of techniques. The aggregation assays showed that many of the Lys acetylations observed in patient samples have no effect, demonstrating that there is no non-specific effect on protein solubility or electrostatic interactions, at least for single Lys modifications. At sites 12, 43, and 80, Lys acetylation

significantly slowed the formation of fibrils, both *in vitro* and in cells. Therefore, increasing acetylation at these sites through the use of KAT stimulators or KDAC inhibitors has potential therapeutic benefits. However, acetylation at Lys 12 or 43 perturbs membrane binding moderately, so increasing acetylation at these sites in α S could disrupt its native function in neurotransmitter vesicle trafficking. Thus, Lys 80 seems like the most promising site for targeted acetylation. Indeed, our previous cell-based studies using Gln mimics have shown that Lys 80 modification reduces aggregation.³⁵ Collectively, our results imply that strategies that can specifically enhance acetylation at Lys 80, without affecting Lys 12 or Lys 43, would be the most favorable approach to reduce α S aggregation pathology. Initial structural analysis indicates that the reason for $^{Ac}K_{80}$ effects may be more complex than simply altering monomer conformational ensembles or fibril morphologies. We are currently pursuing additional structural and biophysical characterization of all three acetylated constructs.

It should be noted that it is not clear at this point whether acetylation at these sites is known to be altered in synucleinopathy patients. Taking advantage of our capability to produce authentically acetylated α S, we determined the extent of acetylation within human protein samples by quantitative liquid chromatography MS (LC-MS). The ^{Ac}K α S standards allowed us to correct for changes in trypsinization and ionization efficiency of acetylated peptides, the latter of which turned out to be very low for the $^{Ac}K_{80}$ peptide due to its large size (a result of the missed K_{80} cut site due to acetylation). The level of acetylation was variable – no clear trend was observed between healthy control and patients – nor between patients of different diseases. Nevertheless, the MS data suggest that the 10 and 25% acetylation that we used for aggregation experiments are in the (patho)physiological range. Given the results reported here, it will be valuable to generate antibodies to acetylated peptides for the $^{Ac}K_{12}$, $^{Ac}K_{43}$ and $^{Ac}K_{80}$ epitopes to more easily quantify the levels of acetylation in both soluble and fibrillar α S for immunofluorescence microscopy and Western blotting studies.

More broadly, our experiments show the value of a ncAA mutagenesis approach in systematically investigating a PTM that occurs at many locations in a protein. Since the yields were similar between NCL and ncAA mutagenesis, the ability to scan many sites by simple site-directed mutation to a TAG codon clearly makes ncAA mutagenesis the method of choice for our application. We efficiently scanned 12 different modification sites and fluorescently labeled proteins for binding studies. The ncAA approach was also crucial to generating isotopically labeled, acetylated α S for solution-phase NMR experiments and MS analysis. The isotopic labeling approach could be used in future solid-state NMR experiments to give detailed structural insight into slowed aggregation and distinct fibril morphology.

Our future experiments will include assessing the site-specificity of other KATs and KDACs for sites in α S in a similar fashion to the HDAC8 experiments here, studies enabled by our ability to easily produce ^{Ac}K α S constructs. We can study modulation of HDAC8 and these other enzymes for their ability to specifically increase acetylation at Lys 80 without altering acetylation at Lys 12 or 43. We will also investigate effects on α S aggregation in cellular models in the presence of small molecule modulators of HDAC8 and these other enzymes. Furthermore, combining ncAA mutagenesis and NCL would allow us to study more complex PTM effects in α S, such as the combinatorial effects between multiple lysine acetylations or crosstalk between acetylation and other PTMs.

CHAPTER 3: GLUTAMINE IN PART MIMICS NEUROPROTECTIVE EFFECTS OF THE AUTHENTIC LYSINE ACETYLATION ON ALPHA-SYNUCLEIN

Ming-Hao Lee performed HSQC NMR studies (David Eliezer's group). Evan Yanagawa produced isotopically labeled proteins. Ruwei Zhu (Chao Peng's group) performed aggregation seeding experiments.

Relevant methods: §7.1, §7.3, §7.4, §7.10, §7.11, §7.15

§3.1 Introduction

Alpha-synuclein (α S) is a presynaptic protein that plays a crucial role in synaptic vesicle trafficking and neurotransmitter release. However, its aggregation is a defining feature of synucleinopathies, including Parkinson's Disease. The precise mechanisms driving α S misfolding and aggregation remain incompletely understood, but post-translational modifications (PTMs) have emerged as critical factors influencing its aggregation propensity and toxicity. Among the various PTMs identified on α S, lysine acetylation has gained attention for its potential regulatory role in α S aggregation and toxicity^{35,67,105}. Our previous research investigated the effects of lysine acetylation on α S at disease-relevant sites using genetic code expansion¹⁰⁶. The findings demonstrated that Lys acetylation at specific sites, such as K₁₂, K₄₃, and K₈₀, inhibits α S aggregation *in vitro* and in primary neurons, suggesting a potential neuroprotective role. Among these sites, slightly less membrane binding was observed for K₁₂ or K₄₃ acetylation, while there was no significant effect observed for K₈₀ acetylation, which implicates that K₈₀ is a therapeutic target where promoting its acetylation inhibits α S aggregation without affecting its native role.

Given the challenges of incorporating site-specific, authentic Lys acetylation in living cells or *in vivo*, researchers often employ glutamine (Gln) substitution as a mimic of acetylation due to relatively similar

structure and charge neutralization effect. This approach is widely used in *in vivo* and intracellular overexpression studies to approximate the effects of acetylation in a more experimentally tractable manner. However, the efficacy of Gln as a acetyl lysine (^{Ac}K) mimic is highly context-dependent, as the structural and functional impact of Lys-to-Gln substitutions varies depending on the protein and the specific modification site, likely due to the differences in hydrophobicity and size¹⁰⁷⁻¹¹⁰.

In this study, we aimed to evaluate whether Gln substitution at key Lys acetylation sites in α S can faithfully replicate the neuroprotective effects of authentic acetylation. By comparing the biophysical and functional consequences of Lys acetylation and its Gln mimic at relevant positions, we sought to determine the extent to which Gln can serve as an effective mimic for acetylation in α S. Understanding these relationships will enhance our ability to investigate PTM effects *in vivo* and could inform strategies for modulating α S aggregation in synucleinopathies.

§3.2 Results

Gln mimicking ability in α S *in vitro* aggregation

For acetylation at K₁₂, K₄₃ and K₈₀, we recombinantly expressed Gln mutants and examined if Gln replicates the effects of authentic acetylation. We tested whether Gln mutants replicate the slowed *in vitro* aggregation kinetics at sites 12, 43 and 80, and found that glutamine mutation at site 43 or 80 results in similar effects whereas glutamine mutation at site 12 had an opposite effect (Figure 14). Notably, this effect by K₈₀Q mutation is consistent with a previously published result¹¹¹. We also isolated fibrils and quantified monomers incorporated at the end point of aggregation using a gel-based assay. K₁₂Q at 10% and K₈₀Q at both 10% and 25% resulted in reduction of aggregation, which was not observed with authentic acetylation constructs (Figure 14). Our data indicate that Gln mimics ^{Ac}K in aggregation kinetics

effects at K₄₃ or K₈₀, but not at K₁₂. The positive charge reduction is likely be the cause for the decreased aggregation rate by acetylation at K₄₃ or K₈₀, given that the results are well replicated by Gln mutants.

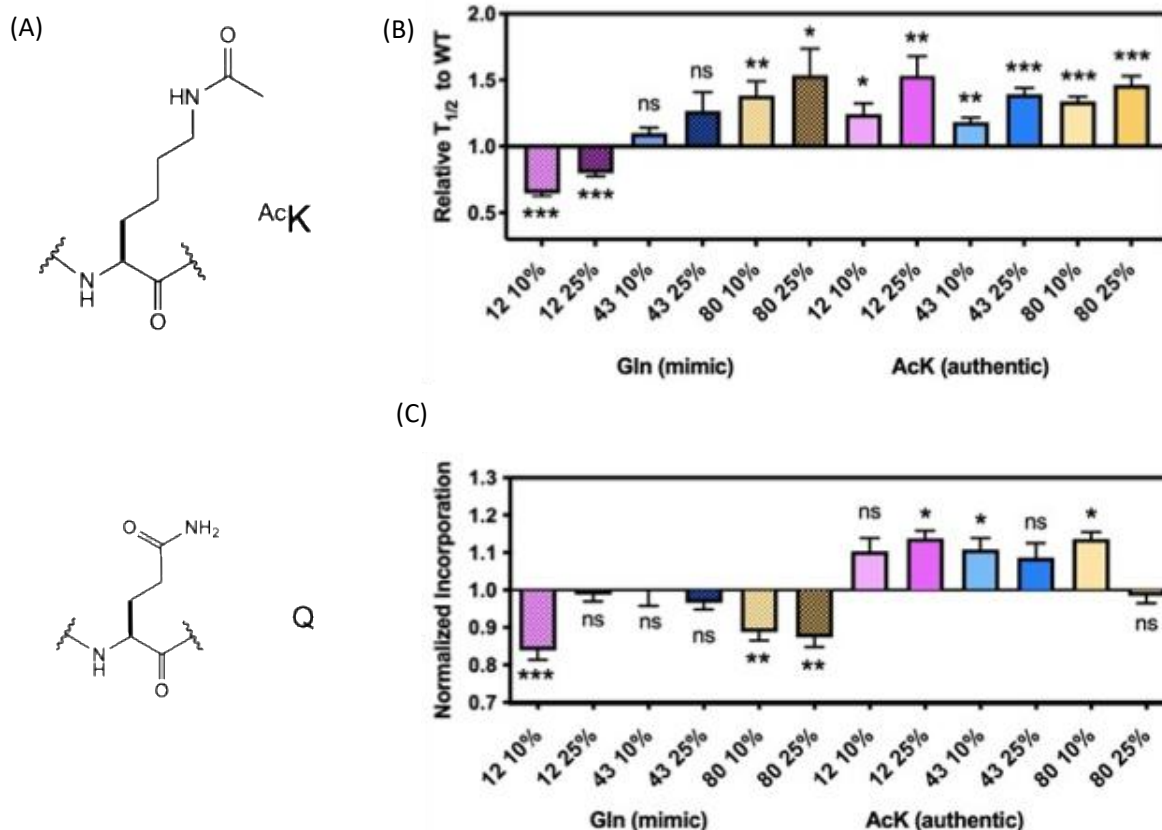


Figure 14. Evaluation of α S-Gln mutants as Lys acetylation mimic in α S aggregation.

(A) Structural comparison of acetylated Lys (^{Ac}K) and Gln (Q), (B) Aggregation kinetics were monitored by fluorescence intensity change of ThT. Time it takes to reach 50% fibrilization ($T_{1/2}$) for each condition was normalized to that of WT. Seeded aggregation was performed with α S monomers where mimic α S was mixed with α S WT at 25%:75% ratio. SEM, R=6. Authentic Lys acetylation data were adapted from Chapter 2 for comparison. (C) Monomers incorporated into fibrils were quantified by SDS-PAGE gels and normalized to WT values. Mean with standard error, R=6.

Seeded aggregation in mammalian cells

Following these *in vitro* aggregation results, we investigated the effects of Gln acetylation mimics on pathological aggregation seeding in a mammalian cell model. We overexpressed α S – Q₁₂, Q₄₃ or Q₈₀ in HEK cells and seeded its aggregation by transduction of α S PFFs. Pathological aggregates formed were quantified by immunostaining with antibodies against α S with phosphorylation at S₁₂₉, following previously published protocols³⁵. We observed reduced aggregates with Q₄₃ and Q₈₀, but not with Q₁₂ (Figure 15). These data are consistent with our *in vitro* aggregation experiments, indicating that acetylation at K₄₃ and K₈₀ disrupt fibril formation. Since the Q₁₂ mutant failed to mimic ^{Ac}K₁₂ behavior *in vitro*, we are cautious about interpreting the lack of cellular effects.

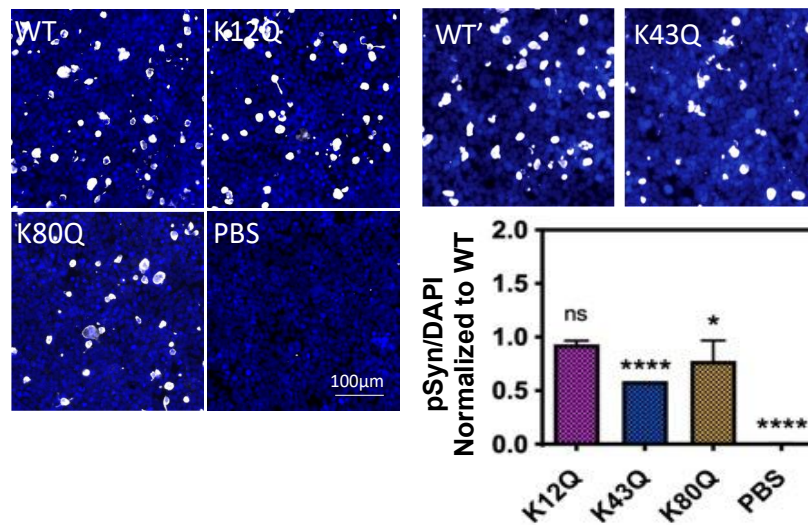


Figure 15. Effects of glutamine mutation on aggregation seeding in HEK cells.

Pathological aggregates were quantified by immunostaining with antibodies against α S with phosphorylation at Ser₁₂₉. Mean with standard error, R= 12 (K₁₂Q), 15 (K₄₃Q), 12 (K₈₀Q) or 7 (PBS). K₁₂Q and K₈₀Q data were collected separately from K₄₃Q data and each mutant was normalized to a paired WT trial. The K₄₃Q mutant was previously reported in Zhang et al.³⁵

Structural characterization of α S-Gln mimic monomers and fibrils

To gain information on the structural impact of Gln acetylation mimics at these sites on monomer conformation and give insights to effects on aggregation, we acquired proton-nitrogen heteronuclear single quantum coherence ($^1\text{H}, ^{15}\text{N}$ – HSQC) NMR spectra for Q₁₂, Q₄₃ or Q₈₀ and compared them to HSQC spectra for WT and authentic acetyl Lys α S. We expressed the α S Gln mutants in M9 minimal media containing ^{15}N -labeled ammonium chloride. Comparing the HSQC spectra for α S-WT and α S Gln mutants (Figure 16), peak shifts were observed mostly in signals from residues surrounding the mutation site, suggesting that the structural changes are local for the most part and there are no major impacts on monomer structure. These changes are somewhat aligned with our observations with corresponding, authentically acetylated constructs, especially for Lys acetylation at K₈₀, while in the N-terminal region Gln mutants seem to result in more chemical shifts.

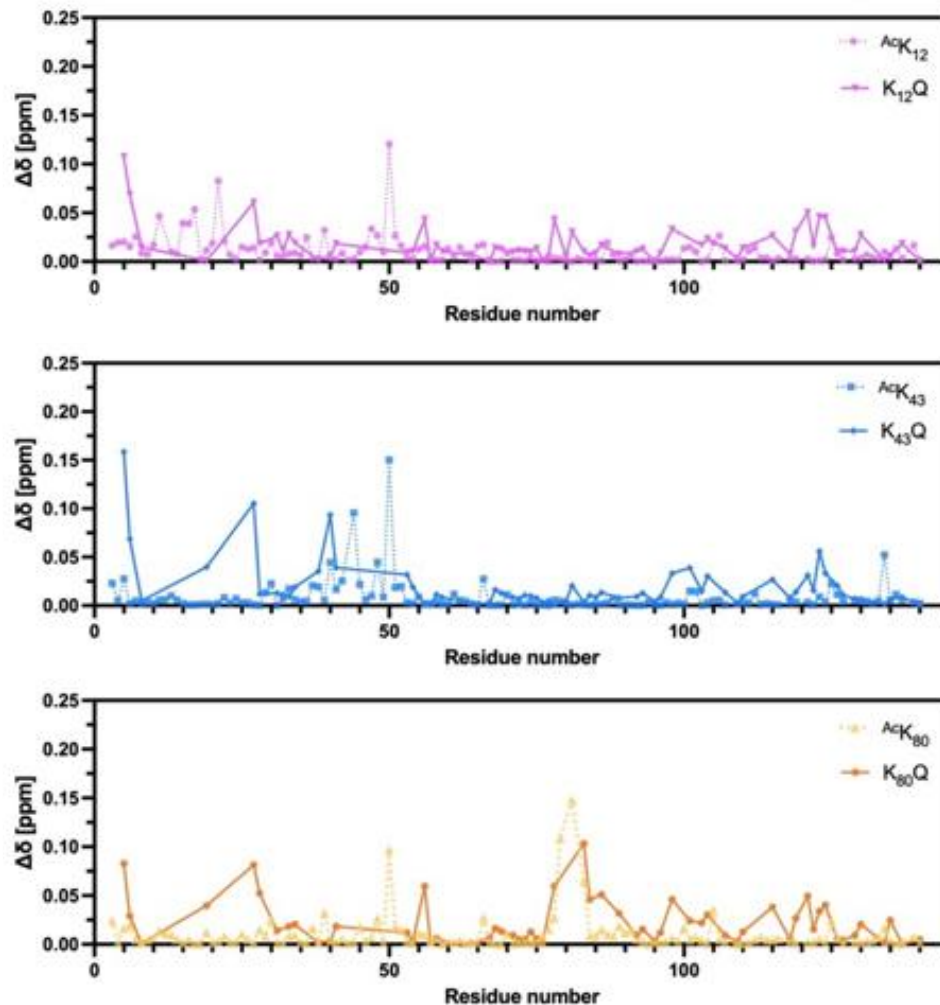


Figure 16. Effects of Gln mimics on α S conformation.

Chemical shift perturbation for each residue calculated from ^1H - ^{15}N HSQC spectra collected with ^{15}N -labeled α S variants, compared to α S WT.

To get preliminary insights on fibril structure effects, we performed transmission electron microscopy (TEM) imaging on fibrils formed from α S-Gln acetylation mimics (α S-Q₁₂, Q₄₃ or Q₈₀), mixed with α S WT, at 25% of the total monomer concentration and compared to the TEM results that authentic

acetylation afforded (Figure 17). Interestingly, we did not observe mixed morphology for PFFs prepared with α S-Q₁₂, unlike PFFs prepared with α S-^{Ac}K₁₂. This may be related to our observation that the Gln mutation did not reproduce the kinetic effects of the authentic ^{Ac}K at position 12, however more in-depth structural characterization would be necessary to understand molecular details of α S-Q₁₂ as a poor mimic in α S aggregation.

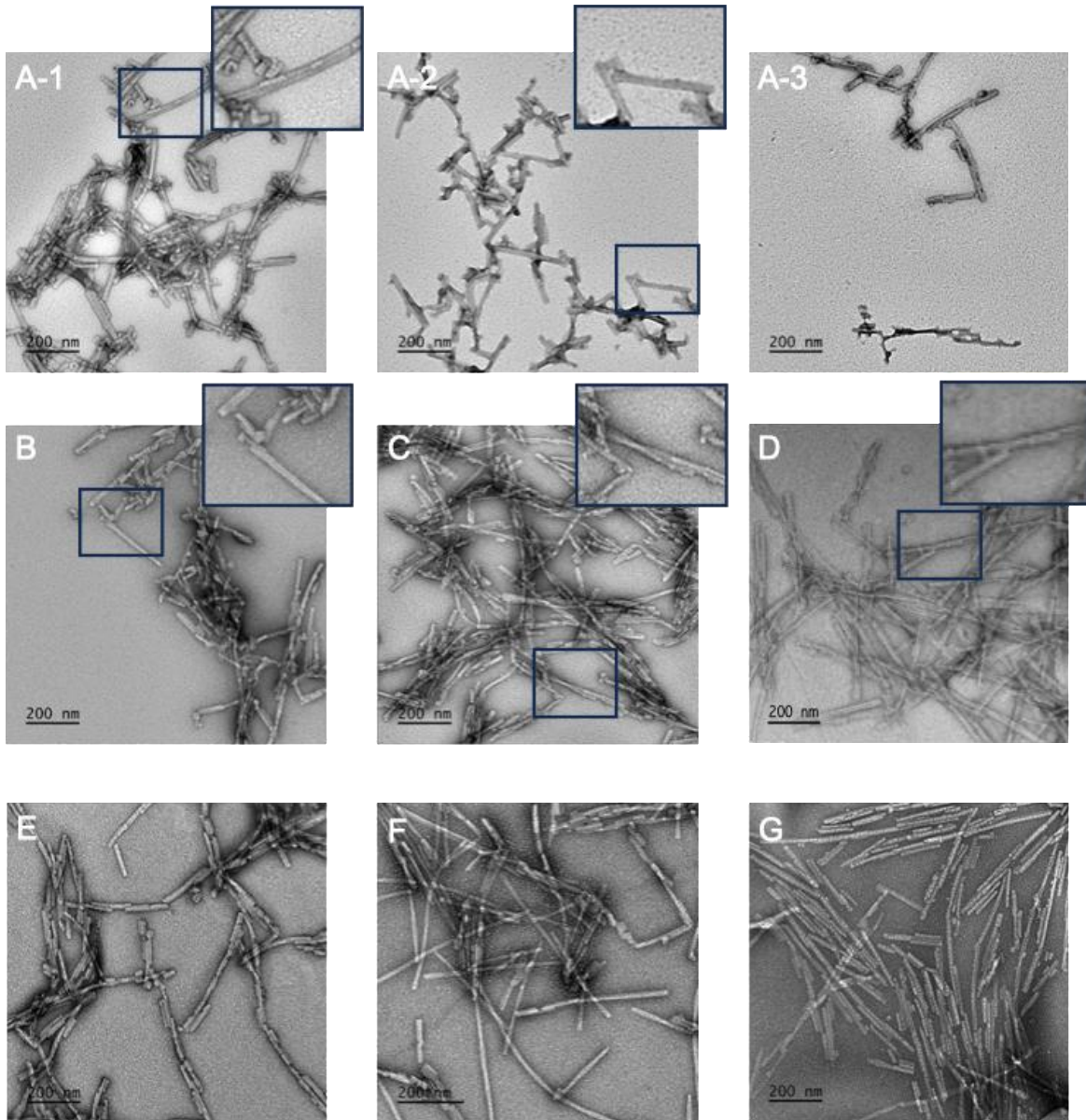


Figure 17. Transmission Electron Microscopy images of α S Lys acetylation constructs and α S Gln mutants.

(A-1, A-2, A-3) α S-^{Ac}K₁₂ (B) α S-^{Ac}K₄₃ (C) α S-^{Ac}K₈₀ (D) α S-WT (E) α S-Q₁₂ (F) α S-Q₄₃ (G) α S-Q₈₀

Gln mimicry in lipid-bound α S

We then asked if Gln replicates the effects of authentic acetylation on native roles of α S. Gln mutation at site 43 did not change helicity on sodium dodecyl sulfate (SDS) micelles in circular dichroism (CD) experiments, unlike authentic acetylation for which we observed reduction in helicity (Figure 18). This difference could be due to reduced side-chain length and hydrophobicity of Gln compared to authentic Lys acetylation.

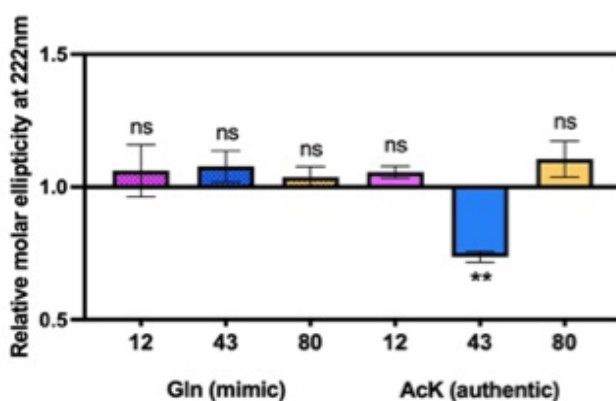


Figure 18. Effects of Gln mimics on helicity of SDS micelle-bound α S.

To understand the effects of Gln mutational mimic in more physiological context, we performed HSQC experiments in the presence of small, unilamellar vesicles (SUVs) that are composed of 60:25:15 1,2-dioleoyl-sn-glycero-3-phosphocholine/1,2-dioleoyl-sn-glycero-3-phosphatidylethanolamine/1,2-dioleoyl-sn-glycero-3-phospho-L-serine (DOPC/DOPE/DOPS). The NMR peak chemical shifts were very similar to spectra for free α S. α S signal is reduced when bound to vesicles, due to slowly tumbling lipids on vesicles (seen in α S residues 1-100). The loss of the signal compared to corresponding vesicle-free α S can therefore be used to determine how much vesicle binding is occurring. We observed that Gln mutational

mimics had a very similar impact on vesicle binding (Figure 19), compared to authentic Lys acetylation - Q₁₂ and Q₄₃ led to ~80% reduction of intensity, whereas Q₈₀ and WT led to ~60% reduction of intensity. This suggests that Q₁₂ and Q₄₃ reduce vesicle binding but not Q₈₀, and this agrees very well with our observations with authentic acetylation at corresponding sites¹⁰⁶. More quantitative methods, such as fluorescence correlation spectroscopy, would be needed to quantify binding affinity.

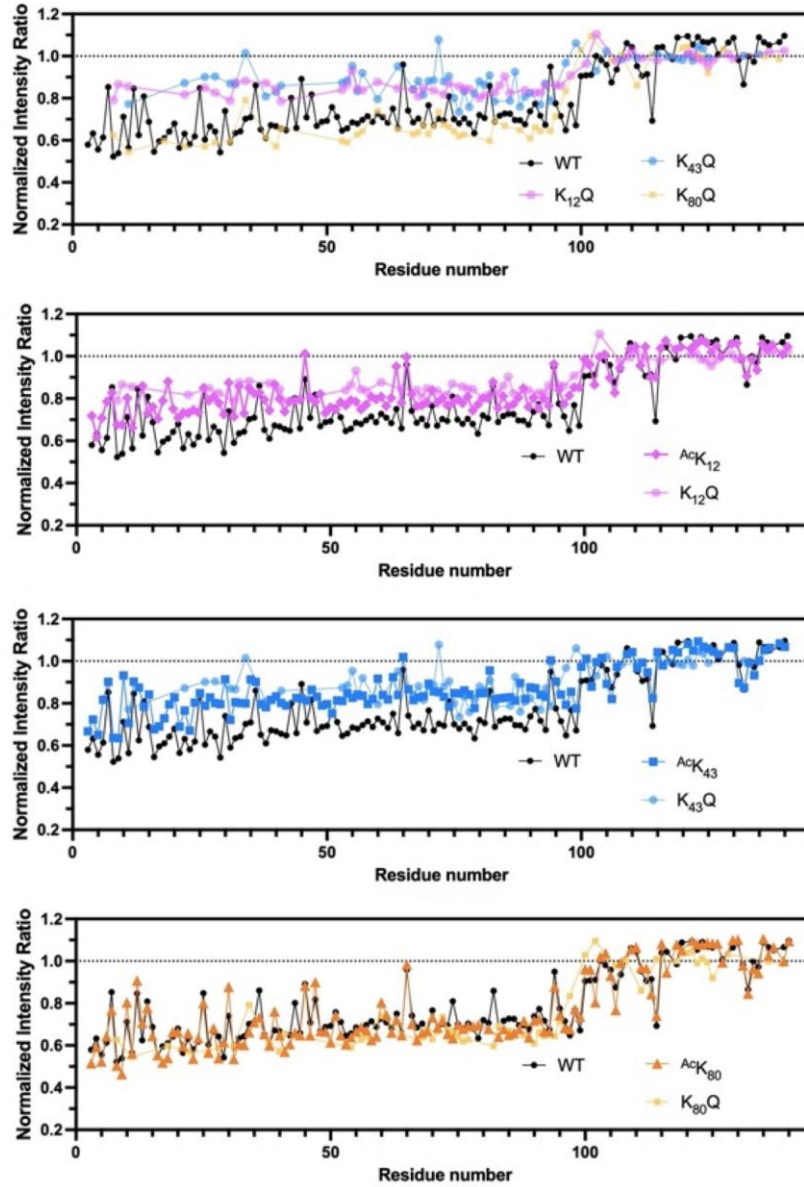


Figure 19. Effects of Gln mimics on vesicle binding.

NMR intensity ratio for each residue calculated from ^1H - ^{15}N HSQC spectra collected with ^{15}N -labeled αS variants in the presence or absence of SUVs, normalized by the average ratio for residues 101-140.

§3.3 Conclusion

In this study, we systematically evaluated the ability of Lys-to-Gln substitutions to mimic Lys acetylation at previously identified three key sites in α S: K₁₂, K₄₃, and K₈₀. Through a combination of *in vitro* aggregation assays, structural characterization, and lipid-binding studies, we uncovered site-specific differences in the fidelity of Gln as an acetylation mimic.

Our findings demonstrate that for K₄₃ and K₈₀, Gln effectively replicates the *in vitro* aggregation-inhibitory effects of authentic lysine acetylation. Similar effects were also observed in a mammalian cell model of fibril seeding. This suggests that the primary mechanism behind the reduced aggregation rate at these sites is neutralization of lysine's positive charge. However, at K₁₂, Gln did not reproduce the effects of acetyl lysine, highlighting the context dependence of ^{Ac}K mimicry. This discrepancy be due to differences in steric properties, hydrogen bonding capacity, or hydrophobicity.

Low resolution structural analyses further revealed that while ^{Ac}K₁₂ led to heterogenous fibril morphology, Gln substitution at the same position resulted in fibrils with uniform structures. This finding emphasizes the need for caution when using Gln as a mimic in structural studies. Moreover, while Gln and ^{Ac}K had similar effects on α S binding to vesicles, secondary structure analyses on micelle-bound α S suggested that ^{Ac}K, but not Gln, reduced helical content at K₄₃, implicating potential site-dependent functional differences.

Taken together, our study highlights the importance of validating Lys-to-Gln substitutions as acetylation mimics in a site-specific manner. Our findings provide valuable insights for future studies employing Gln mutational mimics to investigate α S acetylation in cellular and *in vivo* settings or multiple Lys

acetylation. It is suggested that alternative approaches, such as genetic code expansion, enzymatic acetylation, chemical protein synthesis or closer mimics may be necessary for studying certain acetylation sites with high accuracy.

CHAPTER 4: ADDITIONAL TOOLS TO STUDY LYSINE ACETYLATION OF ALPHA-SYNUCLEIN

Relevant methods: §7.7, §7.8, §7.11

§4.1 Introduction

Lysine acetylation is a key post-translational modification (PTM) that regulates protein function, stability, and interactions. In α -synuclein (α S), acetylation at specific lysine residues has been implicated in modulating its aggregation, membrane binding, and potential neurotoxicity.

While site-specific and homogenous incorporation of authentic acetylation has been achieved using chemical synthesis or genetic code expansion (Chapter 2), these approaches can be technically challenging and are often limited to *in vitro* applications and single sites within the protein. Lys-to-Gln mutations can be used to mimic Lys acetylation in such cases, however we have shown that it is not always a good mimic (Chapter 3), as has been previously reported more generally¹¹². To expand the toolkit for studying lysine acetylation, researchers have explored alternative chemical strategies that offer distinct advantages in stability and functional studies¹¹³. However, these methods differ significantly in their ease of incorporation and practical applications.

Among these approaches, thioether acetylation mimics (^{Ac}K*), generated via thiol-ene chemistry, provide a relatively straightforward way to introduce stable acetylation analogs. This method involves modifying cysteine residues to create thioether-linked acetyl groups, which very closely mimic the physical properties of authentic acetylation while offering increased resistance to enzymatic deacetylation¹¹⁴. We

here used thioether acetylation mimics to probe the structural and functional consequences of lysine acetylation in α S, particularly in protein conformation and aggregation. Their relatively simple synthetic accessibility has a potential as a practical tool for studying acetylation effects when multiple modifications are necessary or for applications that require significant quantities of materials.

In contrast, a thioamide analog of acetyllysine (^{AcS}K) presents a greater synthetic challenge. Unlike main-chain thioamides which typically require chemical protein synthesis¹¹⁵, ^{AcS}K could also be introduced using genetic code expansion with an engineered aminoacyl-tRNA synthetase – however, incorporation efficiency is typically worse than acetyllysine¹¹⁶. Despite this difficulty, thioamide acetyllysine offers distinct advantages, including enhanced stability against enzymatic deacetylation and potential utility as a spectroscopic probe due to its fluorescence quenching properties¹¹⁷.

In this chapter, I briefly describe the efforts we have made in utilizing each of these strategies for studying lysine acetylation and how we plan to continue further investigations.

§4.2 Results

Synthesis of α S thioether acetylation mimics

The thiol-ene reaction is a radical-mediated addition of a thiol to an alkene that gives a thioether, which has been used to site-specifically incorporate acetylation mimics at cysteine positions in proteins, although it has not been previously used with α S (Figure 20A).¹¹⁴

Cysteine mutants at desired positions were expressed following site-directed mutagenesis and purified (expression yield of cysteine mutants: 5.34 - 13.2 mg per L of *E. coli* culture, Figure 20B-C, Table 1). Thiol-ene reactions were performed in pH 4 acetate buffer by reacting the mutant with *N*-vinylacetamide in the presence of a radical initiator under 365 nm light. Methionine was added as a scavenger for singlet

oxygen, which may be generated during the photo reaction. The reaction proceeded quantitatively after 30 minutes, with minimal oxidation. The products were purified on RP-HPLC and were exchanged into buffer using spin concentrators. Isolated yields of thioether mimics calculated upon buffer exchanging were 14%-76% (Figure 20D-E, Table 1). Some of the low yields were due to dimer formation of the cysteine mutant. Further addition of reduced glutathione would be the best solution to this problem, as it is already used for the reaction and TCEP has been documented to cause desulfurization, converting Cys to Ala¹¹⁴.

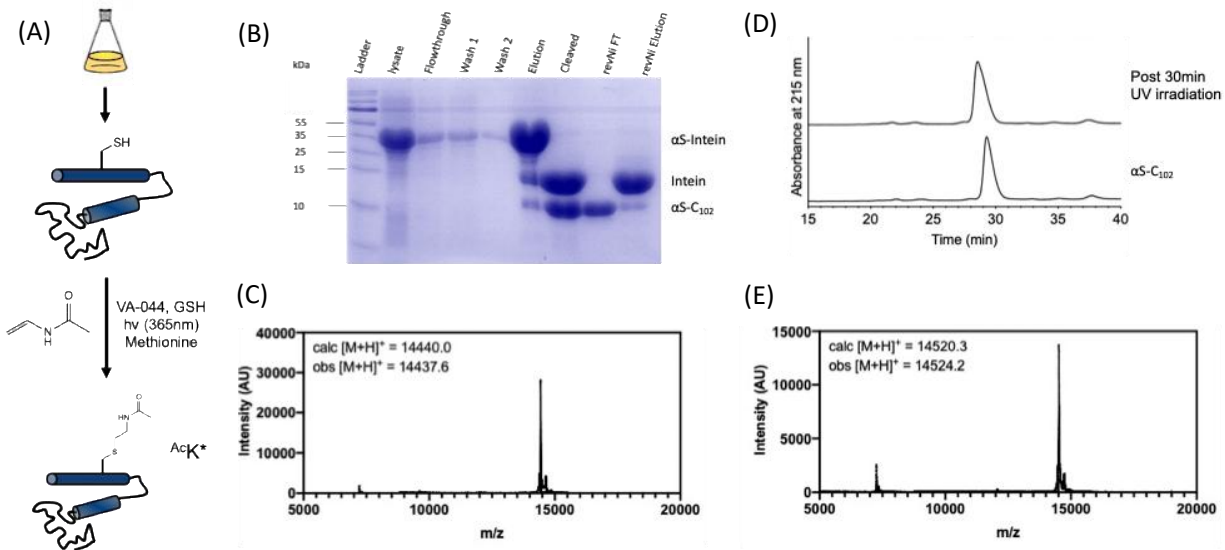


Figure 20. Synthesis of thioether Lys acetylation mimic via thiol-ene reaction

$\alpha\text{S}^{-\text{Ac}}\text{K}^*_{102}$ is shown for representation. (A) Synthesis schematics (B) SDS-PAGE gel for purification of $\alpha\text{S}\text{-C}_{102}$ (C) MALDI spectra for purified Cys mutant $\alpha\text{S}\text{-C}_{102}$ (D) Analytical HPLC trace of $\alpha\text{S}\text{-C}_{102}$ (starting material and crude reaction after 30-min, thiol-ene reaction (35-45%B over 30 mins) (E) MALDI spectra of purified thioether Lys acetylation mimic, $\alpha\text{S}^{-\text{Ac}}\text{K}^*_{102}$.

	Cys mutant expression yield	Final product (mg)	Isolated yield
AcK* ₁₂	9.95 mg/L	1.18	39%
AcK* ₂₁	5.34 mg/L	1.54	29%
AcK* ₂₃	5.79 mg/L	0.40	14%
AcK* ₃₂	9.32 mg/L	3.50	75%
AcK* ₃₄	12.8 mg/L	2.59	52%
AcK* ₄₃	9.01 mg/L	3.43	76%
AcK* ₄₅	9.46 mg/L	2.06	43%
AcK* ₅₈	8.60 mg/L	1.49	22%
AcK* ₆₀	9.94 mg/L	3.25	61%
AcK* ₈₀	11.5 mg/L	3.23	53%
AcK* ₉₆	5.86 mg/L	1.45	43%
AcK* ₁₀₂	13.2 mg/L	4.19	53%

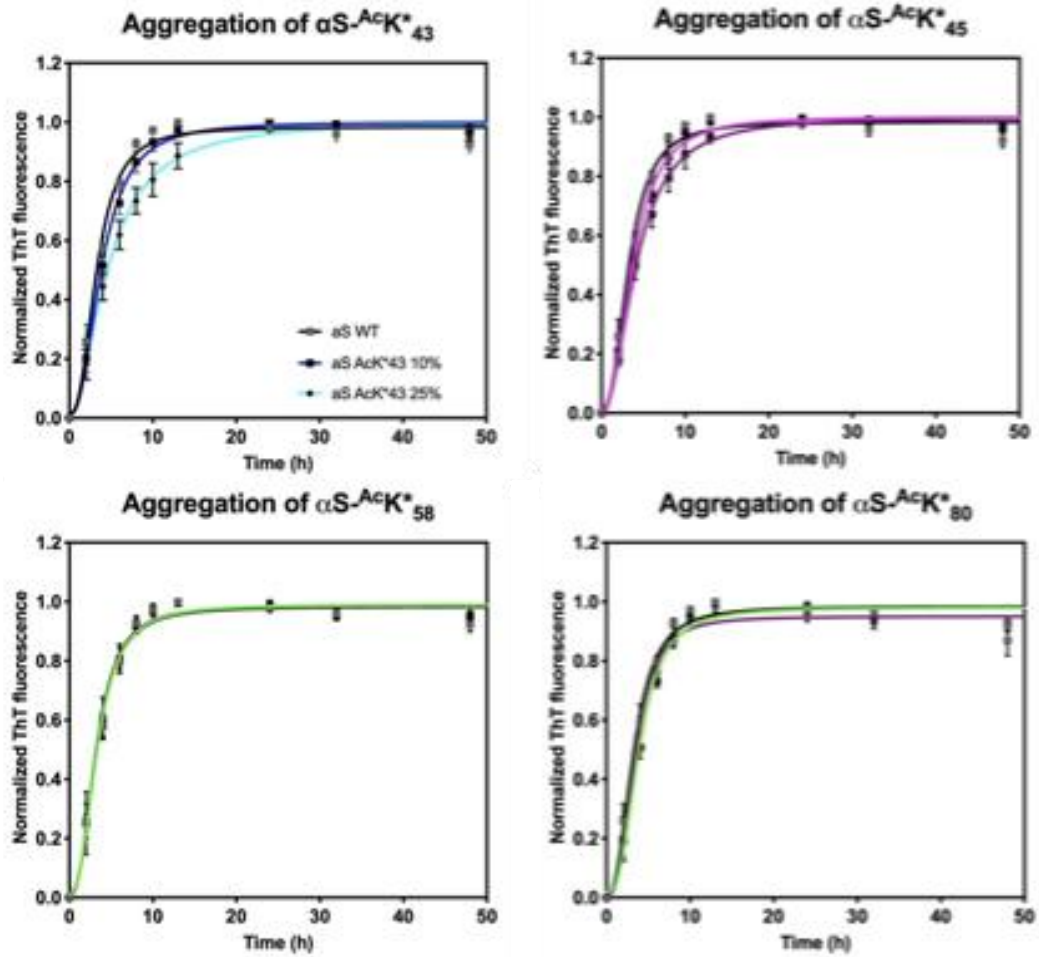
Table 1. Yield for production of α S thioether Lys acetylation mimic at each acetylation site.

In vitro aggregation kinetics shows partial success in mimicking

With all the thioether Lys acetylation mimics in hand, we investigated the effects of thioether acetylation mimics on *in vitro* aggregation kinetics for sites 43, 45, 58 and 80. The relative increase of thioflavin T (ThT) fluorescence was used to track aggregation, where $T_{1/2}$ refers to the time to reach half maximal fluorescence. We then compared these results to our observations with authentic acetylation (Chapter 2).

We observed very similar slowing effect for site 43, while in other sites limited success in mimicking the effects (Figure 21). It is notable to mention that these thioether mimics may be more susceptible to oxidation compared to authentic Lys acetylation, which could affect aggregation. More investigations are necessary to elucidate the nature of oxidation during aggregation and effects that arise from it.

(A)



(B)

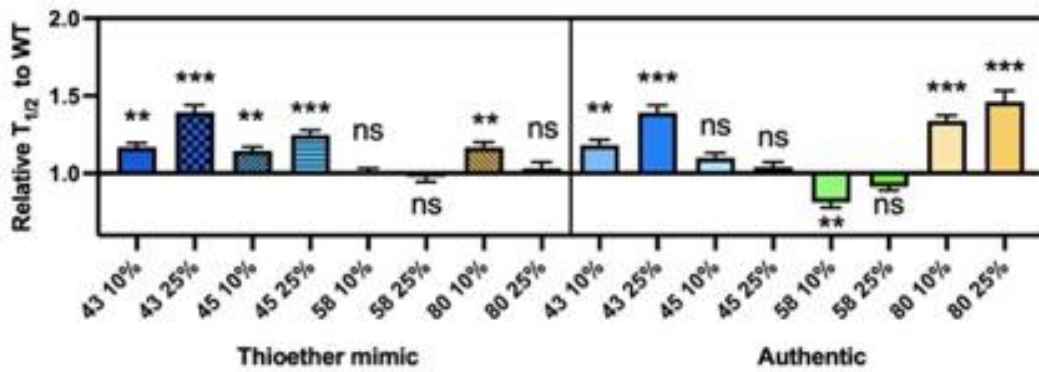


Figure 21. Aggregation kinetics of thioether Lys acetylation mimics.

(A) Aggregation kinetics tracked by change in ThT fluorescence. (B) Relative $T_{1/2}$ values to corresponding WT control, compared between thioether mimics and authentically acetylated constructs.

Monomer local conformation may be different for thiol-ene at site 80

To gain information on the structural impact of the thioether Lys acetylation mimic on monomer conformation and give insights to differential effects on aggregation, we acquired proton-nitrogen heteronuclear single quantum coherence spectra ($^1\text{H}, ^{15}\text{N}$ – HSQC) for $^{\text{Ac}}\text{K}^*_{80}$ and compared them to that for wild type (WT) and authentic Lys acetylation. To access ^{15}N -labeled αS , we expressed the αS Cys mutants in M9 minimal media containing ^{15}N -labeled ammonium chloride, followed by thiol-ene reaction with non-isotopically labeled *N*-vinylacetamide.

The HSQC experiment was done as a scouting experiment – only the shifted peaks were assigned, using a preceding work as a reference⁸⁷. A major chemical shift was observed only for T81, suggesting a modest local conformational change (Figure 22). It is notable, however, that the direction of the T81 chemical shift perturbation is opposite from the case with the authentically acetylated αS . This, in addition to the absence of an E83 peak shift implies a distinct local conformation around Lys 80 between $^{\text{Ac}}\text{K}_{80}$ and $^{\text{Ac}}\text{K}^*_{80}$.

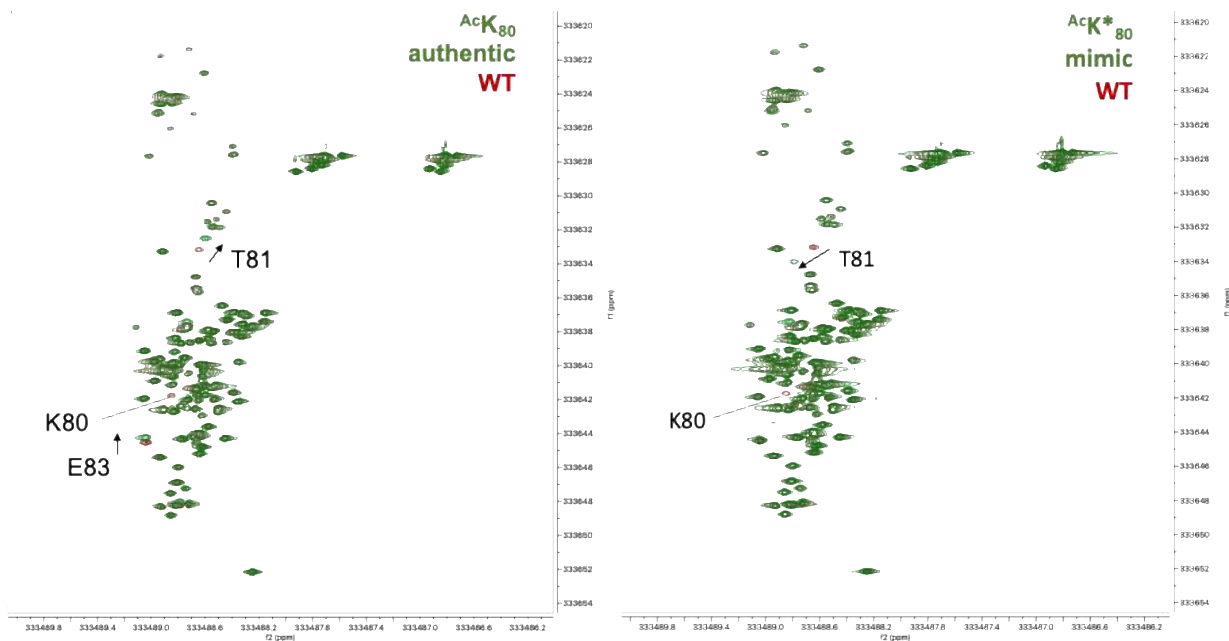
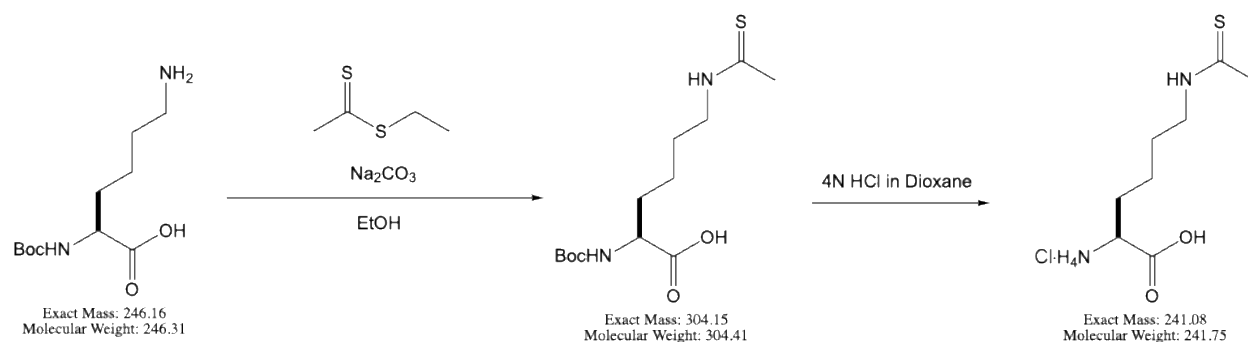


Figure 22. Monomer conformation of authentic Lys80 acetylation and thioether mimic.

$^1\text{H}, ^{15}\text{N}$ – HSQC spectra collected in-house for $\alpha\text{S}^{\text{-AcK}_{80}}$ and $\alpha\text{S}^{\text{-AcK}^*_{80}}$, each overlaid with corresponding WT spectra.

Synthesis of side-chain thioamide acetyl Lys

Synthesis of thioacetyl Lys $^{\text{AcS}}\text{K}$ was performed in order to evaluate its genetic incorporation either in mammalian cells or *E. coli*. The first step of the synthesis followed our previously published method¹¹⁸. The second step was done differently, where deprotection of the *tert*-butoxycarbonyl (Boc) group was done in HCl, not in trifluoroacetic acid (TFA), to give the final product as a milder acidic salt (Scheme 1). The yield for step 1 after workup was 60% (1.1 g). Yield for step 2 and product characterizations are currently underway.



Scheme 1. Reaction scheme for the synthesis of thioamide analog of acetyl Lys.

§4.3 Conclusion

We described above our efforts to utilize two close mimics of Lys acetylation, thioether acetylation mimics and side-chain thioamide acetylLys, the former particularly in the context of α S research. The hope is that by integrating these chemical approaches with existing methods, researchers can gain deeper insights into the regulatory role of acetylation in α S function and pathology.

Generation of thioether mimics through Cys mutant expression and thiol-ene reaction was successful, though it must be noted that residual oxidation (+16 Da) was always observed to varying extents, and this needs to be improved. We have not determined if this oxidation was Met oxidation or on the thioether, but it is notable that addition of free Met in the reaction significantly helped with this. *In vitro* aggregation tests of the mimicking abilities of these constructs gave mixed results – these were valuable mimics at K₄₃ but not at K₈₀. Our HSQC data suggests that the mimic ^{Ac}K*₈₀ has slightly different local conformation compared to authentic ^{Ac}K₈₀. This could also be due to differentially oxidized proteins during aggregation, and this is another area that needs further investigation – how much oxidation occurs in the course of

aggregation for each construct, whether the results are significantly affected when oxidation is prevented – i.e. in reducing environment or with additives like EDTA.

For side-chain thioamide ^{AcS}K, the next step is for our collaborators to each evaluate its incorporation by GCE, respectively in mammalian cells or in *E. coli*. Upon success in their GCE systems, thioamide acetyllysine will be a valuable and accessible tool to study Lys acetylation, especially when deacetylation half-life is important or when its fluorescence quenching could be used as a probe. While maintaining a structure highly similar to authentic acetylation, thioamides may also introduce subtle differences in hydrogen bonding or electronic properties that may cause different aggregation propensities, and this needs to be evaluated in a site- and context-dependent manner. However, their potential for additional reactivity remains to be fully explored.

CHAPTER 5: GENETIC CODE EXPANSION AND ENZYMATIC MODIFICATIONS AS ACCESSIBLE METHODS FOR STUDYING SITE-SPECIFIC POST-TRANSLATIONAL MODIFICATIONS OF ALPHA-SYNUCLEIN

Ibrahim Saleh and Bernard Abkah performed FCS, with assists from Jennifer Ramirez and Marie Shimogawa. Ibrahim Saleh helped with production of isotopically label protein. Ming-Hao Li performed HSQC NMR studies (David Eliezer's group). Wai Kit Chia performed radioligand competition binding assays.

Relevant methods: §7.5, §7.6, §7.12, §7.13, §7.14

§5.1 Introduction

Alpha-synuclein (α S) is classified as intrinsically disordered proteins (IDPs) that play crucial roles in cellular functions and are central to the pathology of numerous neurodegenerative diseases. In healthy contexts, α S exists primarily in the presynaptic terminals of neurons and its native roles are thought to be in vesicle trafficking and regulating neurotransmission^{57,58}. In pathological contexts, its aggregates are found from patients of synucleinopathies, including Parkinson's Disease and multiple system atrophy (MSA). Critical to the functionality and dysregulation of IDPs are post-translational modifications (PTMs), which can influence interactions with other biomolecules and formation of pathological assemblies. Understanding the precise impact of site-specific PTMs on IDPs such as α S and tau is crucial for elucidating their roles in health and disease.

Traditionally, the study of site-specific PTMs in proteins has largely been approached through various methods including site-specific mutagenesis, chemical or semi- synthesis, and enzymatic reactions, each with inherent limitations. While mutagenesis allows for facile introduction of mutation-

based mimics of PTMs, these alterations do not always recapitulate the chemical and structural nuances of naturally occurring PTMs⁴⁹. On the other hand, the use of peptide ligation techniques, although precise, often require sophisticated synthetic expertise and can be resource intensive⁶². Enzymatic methods, although limited by the availability of specific, efficient enzymes, have proven successful in certain instances where site-specificity and yield satisfy the experimental needs^{49,56,119}. We highlight cases involving α S where enzymatic methods have effectively introduced PTMs, exemplifying successful outcomes from these "lucky" scenarios.

However, for broader applicability and ease of use, genetic code expansion (GCE) is a robust alternative¹²⁰. This approach allows the direct, site-specific incorporation of non-canonical amino acids that correspond to natural PTMs with little more effort than conventional mutagenesis, expanding the accessibility of precise PTM studies to laboratories with limited access to specialized chemical synthesis setup. This technique enables researchers to investigate the effects of PTMs more directly and comprehensively.

In this chapter, we showcase the use of either enzymatic modifications or GCE to study three PTM targets: phosphorylation of tyrosine 39 in α S (pY₃₉, Enzymatic), phosphorylation of serine 87 in α S (pS₈₇, GCE and phosphorylation of serine 129 in α S (pS₁₂₉, Enzymatic). We then characterize how these PTMs affect radioligand binding, protein conformation, vesicle binding, phase transition of these proteins - factors critical in their native, pathological, or diagnostic contexts. By integrating successful enzymatic modifications with GCE, we aim to provide guidance for biochemists to achieve a nuanced understanding of PTM impacts on IDPs.

§5.2 Results

In this work, we focus on PTM targets that could be introduced only by enzymatic modifications or GCE, which are less labor intensive and more accessible to biochemists that do not necessarily have peptide chemistry setup or expertise. We describe three examples: i) phosphorylation of serine 87, or pS₈₇, in α S (GCE); ii) phosphorylation of tyrosine 39, or pY₃₉, in α S (Enzymatic); iii) phosphorylation of serine 129, or pS₁₂₉, in α S (Enzymatic).

Production of PTM-modified proteins by GCE

Using methods similar to those that we have previously described for recombinantly expressing α S with ncAAs in *E. coli*, one can produce α S with phosphorylation of serine 87 (i), α S -pS₈₇) as shown in Figure 23. We use two plasmids, one encoding the aaRS for phosphoserine or ϵ -acetyllysine and its cognate tRNA, the other encoding a protein of interest with a TAG stop codon at the site of ncAA incorporation. Our protein of interest bears a C-terminal traceless intein-His₆ tag which not only allows for isolation of full-length products from species truncated at the TAG codon but could also be cleaved off with thiols during purification and provide scarless protein products. For pSer GCE, *E. coli* cells with a Δ serB phosphatase genomic knockout (BL21 Δ serB or B95 Δ serB cells developed by Cooley et al.¹²¹, the latter lacks release factor 1) was used so that pSer is intracellularly concentrated and readily used for GCE without the need to exogenously add pSer. Following affinity purification, the product was separated from impurities on HPLC, which include de-phosphorylation (-80 Da), Gln misincorporation, and an unknown +72 Da species (Figure 24), then buffer exchanged. We found BL21 Δ serB cells to be more high yielding than B95 Δ serB cells, due to the higher level of protein expression and slightly lower fraction of impurities. As a potential method to determine the homogeneity of phosphorylated samples, we performed Phos-tag gel electrophoresis, where the phosphate-binding ligand usually slows the mobility of phosphorylated proteins¹²². We observed a mobility shift of α S -pS₈₇ - the extent of the shift seems to depend slightly on buffer components (Figure 23, see marked bands in “Ni cleanup” and “HPLC

purified”). We observed nearly quantitative isolation of phosphorylated product from unphosphorylated species upon HPLC (Figure 24: HPLC, Figure 26: MALDI-MS of HPLC-purified product). It is notable, however, that +72 Da species may not result in mobility shift on this gel.

To demonstrate the power of the GCE method over NCL-based incorporation, we additionally prepared following α S - pS₈₇ constructs: first, a Cys mutant α S -pS₈₇ labeled with a fluorophore maleimide for FCS, which previously yielded too low by NCL in our hands to obtain a full vesicle binding curve¹²³; second, ¹⁵N isotopic labeling of α S - pS₈₇. The latter followed the strategies introduced by Cooley et al.¹²⁴ – it was necessary to start the culture with rich media and then switch to a minimal media so that Ser auxotroph *E. coli* Δ serB cells are kept alive while minimizing ¹⁴N incorporation. The proteins were expressed at lower temperature but for longer to minimize the activity of endogenous phosphatases and a yield loss. HPLC was able to purify out phosphorylated α S from de-phosphorylated side products, which shows that a larger fraction of α S was de-phosphorylated in the ¹⁵N isotopic labeling protocol (Figure 24: HPLC, Figure 25: MALDI-MS of HPLC-purified product).

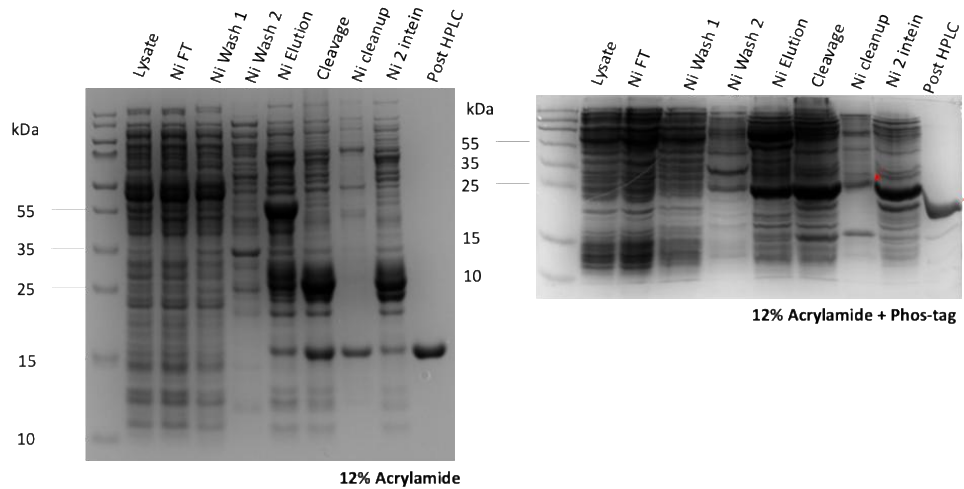


Figure 23. Affinity purification of α S with phosphorylation at S87, produced by genetic code expansion.

SDS-PAGE gels show affinity purification of α S -pS₈₇ from BL21 Δ serB cells, both run with 12% acrylamide and stained with Coomassie blue. Left = 12% acrylamide, Right = 12% acrylamide and Phos-tag.

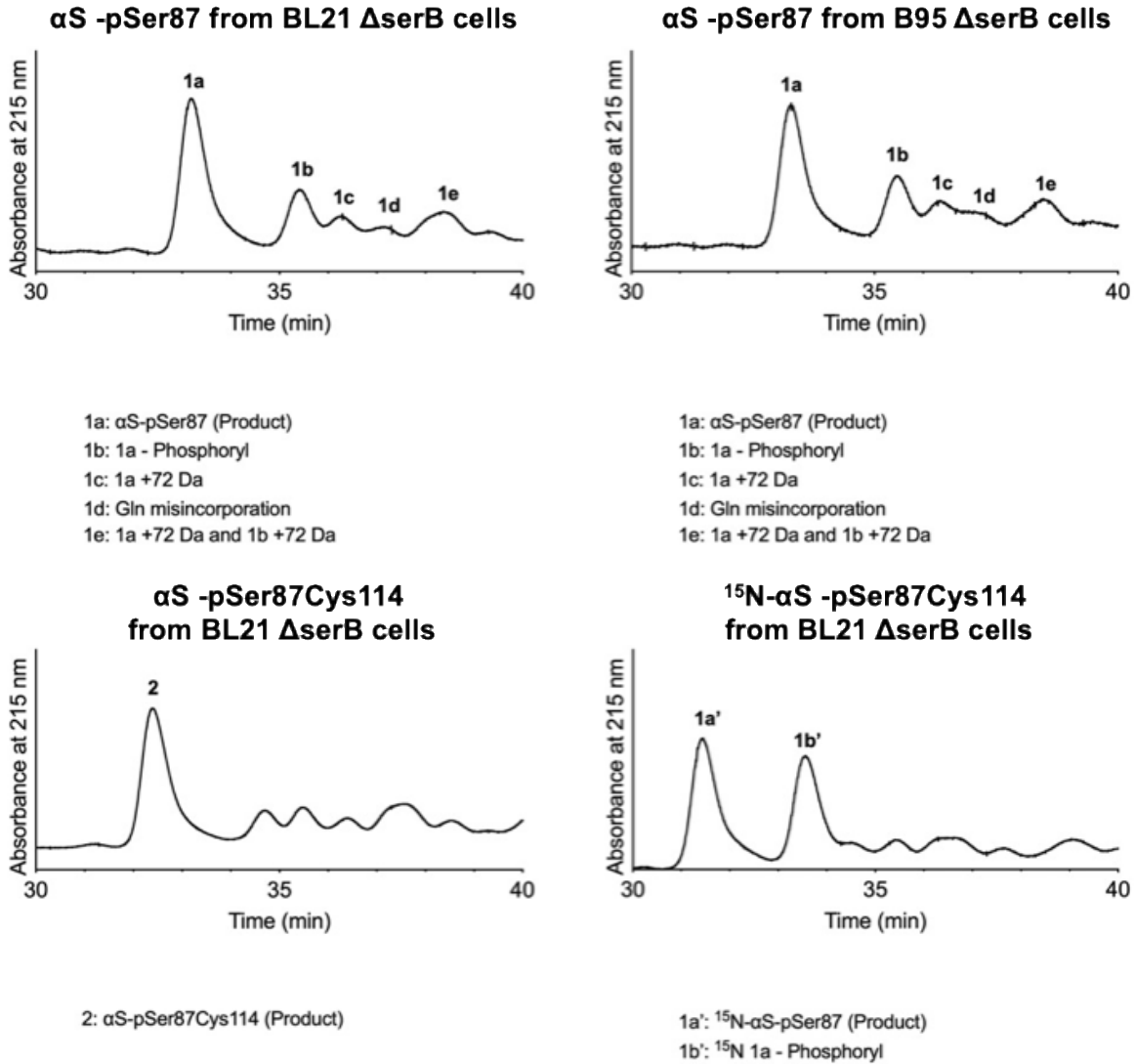


Figure 24. HPLC chromatogram collected for affinity-purified phosphoserine GCE products.

Affinity-purified α S -pS₈₇ from BL21 Δ serB cells or B95 Δ serB cells, α S -pS₈₇C₁₁₄ and 15 N α S - pS₈₇ from BL21 Δ serB cells. Peak identity was confirmed by MALDI-MS.

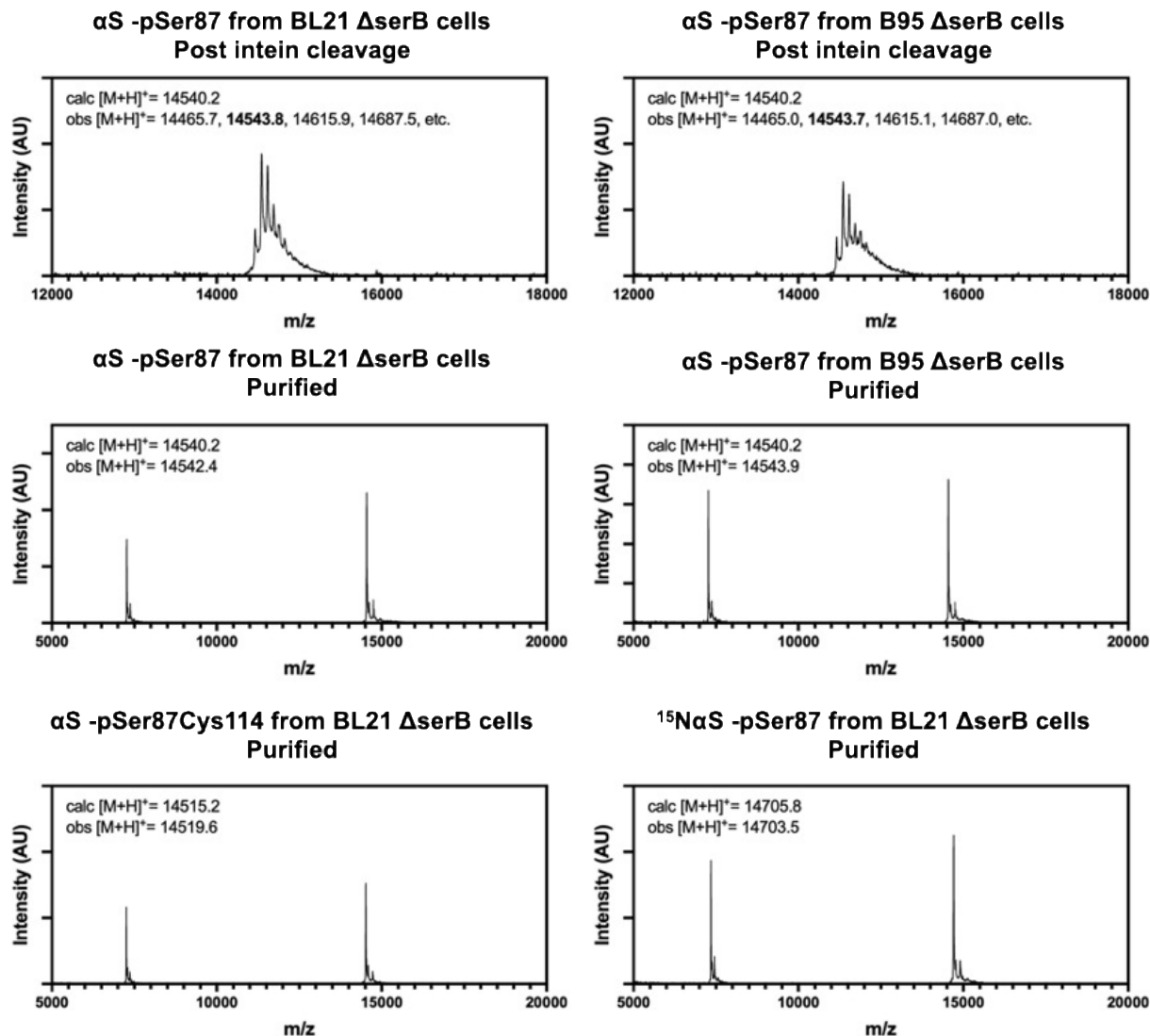


Figure 25. MALDI-MS characterization of affinity-purified or HPLC-purified α S - pS87 constructs.

Production of PTM-modified proteins by enzymatic modification

Production of α S- pS₁₂₉ was done as in our reported work⁵⁶, by co-expressing α S with a Ser/Thr kinase PLK2 in *E. coli*. This is fortunately possible thanks to the ability of PLK2 to phosphorylate Ser129 *in vivo* selectively and quantitatively without posing toxicity to *E. coli*. This method gives us a very high yield and therefore for this phosphorylation site, this was our method of choice over the GCE approach.

Interestingly, we observed no mobility shift of this phosphorylated product on Phos-tag gel (Figure 27). This is likely due to the acidic nature of the C-terminal region of α S.

Production of α S-pY₃₉ was done in an *in vitro*, chemoenzymatic manner using recombinantly expressed catalytic domain of tyrosine kinase (c-Abl), similar to our published approach, except that enzymatic modification was done on full-length α S instead of an N-terminal fragment. We chose to do this because of an acceptable level of efficiency (~50%, with 25% modification needed for experiments) and site-selectivity of c-Abl for Tyr39 phosphorylation as well as the benefit of skipping the laborious procedure needed for NCL. It has been noted that especially in prokaryotes like *E. coli*, c-Abl needs to be co-expressed with the phosphatase YopH or with kinase inhibitors to counteract and suppress its toxicity, and this likely makes it practically impossible to co-express the kinase with α S-Tyr39 and get it phosphorylated in *E. coli* cells¹²⁵. Upon incubation with c-Abl, we observed mobility shift for ~50% of α S on Phos-tag gel, indicating successful phosphorylation in a non-C-terminal region (phosphorylation in the already acidic C-terminal domain, Figure 26). Phosphorylation was also analyzed by HPLC and MALDI-MS, confirming the ~50% conversion (Figure 27). Following Glu-C digestion, we were able to identify only the α S₃₆₋₄₆ peptide as a phosphorylated peptide. MS/MS analysis of this peptide showed that Tyr39 is phosphorylated (Figure 27).

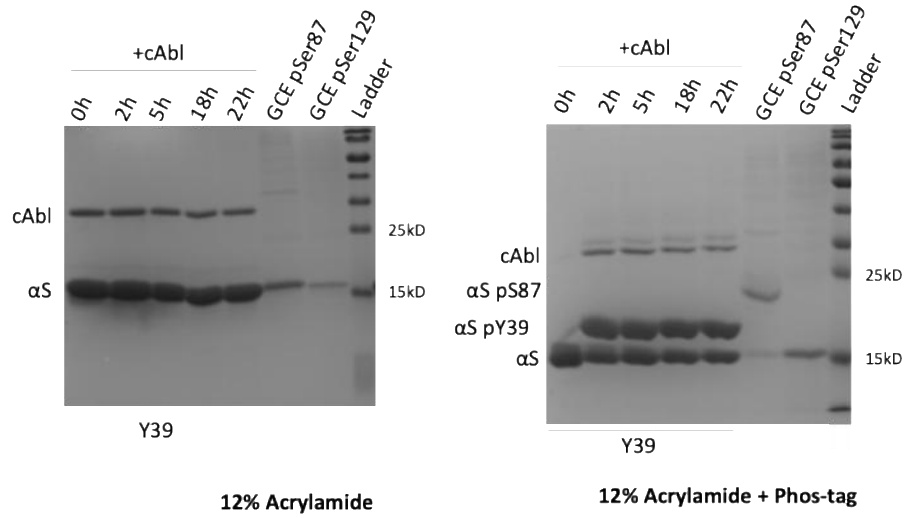


Figure 26. Phos-tag SDS-PAGE gels ran with αS phosphorylated at different sites.

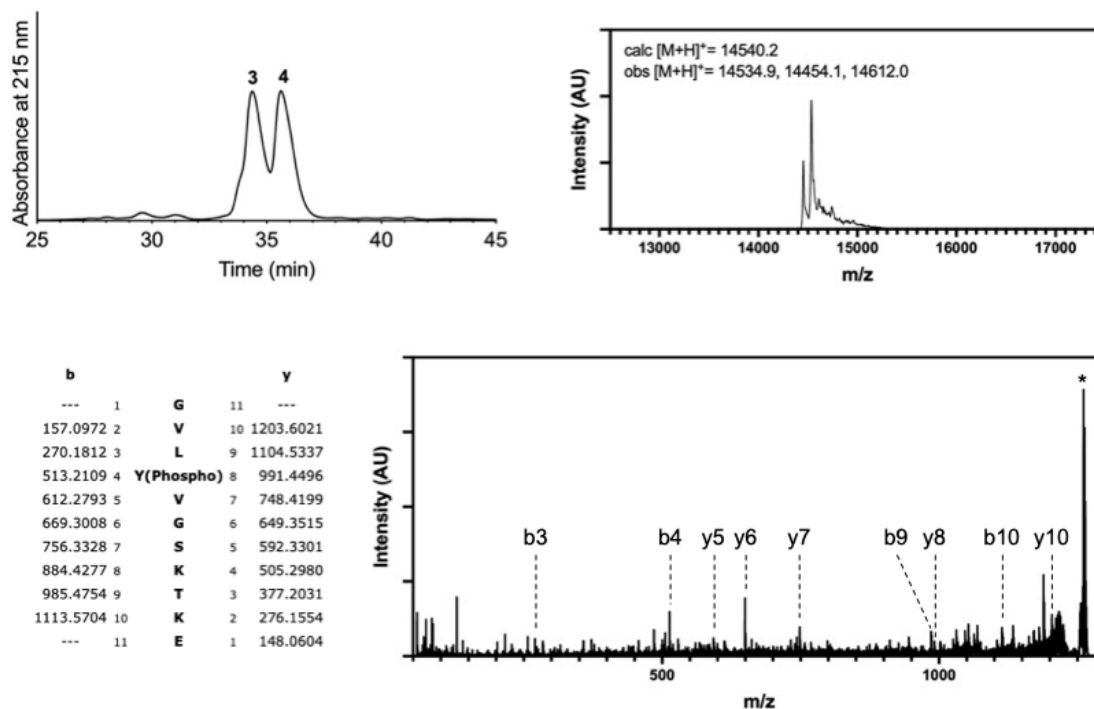


Figure 27. Analysis of α S phosphorylated by Tyr kinase c-Abl.

Top, HPLC chromatogram (upper left) and MALDI-MS (upper right) run on the same batch phosphorylation reaction, after incubated for 2h. Bottom, MALDI-MSMS data for the α S₃₆₋₄₆ peptide.

Effects of pTyr39 on radioligand binding to α S fibrils

Radioligands, such as positron emission tomography (PET) tracers, are powerful tools for imaging α S aggregates in cells and *in vivo* that can provide insights into misfolding and aggregation in Parkinson's disease. In collaboration with the Mach Research Group, we previously developed PET probes to bind selectively and with high affinity to specific sites of α S fibrils in order to visualize disease-associated aggregates^{126,127}. We used the original solid-state NMR structure (PDB: 2N0A) published by Rienstra and coworkers for this effort, which is similar to many unmodified α S fibril structures published to date,

including ones solved by cryo-EM⁵⁰. Building on this, one could take radioligand PET probes with known binding sites in unmodified α S fibrils (Tg-190b for “Site 2” and BF2846 for “Site 9”) and investigate their binding to post-translationally modified α S fibrils, then use this information to better understand the conformational differences introduced by specific modifications. Since PTMs can significantly alter α S fibril structure and behavior, radioligand binding provides a functional readout that can hint at how these modifications influence fibril conformation. In this example, we investigate the fibril conformation of α S-pY₃₉ with physiological modification stoichiometry (10-25%³⁵). This PTM was of particular interest, not only because Tyr39 is within the known binding site, Site 2, of the PET probe Tg-190b, but also motivated by the pioneering work by Zhao et al. – they chemically synthesized α S-pY₃₉ and showed that the cryo-EM structure of the fibril prepared from α S-pY₃₉ with 100% modification occupancy was dramatically rearranged from known unmodified α S fibril structures¹²⁸. This interested us in investigating the fibril conformation when prepared from monomers containing physiological stoichiometry of pY₃₉ (“25% pY₃₉ fibrils”).

Binding of Tg190b, the Site 2 binder, was significantly disturbed by the presence of pY₃₉ (K_d ~5.2 nM to 35 nM, Figure 5.6), whereas binding of BF2846, the Site 9 binder, to the 25% pY₃₉ fibrils was comparable to unmodified (K_d ~2.4 nM to 1.4 nM, Figure 28). This suggests that at physiological stoichiometry (25%), α S-pY₃₉ fibrils have similar structure to that of unmodified. Further investigations, using ultrastructure techniques, are necessary to understand the aggregation process of mixed monomers, particularly whether α S- pY₃₉ and unmodified α S gets incorporated into the same strand of fibrils.

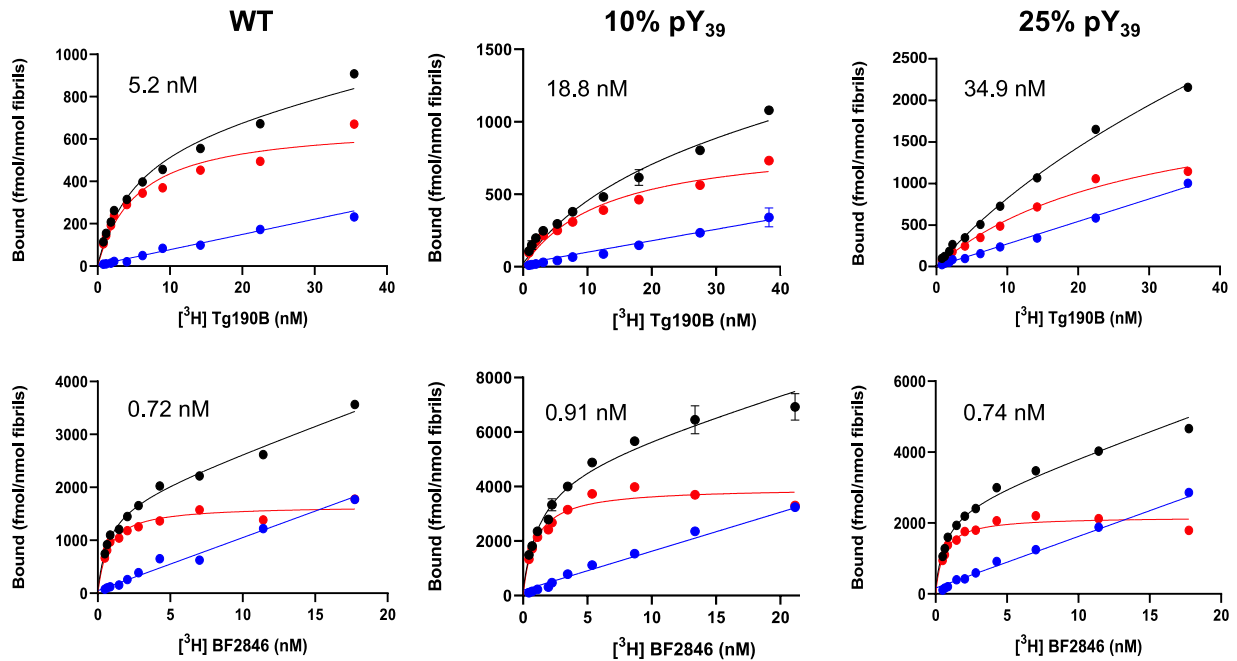


Figure 28. Radioligand competition binding to fibrils containing pTyr at physiological stoichiometry.

Competition binding of radioligands Tg190B (top) and BF2846 (bottom) to 25% α S- pY₃₉ fibrils (right), compared to their binding to unmodified α S fibrils (left).

Biophysical characterization of conformation and vesicle binding of α S-pS₈₇

Phosphorylation at Ser87 has been studied by multiple groups, with a focus on aggregation - the Lashuel group showed that their levels are increased in synucleinopathy patient brains, followed by *in vitro* and rat studies, where it slows down and reduces aggregation, resulting in less toxicity^{40,23}. Notably, they used either mutational mimics or enzymatic phosphorylation by CK1 coupled to a blocking mutation of S₁₂₉A. The Churchill Group used GCE and incorporated authentic pS₈₇ modification with minimal sequence scars from TEV cleavage, which exhibited similar dopamine or Cu²⁺-induced oligomerization trends but

significantly increased toxicity in SH-SY5Y neuronal cell model¹²⁹. Lastly, the Li and Liu groups performed protein semi-synthesis, resulting in completely authentic α S-pS₈₇ construct, and their a cryo-EM study showed its unique fibril structure – unlike the case of pY₃₉, pS₈₇ could not be stabilized by nearby positively charged residues and causes the broader C-terminal region of α S to be excluded from the fibril core while including the entire N-terminal region (PDB: 8JEY)⁴¹.

On the other hand, the effects of pS₈₇ on the native role of α S are relatively understudied: the Lashuel Group studied α S conformation in the presence and absence of lipid membranes, indicating that pS₈₇ alters the conformation of the helix that forms when bound to SDS micelles and that it reduces helicity on vesicles⁴⁰. Again, they used the proteins modified with mutational mimics/blocks and enzymatic modification for this.

To understand the effects of pS₈₇ on vesicle binding, we first acquired proton-nitrogen heteronuclear single quantum coherence spectra (¹H,¹⁵N – HSQC) in the presence and absence of small, unilamellar vesicles (SUVs) that are composed of 60:25:15 1,2-dioleoyl-sn-glycero-3-phosphocholine/1,2-dioleoyl-sn-glycero-3-phosphatidylethanolamine/1,2-dioleoyl-sn-glycero-3-phospho-L-serine (DOPC/DOPE/DOPS). The NMR peak chemical shifts relative to spectra for free α S were very minimal. We observed that both pS₈₇ and WT led to a ~60% reduction of intensity (Figure 29). This reduction is caused by binding to vesicles, where lipids are slowly tumbling (seen in α S residues 1-100). This result suggests that pS₈₇ does not affect vesicle binding.

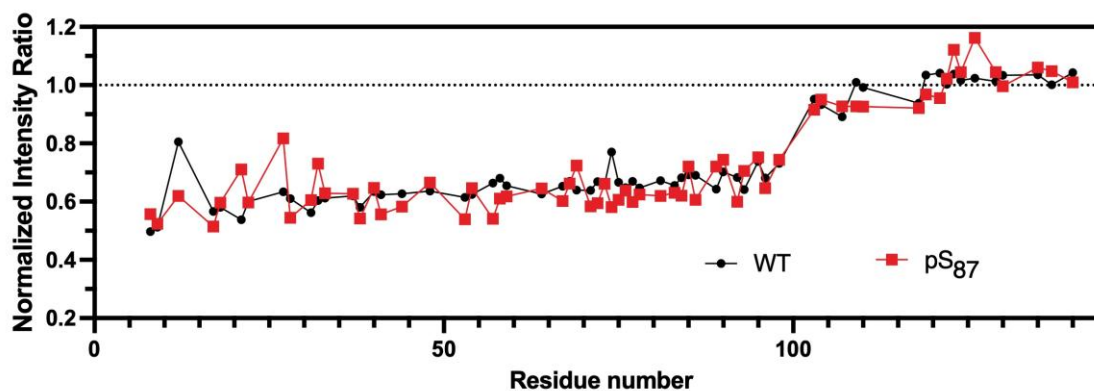


Figure 29. Effects of pSer87 on vesicle binding, investigated by NMR.

NMR intensity ratio for each residue calculated from ^1H - ^{15}N HSQC spectra collected with ^{15}N -labeled αS variants in the presence or absence of SUVs, normalized by the average ratio for residues 101-140.

To quantitatively determine binding affinity, we performed fluorescence correlation spectroscopy (FCS), an established method for quantifying biomolecule interactions, including αS vesicle binding⁹⁰. FCS and NMR are complementary techniques in this context: FCS provides quantitative results with slight perturbation, while NMR offers qualitative insights without perturbation. It is also notable that this binding affinity measurement could not be completed when we previously generated pS₈₇ by chemical protein synthesis¹²³. For this experiment, we first fluorescently labeled αS variants with a Cys mutation at site 114, by reacting them with Atto488-maleimide overnight at room temperature, resulting in labeled, phosphorylated construct (αS -pS₈₇C₁₁₄^{Atto488}, “pS87”) and labeled, unphosphorylated construct (αS -C₁₁₄^{Atto488}, “WT”). We synthetically prepared lipid vesicles composed of 50:50 1-palmitoyl-2-oleoyl-sn-glycero-3-phospho-L-serine/1-palmitoyl-2-oleoyl-glycero-3-phosphocholine (POPS/POPC). The diffusion times of free αS and vesicles were initially measured. To evaluate αS -vesicle binding, a fixed amount of αS was added to varying concentrations of vesicles, and the fraction of protein bound was determined by fitting a two-component autocorrelation function. The fraction bound at each vesicle

concentration was then used to generate a binding curve for each α S construct. We observed no significant difference in vesicle binding affinity caused by phosphorylation at Ser87 (Figure 30; $K_{d,app}^{WT} = 3.7 \pm 0.5 \mu\text{M}$, $K_{d,app}^{pS87} = 5.2 \pm 0.5 \mu\text{M}$). This result is consistent with our observations in the NMR vesicle binding experiments, complementing quantitative measurements with non-perturbing measurements.

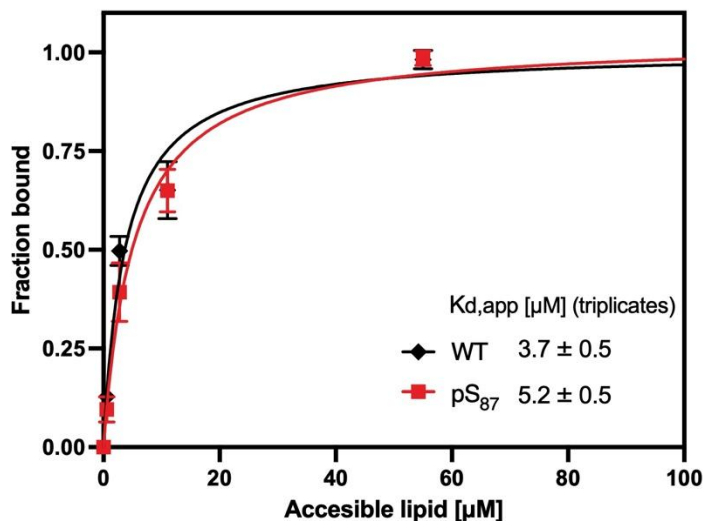


Figure 30. Effects of pSer87 on vesicle binding, investigated by FCS.

§5.3 Conclusion

In this work, we explored the production and characterization of post-translationally modified α S by GCE or modifications by PTM-modifying enzymes. These methods allow for site-specific incorporation of phosphorylation, while being broadly accessible to biochemistry laboratories that may lack peptide chemistry expertise. Additionally, we demonstrated the utility of these approaches for isotopic labeling, allowing for structural and biophysical studies. While Phos-tag gel electrophoresis provided a useful tool

for assessing phosphorylation status, we also highlighted the need for careful interpretation, as band shifts can be influenced by the intrinsic charge of the phosphorylated region.

Beyond protein production, we examined the biophysical and functional consequences of these modifications, particularly focusing on phosphorylation at Ser87, Ser129, and Tyr39 in α S. Our results indicate that GCE-based phosphorylation at Ser87 enables studies that were previously challenging with chemical protein synthesis, allowing for structural and vesicle-binding analyses.

By integrating radioligand binding studies with PTM-modified fibrils, we demonstrated how PET probe interactions can serve as a functional readout of structural changes induced by modifications. Our findings suggest that pY₃₉, even at physiological sub-stoichiometric ratios, perturbs PET probe binding only at Site 2, reflecting blocked interactions by phosphorylation or localized structural changes of the fibrils. Future work involving ultrastructural characterization will be essential for understanding the underlying molecular basis of this altered binding affinity.

Lastly, we examined how PTMs influence α S's native functions, including membrane interactions. Vesicle-binding studies using NMR and FCS showed that pS₈₇ does not significantly impact α S-vesicle interactions. This finding contrasts with previous studies using phosphomimetic mutations or enzyme-blocking mutations, which showed that this PTM reduces helicity of the protein on vesicles. This highlights the importance of employing authentic modifications rather than relying on mimics when studying PTM effects.

Overall, this work showcases the value of GCE and enzymatic methods for producing PTM-modified proteins and their application in biophysical and structural characterization. With these tools, we provide new insights into the role of phosphorylation in α S, contributing to a deeper understanding of PTM-mediated regulation in neurodegenerative disease pathology.

CHAPTER 6: CONCLUSION AND PERSPECTIVES

This dissertation has explored the role of site-specific post-translational modifications (PTMs) in α -synuclein (α S) by employing genetic code expansion (GCE), enzymatic modification, and protein semi-synthesis. These approaches have allowed for precise incorporation of modifications such as lysine acetylation and phosphorylation, enabling an in-depth study of their effects on aggregation, membrane interactions, fibril structure, and seeding capability. Particularly with Lys acetylation, multiple mimics were additionally explored and compared. By establishing and applying these methodologies, this work contributes both technical showcase in PTM incorporation and biological insights into how α S modifications influence its pathogenic and physiological roles.

In Chapter 2, we examined the functional and pathological consequences of lysine acetylation at all disease-relevant sites in α S using GCE-based site-specific incorporation. The choice of GCE over native chemical ligation (NCL) for acetyllysine incorporation made it much more efficient to scan through each of 12 different modification sites. Acetylation of K₁₂, K₄₃, and K₈₀ was found to significantly slow formation of fibrils, both *in vitro* and in neurons. With acetylation of K₁₂ and K₄₃ moderately affecting membrane binding, acetylation at K₈₀ seems to be a more promising therapeutic target, where enhancers of Lys acetyltransferases (KATs) or inhibitors to Lys deacetylases (KDACs) could help increase the level of acetylation at this site. In our preliminary work, HDAC8 exhibited higher deacetylation level for acetylation at Lys 80 than many other sites, but not selectively over Lys 43. This makes HDAC8 not very ideal for therapeutic targeting. Our next step will be to screen and investigate specificity of KATs and KDACs, narrowing down possible targets. Our structural efforts into slowed aggregation by acetylation at Lys 80 implies that the mechanism for this effect may be more complex than affecting monomer conformations or fibril structures. Future investigations will be done on morphology of fibrils acetylated

at Lys 12 or Lys 43, as well as monomer dynamics and structural impacts on oligomeric, intermediate states, as well as effects.

In Chapter 3, we explored the commonly used glutamine (Gln) substitution as a mimic for lysine acetylation, a technique frequently employed in cellular or *in vivo* studies where authentic acetylation is difficult to introduce. While Gln mimics some of the electrostatic and structural effects of acetylation by neutralizing the lysine's positive charge, we found that its effectiveness varies by modification site and depends on the context. Q₄₃ and Q₈₀ successfully replicated the effects of authentic Lys acetylation in aggregation assays, whereas Q₁₂ failed to do so. In vesicle binding, all sites successfully mimicked the effects of authentic acetylation. This study highlights the importance of validating commonly used PTM mimics on a site-by-site basis and in each context, as their effectiveness in recapitulating authentic acetylation's effects on α S aggregation and function is not universal.

In Chapter 4, we expanded our methodological toolkit for studying Lys acetylation of α S by exploring alternative chemical strategies, such as thioether acetylation mimics and thioamide acetyllysine analogs. Thioether acetylation mimics, generated via thiol-ene chemistry, offered an efficient approach to studying acetylation effects. They would particularly be useful in cases where GCE is impractical, such as when multi-site incorporation is needed, multi-PTM incorporation makes the synthesis complicated or when characterization experiments require a lot of materials. Our preliminary studies showed that its mimicry was site-dependent – at Lys 43 it mimicked the effects of authentic acetylation ability in aggregation assays while at Lys 80, it exhibited distinct results in both aggregation assays and monomer conformation investigated by NMR. In contrast, thioamide acetyllysine presents a fluorescence-quenching probe with the added advantage of being resistant to enzymatic deacetylation. These alternative strategies provide researchers with additional tools to study lysine acetylation in α S.

Chapter 5 shifted focus toward phosphorylation, another key PTM in α S pathology, specifically investigating the effects of phosphorylation at Ser87 (pS₈₇) and phosphorylation at Tyr39. pS₈₇ was

incorporated using GCE, enabling site-specific modification and isotopic labeling for NMR studies. In contrast, pY₃₉ was introduced via enzymatic phosphorylation using c-Abl kinase, achieving ~50% modification efficiency, which was sufficient for our experiment. Our studies revealed that pS₈₇ had minimal impact on vesicle binding, and pY₃₉ does not influence fibril structure at physiological stoichiometry (10-25%), unlike when it is at 100%, as detected by changes in binding of site-specific radioligands. This work showcases the utility of GCE and enzymatic methods for producing phosphorylated α S and their application in biophysical and structural characterization.

Beyond the core chapters, the appendices include additional investigations into PTMs and methodological advancements. Appendix A describes semi-synthetic incorporation of glutamate arginylation in α S, a rare PTM whose biological significance is still being elucidated. Appendix B investigates whether a cysteine-based mimic of arginylation reproduces the effects of authentic arginylation, with promising results both in vitro and in neurons. Appendix C details synthetic strategies for generating peptides and proteins with site-specific glutamate arginylation, including the synthesis of arginylated peptide libraries. Appendix D describes the synthesis of semi-synthetic CoA- α S construct designed to study NatB-mediated N-terminal acetylation.

While this work has provided valuable insights into the role of site-specific PTMs in α S aggregation and function, several important questions remain. One key avenue for future research is the study of combinatorial PTMs, as multiple modifications often act in concert to regulate protein behavior. Preliminary work motivated by interactions observed in the pY₃₉ fibril structure (Figure 32, PDB:6LIT)¹²⁸ suggest a potential, synergistic effect between pY₃₉ and ^{Ac}K₄₃, as observed in aggregation assays where mixtures of monomeric α S containing each modification exhibited altered fibril formation rates compared to singly modified α S (Figure 31). This could be due to an additive effect of each PTM, and it is important to experiment with modifications in the same chain. However, generating a single α S construct bearing both modifications remains a major challenge. Our semi-synthesis design involves the production

of α S₁₋₅₅-^{Ac}K₄₃-MES fragment through GCE, then enzymatic phosphorylation, before being used for NCL (Scheme 2). The challenge was largely due to the combination of enzymatic phosphorylation of Tyr39 being inefficient, as well as GCE not being very high yielding, although the latter could be dealt with by scale-up. Developing new synthetic strategies, such as the use of thioether mimic at this position or improving kinase purification protocol will be critical for further exploring PTM crosstalk in α S at these PTMs.

Besides, it is ideal for combinatorial PTM studies to involve identifications of the combinations in healthy humans and patients. This is especially important as our current knowledge in human-identified PTMs is based on a bottom-up mass spectrometry (MS) work, which does not inform on co-existence of PTMs on the same protein. Middle-down MS or top-down MS would fill this gap, and this effort is in progress by our collaborator. For particular combinations of interest, immunostaining would inform on co-localization of different PTMs. Methodology development will be needed to elucidate co-existence of these PTMs in a single chain.

Another key question is how PTMs influence α S aggregation mechanism at an atomic level. This question gets even more complicated at physiological stoichiometry (often <100%) of the PTMs. Structural studies using cryo-EM have begun to reveal how PTMs reshape fibril polymorphs, but more work is needed to determine whether PTM induces conformational changes on intermediate states and how these structural effects correlate with toxicity and disease progression.

Finally, expanding PTM investigations beyond acetylation, phosphorylation, and glutamate arginylation will be essential for developing a comprehensive understanding of α S regulation. Future studies could explore ubiquitination, SUMOylation, and oxidative modifications, which have all been detected in α S pathology but remain relatively understudied in a site-specific manner. For Lys modifications, it would be interesting to see how different Lys PTMs compete with each other at the same site and cross-talk, as has been suggested in tau between Lys acetylation and ubiquitination¹³⁰.

These aforementioned future efforts will further enhance our understanding of PTM-mediated regulation in synucleinopathies, ultimately contributing to the development of therapeutic strategies targeting α S aggregation and toxicity.

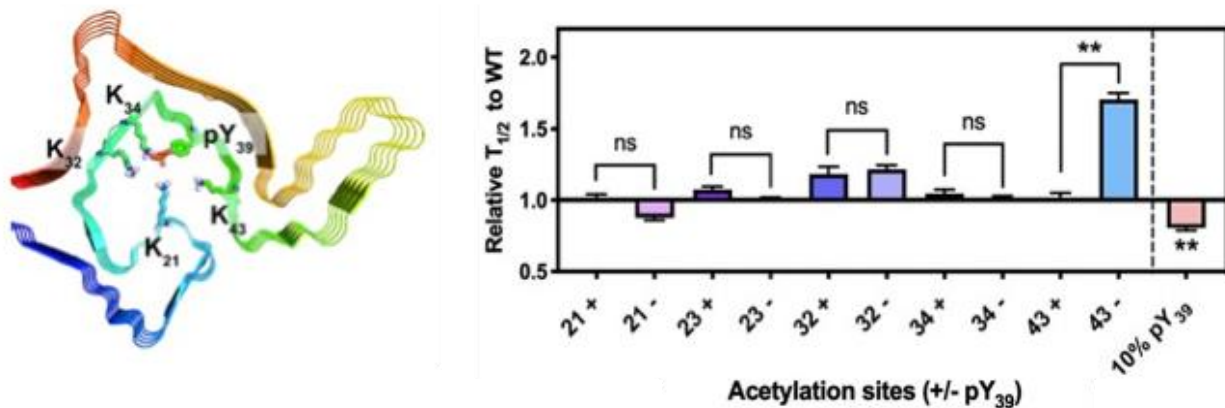
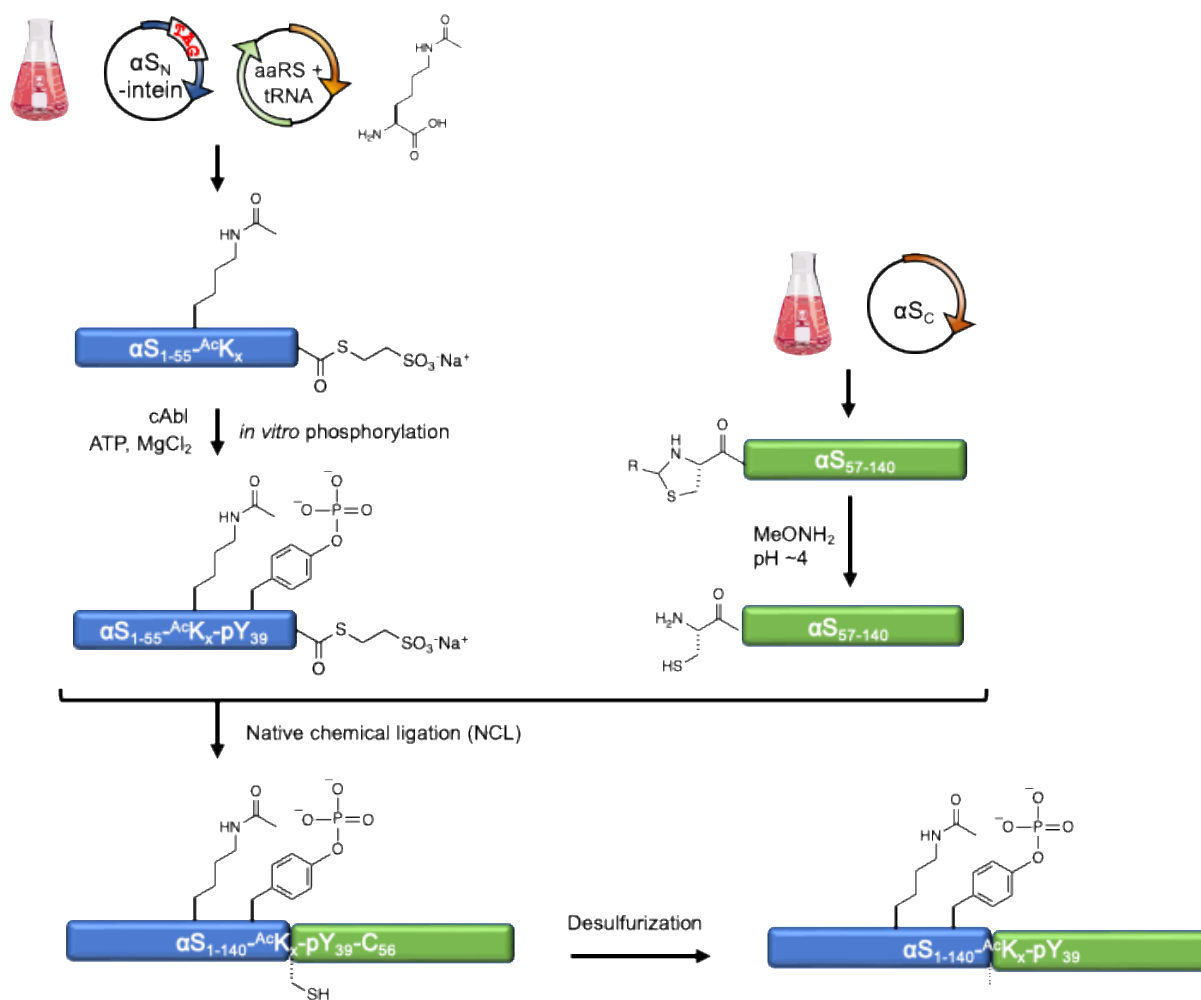


Figure 31. Preliminary combinatorial PTM study with pTyr9 and acetylation at nearby Lys.

Left, cryo-EM structure of synthetically prepared pY₃₉ fibril (PDB:6LIT)¹²⁸. The phosphate group forms salt bridges with side chains of K₂₁, K₃₂ and K₃₄. K₄₃ side chain points towards the phosphate. Right, aggregation kinetic studies performed for mixture of 10% ^AK_X and 10% pY₃₉ as well as single PTM controls (X = 21, 32, 34 or 43). Aggregation kinetics were monitored by fluorescence intensity change of ThT. Time it takes to reach 50% fibrilization (T_{1/2}) for each condition was normalized to that of WT. Seeded aggregation was performed with αS monomers where PTM αS was mixed with αS WT at 10%+10%:80% (mixture) or 10%:90% (single PTM control) ratio. SEM, R=6



Scheme 2. Semi-synthesis of αS bearing both Lys acetylation and pY₃₉. (X = 21, 32, 34 or 43)

CHAPTER 7: MATERIALS AND METHODS

§7.1 General information

Reagents for peptide synthesis, including 2-(*1H*-benzotriazol-1-yl)-1,1,3,3-tetramethyluronium hexafluorophosphate (HBTU), *N,N*-diisopropylethylamine (DIPEA), and Fmoc-amino acids, were purchased from EMD Millipore (Burlington, MA, USA) or ChemImpex International (Wood Dale, IL, USA). Reagents for native chemical ligation (NCL): NaNO₂, *tris*(2-carboxyethyl)phosphine (TCEP), and mercaptophenyl acetic acid (MPAA) were purchased from Sigma-Aldrich (St. Louis, MO, USA). *E. coli* BL21(DE3) cells and *E. coli* Dh5 α cells were purchased from New England Biotechnologies (Ipswich, MA, USA). DNA oligomers were purchased from Integrated DNA Technologies, Inc (Coralville, IA, USA). DNA extraction and Miniprep kits were purchased from Qiagen (Hilden, Germany). Buffers were made with MilliQ filtered (18 M Ω) water (Millipore; Billerica, MA, USA). Preparation of the pTXB1- α S-intein-H₆ plasmid containing α -synuclein (α S) with a C-terminal fusion to the *Mycobacterium xenopi* GyrA intein and C-terminal His₆ tag was described previously.¹ This plasmid was used as a starting point for the preparation of α S (mutants) -intein constructs. For overexpression of α S in HEK cells, the expression vector pcDNA5/TO was purchased from Thermo Fisher Scientific (Waltham, MA). pTECH-chAcK3RS (IPYE) was a gift from David Liu via Addgene (plasmid # 104069; <http://n2t.net/addgene:104069>; RRID:Addgene_104069; Watertown, MA, USA). Acetyllysine was purchased from ChemImpex. Nicotinamide was purchased from Alfa Aesar (Tewksbury, MA, USA). Atto 488 maleimide was purchased from Sigma-Aldrich. Matrix-assisted laser desorption/ionization mass spectrometer (MALDI-MS) data were collected with a Bruker Ultraflex III MALDI-MS instrument or a Bruker Microflex MALDI-MS (Billerica, MA, USA). UV/Vis absorbance spectra were obtained with a

Hewlett-Packard 8452A diode array spectrophotometer (currently Agilent Technologies; Santa Clara, CA). Gel images were obtained with a Typhoon FLA 7000 (GE Lifesciences; Princeton, NJ, USA). Thioflavin T (ThT) absorbance spectra were collected on a Tecan SPARK plate reader (Mannedorf, Switzerland). Proteins were purified on a 1260 Infinity II preparative high-performance liquid chromatography (HPLC) system (Agilent Technologies). NCL reactions were monitored on a 1260 Infinity II Analytical HPLC system (Agilent Technologies) using a Jupiter C4 column (Phenomenex; Torrance, CA, USA). Water + 0.1% trifluoroacetic acid (TFA) (solvent A) and acetonitrile + 0.1% TFA (solvent B) were used as the mobile phase in HPLC.

§7.2 Protein semi-synthesis for generation of α S^{-Ac}K₈₀

To synthesize α S acetylated at K₈₀, an N-to-C three-part native chemical ligation (NCL) was performed between the fragments α S₁₋₇₆, α S₇₇₋₈₄-^{Ac}K₈₀, and α S₈₅₋₁₄₀. All fragments and intermediate products were purified by reverse-phase high-performance liquid chromatography (RP-HPLC) over a C4 column.

N-terminal thioester fragment α S₁₋₇₆-MES (**1a**) and C-terminal fragment α S₈₅₋₁₄₀-C₈₅ (**4**) were constructed through deletion polymerase chain reaction (PCR) of previously published α S fragment constructs. They were each recombinantly expressed as a fusion with a polyhistidine-tagged GyrA intein from *Mycobacterium xenopi*. The N-terminal thioester was generated by adding excess sodium mercaptoethane sulfonate (MESNa) to cleave the intein by N,S-acyl shift.² (reported yield 24.1 mg/L.³) Endogenous methionyl aminopeptidase processes the N-terminus of the 85-140 peptide to expose the N-terminal cysteine,⁴ which further reacts with aldehydes or ketones *in vivo* to form thiazolidine derivatives.⁵ The thiazolidine derivatives were deprotected with methoxyamine to give a free N-terminal cysteine (4.40 mg/L). The middle peptide α S₇₇₋₈₄-Pen₇₇-^{Ac}K₈₀-NHNH₂ (**2**, Pen: penicillamine⁶) was

synthesized as a C-terminal acyl hydrazide through Fmoc-based, solid-phase peptide synthesis (Yield: 12.4 mg, 12 μ mol, 48%).

α S₁₋₇₆-MES (**1a**) and α S₇₇₋₈₄-Pen₇₇^{Ac}K₈₀-NHNH₂ (**2**) were ligated overnight under routine NCL conditions in the presence of MPAA. (Yield: 1.46 mg, 172 nmol, 57%). The purified product (**3a**) was activated to MES thioester (**3b**) (Yield: 1.29 mg, 126 nmol, 73%). The second ligation between α S₁₋₈₄-Pen₇₇^{Ac}K₈₀-MES (**3b**) and α S₈₅₋₁₄₀-C₈₅ (**4**) was performed in the presence of methyl thioglycolate⁷ to allow for desulfurization without intermediate purification. The product α S^{Ac}K₈₀ (**5b**) was obtained in 43% yield (0.90 mg, 62 nmol).

§7.3 Construction of expression plasmids

The following primers were designed for site-directed mutagenesis to introduce TAG (= Z) codons at each lysine acetylation site or codons for Gln mutations at sites 12, 43 or 80. Site-directed mutagenesis for TAG mutations were performed on the plasmid encoding α S-MxeGyrA-His₆ and site-directed mutagenesis for Gln mutations were performed on the same plasmid and on the mammalian expression vector pcDNA5/TO, encoding α S.

Primer sequences:

α S-Z ₁₂	Forward	5'-CAAAGGCCTAGGAGGGAGTT-3'
	Reverse	5'-AAAGTCCTTTCATGAATACATCCATATGTATA-3'

α S-Z ₂₁	Forward	5'-GTGGCTGCTGCTGAGTAGACCAAACAGGGT-3'
	Reverse	5'-AACTCCCTCCTTGGCCTTTGAAAGTCCTTT-3'
α S-Z ₂₃	Forward	5'-GCTGCTGAGAAAACCTAGCAGGGTGTGGCA
	Reverse	5'-AGCCACAACCTCCCTCCTTGGCCTTTGAAAG
α S-Z ₃₂	Forward	5'-GCAGAAGCAGCAGGATAGACAAAAGAGGGT
	Reverse	5'-CACACCCTGTTTGGTTTTCTCAGCAGCAGC
α S-Z ₃₄	Forward	5'-GCAGCAGGAAAGACATAGGAGGGTGTTC
	Reverse	5'-TTCTGCCACACCCTGTTTGGTTTTCTC
α S-Z ₄₃	Forward	5'-GTAGGCTCCTAGACCAAGG
	Reverse	5'-ATAGAGAACACCCTCTTTTGTCTTTC
α S-Z ₄₅	Forward	5'-GGCTCCAAAACCTAGGAGGGAGTGGTG
	Reverse	5'-TACATAGAGAACACCCTCTTTTGTCTTTCCTGC
α S-Z ₅₈	Forward	5'-GCAACAGTGGCTGAGTAGACCAAAGAGCAA
	Reverse	5'-CACACCATGCACCACTCCCTCCTTGGT
α S-Z ₆₀	Forward	5'-GTGGCTGAGAAGACCTAGGAGCAAGTGACA
	Reverse	5'-TGTTGCCACACCATGCACCACTCC

α S-Z ₈₀	Forward	5'-GCAGTAGCCCAGTAGACAGTGGAGGGA
	Reverse	5'-TGTCACACCCGTCACCACTGC
α S-Z ₉₆	Forward	5'-GCCACTGGCTTTGTCTAGAAGGACCAGTTG
	Reverse	5'-TGCTGCAATGCTCCCTGCTCCCTC
α S-Z ₁₀₂	Forward	5'-CAGTTGGGCTAGAATGAAGAAGG
	Reverse	5'-GTCCTTTTTGACAAAGCCAGTG
α S-Q ₁₂	Forward	5'-TTTCAAAGGCACAAGAGGGAGTTGTGG
	Reverse	5'-GTCCTTTCATGAATACATCC
α S-Q ₄₃	Forward	5'-TGTAGGCTCCCAGACCAAGGAGG-3'
	Reverse	5'-TAGAGAACACCCTCTTTTG-3'
α S-Q ₈₀	Forward	5'-AGTAGCCCAGCAGACAGTGGAG
	Reverse	5'-GCTGTCACACCCGTCACC

§7.4 Production of recombinant α S constructs – Lys acetylation and Gln mutational mimic work

To generate acetylated α S, each plasmid encoding α S with a TAG mutation at the site of interest and a machinery plasmid for acetyllysine incorporation, pTECH-chAcK3RS (IPYE), were co-transformed by heat shock at 42 °C into BL21 (DE3) competent cells. Cells were plated and incubated on

ampicillin/chloramphenicol (Amp/Chlor) plates. Single colonies were picked to inoculate primary cultures in LB media supplemented with 0.1 mg/mL Amp and 0.025 mg/mL Chlor. Primary cultures were incubated overnight or until they were cloudy at 37 °C. Secondary cultures in LB media were inoculated and grown at 37 °C with shaking at 250 rpm until the optical density at 600 nm (OD₆₀₀) reached ~ 0.6. The culture was subsequently cooled to 18 °C. 50 mM nicotinamide and 10 mM ε-acetyl lysine were added to the culture and incubated for ~ 5 min before inducing the expression of the gene of interest with 1 mM isopropyl β-D-1-thiogalactopyranoside (IPTG). To generate isotopically labeled, acetylated αS, protein expression was performed as above, except that cells were grown in M9 minimal media⁸ that contains ¹⁵N-ammonium chloride. To express αS glutamine mutants, the plasmid encoding αS with a Gln mutation at the site of interest was transformed into BL21 (DE3) competent cells. Protein expression was performed as above, but. without the addition of nicotinamide and acetyl lysine. Induced cells were then grown in the shaker-incubator at 18 °C overnight. After centrifugation (4000 rpm, 20 min, 4 °C), cell pellets were re-suspended in buffer (40 mM Tris pH 8.3, with one Roche protease inhibitor tablet) and sonicated in a cup in an ice bath (5 min, 1 s ON, 2 s OFF). The resulting lysate was centrifuged (14,000 rpm, 30 min, 4 °C), and supernatant containing the αS variant was purified over a Ni-NTA affinity column. Intein cleavage was carried out by incubation with 200 mM β-mercaptoethanol (βME) on a rotisserie overnight at room temperature. Cleaved αS variant was dialyzed into 20 mM Tris, pH 8 buffer before purification over a second Ni-NTA column to remove the free intein from the sample. The αS proteins were purified by RP-HPLC over a C4 column (acetylated proteins) or by fast-protein liquid chromatography (FPLC) using a Hi-Trap Q 5 mL column (glutamine mutants), dialyzed into 1x phosphate buffered saline (PBS) and spin-concentrated. For purification of acetylated Cys mutants for fluorescent labeling, TCEP was added to a final concentration of 1 mM prior to HPLC injection and samples were dialyzed into 20 mM Tris 50 mM NaCl pH 7.4 after purification. Upon flash-freezing,

protein stocks were kept at -80 °C until further use. Isotopically labeled α S samples were lyophilized after HPLC purification.

§7.5 Production of recombinant α S constructs – Ser phosphorylation work

Expression of α S with a serine phosphorylation followed the method previously described⁹. The plasmid encoding α S with a TAG mutation at the site of interest (backbone: pRBC, origin of replication: p15A, antibiotic resistance: Amp) and a machinery plasmid for phosphoserine incorporation, pkW2-EFSep (origin of replication: pBR322, antibiotic resistance: Chlor) were co-transformed by a heat shock at 42 °C to BL21 (DE3) competent *E. coli* cells with a $\Delta serB$ genomic knockout. Cells were plated and incubated on Amp/Chlor plates. Single colonies were picked to inoculate primary cultures in 50 mL ZY-non inducing media (NIM) supplemented with 0.1 mg/mL Amp and 0.025 mg/mL Chlor, in a 250 mL baffled flask. Primary cultures were incubated for overnight at 37 °C with 250 rpm shaking.

To generate non-isotopically labeled, Ser-phosphorylated α S, secondary cultures in ZY-AIM media ($OD_{600} \sim 5-8$) were inoculated by adding 1% inoculum of ZY-NIM culture and grown at 37 °C with shaking at 250 rpm until the OD_{600} reached ~ 1.5 . The culture was subsequently cooled to 22 °C and grown with shaking at 250 rpm.

To generate isotopically labeled, Ser-phosphorylated α S, protein expression followed the method previously described¹⁰. Secondary cultures were first started in fresh ZY-NIM media with 10% inoculum and grown at 37 °C with shaking at 250 rpm until OD_{600} reached $\sim 3-4$. Cells were then pelleted by centrifugation at 4000 g for 10 min. Cell pellets were resuspended in an equal volume of minimal MIM 2 media that contains ¹⁵N-ammonium chloride and ¹⁵N-CELTONE. We note that for this work, we did not supplement L-serine. This was grown at 37 °C with shaking at 250 rpm in a baffled flask until the OD_{600}

increased by 1-2 units. Expression of the gene of interest was induced with 1 mM isopropyl β -D-1-thiogalactopyranoside (IPTG). Induced cells were then grown in the shaker-incubator at 22 °C overnight.

In all the buffers used during affinity purification, phosphate inhibitors (20 mM sodium fluoride, 5 mM sodium pyrophosphate, 0.5 mM sodium orthovanadate, final concentration) were added. After centrifugation (4000 rpm, 30 min, 4 °C), cell pellets were re-suspended in buffer (40 mM Tris pH 8.3, 1 Roche protease inhibitor tablet, 1 mM phenylmethylsulfonyl fluoride) and sonicated in a cup in an ice-water bath (5 min, 1 s ON, 2 s OFF). The resulting lysate was centrifuged (14,000 rpm, 30 min, 4 °C), and supernatant containing the protein of interest (POI) was purified over a Ni-NTA affinity column. Intein cleavage was carried out by incubation with 200 mM β ME on a rotisserie overnight at room temperature. Cleaved protein was dialyzed into 20 mM Tris, pH 8 buffer before purification over a second Ni-NTA column to remove the free intein from the sample. The α S proteins were purified by RP-HPLC over a C4 column, dialyzed into 1x phosphate buffered saline (PBS) and spin-concentrated. For purification of phosphorylated Cys mutants for fluorescent labeling, TCEP was added to a final concentration of 1 mM prior to HPLC. Upon flash-freezing, protein stocks were kept at -80 °C until further use. Isotopically labeled α S samples were lyophilized after HPLC purification. Phos-tag gels were run to analyze %phosphorylation.

§7.6 Production of α S-pY₃₉

The procedures for purifying catalytic domain of the c-Abl Tyr kinase as well as phosphorylation of α S were adapted from our previously published work¹¹.

To express and purify c-Abl for phosphorylation studies, BL21 (DE3) *E. coli* cells were transformed with pET His₆-SUMO-TEV-cAbl (Amp resistance) and YopH (Strep resistance) plasmids.

Colonies were selected on LB agar plates containing ampicillin and streptomycin, and primary cultures were grown overnight. Secondary cultures were inoculated and grown in LB medium until reaching an OD₆₀₀ of 0.6–0.7, at which point they were cooled to 16 °C, induced with 0.25 mM IPTG, and incubated overnight. Cells were harvested by centrifugation and lysed by sonication in 50 mM Tris, 500 mM NaCl, 5% glycerol, pH 8.0, supplemented with protease inhibitors. The lysate was cleared by centrifugation at 14,000 rpm for 30 min, and the supernatant was incubated with a Ni-NTA column equilibrated in 50 mM HEPES pH 7.5, supplemented with 5% glycerol. After sequential washes, c-Abl was eluted using an imidazole gradient (60–300 mM). The eluted fractions were analyzed by SDS-PAGE, pooled, and incubated with TEV protease for SUMO tag cleavage during overnight dialysis into 20 mM Tris pH 8.0, supplemented with 5% glycerol and 1 mM TCEP. Following cleavage confirmation, the sample was run on anion exchange chromatography with a 0–350 mM sodium chloride gradient. To remove TEV and further purify c-Abl, the sample was run through size-exclusion chromatography (SEC) using an S75 or S200 column, followed by concentration to 50–150 μM. Aliquots were flash-frozen and stored at -80 °C until further use. Co-expression of YopH was essential to counteract c-Abl toxicity in *E. coli*, and a gradient Ni-NTA purification step was employed to improve separation of c-Abl from YopH.

To generate αS-pY₃₉, wild type (WT) αS was prepared in 50 mM Tris, 150 mM NaCl, pH 7.5, at a final concentration of 50–100 μM. c-Abl was added at a molar ratio of 0.0436 equivalents relative to αS, following an established literature protocol¹². The reaction was initiated by the addition of Mg-ATP (100 mM) and MgCl₂ (1 M) and incubated at 30 °C for 2–4 hours. Phosphorylation progress was monitored by MALDI-MS, and the reaction was halted when approximately 50% modification was achieved. Occasionally, degraded αS was observed, likely due to non-specific cleavage by contaminating TEV. To remove unreacted c-Abl and separate phosphorylated from unmodified αS, the reaction mixture was concentrated and subjected to either SEC (Superdex Increase 75 column) or HPLC (C4 column). The

eluted fractions were analyzed by MALDI-MS to confirm phosphorylation and ensure product purity. The final products were characterized using phos-tag SDS-PAGE and analytical HPLC.

I have additionally created a c-Abl plasmid where TEV recognition sequence is removed so that SUMO could be cleaved more specifically with a SUMO protease Ulp-1. Further investigations are necessary to evaluate the utility of this strategy.

§7.7 Synthesis of thioether acetylation mimics (Thiol-ene addition)

Thiol-ene reactions were performed in acetate buffer (pH~ 4). The buffer was degassed for 10 min, using a syringe-needle attached to a balloon filled with argon gas. Then reaction mixture was prepared in a scintillation vial with a stir bar: α S Cys mutants ~50-100 μ M, 15 mM reduced glutathione, 5 mM VA-044, 50 mM *N*-vinylacetamide, 100 mM methionine. The mixture was then blown with argon for 10 min (the mixture was too viscous for needle bubbling). To run the reaction, the vial was hung in a photoreactor equipped with 365 nm UV light and the reaction was stirred for 30 min. Reaction was monitored by analytical C4 column and purified over semi-preparative C4 column.

§7.8 Synthesis of AcLys thioamide analog (^{AcS}K)

The procedures for the synthesis of H₂N-Lys(Ac^S)-OH were mostly adapted from a previously published method¹³. Boc-Lys-OH (6.0 mmol) was weighed into a 100 ml flask with a stir bar. The round bottom flask was immobilized and ethanol (10 mL) was added. 10% w/v sodium carbonate aq. (10 mL) and ethyl

dithioacetate (6.6 mmol) were subsequently added, with sufficient stirring between each addition. This reaction was performed overnight. For work-up, 20 mL water was added and 3 M HCl was added until the pH reached about 3, and the aqueous layer was then extracted three times with 15 ml DCM. The extract was dried over sodium sulfate, and the filtrate was evaporated to an orange foam (1.1g, 60% yield, purity of the product Boc-Lys(Ac^S)-OH indicated by LC-MS). For Boc deprotection, this orange foam was dissolved into 4N HCl in dioxane and reacted for few hours. The precipitate was washed with cold dioxane and ether, then dissolved into water and lyophilized.

§7.9 Fluorescent labeling

To fluorescently label α S Cys mutants, the protein stocks in 20 mM Tris, 50 mM NaCl, pH 7.4 were incubated with 2-10 eq. TCEP, then 10 eq. Atto 488-maleimide dye was added and incubated at room temperature for 2-4 hours or at 4 °C for overnight until product formation was observed by MALDI-MS. The product was purified by HPLC over a C4 column and dialyzed into 20 mM Tris, 50 mM NaCl, pH 8.

§7.10 Circular Dichroism (CD)

α S samples were filtered through 100 kDa-cutoff spin concentrators and the concentrations were determined by UV-Vis absorbance. Based on the quantification, all the α S samples were first diluted to 15 μ M with 1x PBS. Samples for CD acquisition were then prepared in triplicate by dilution of the protein stock solutions using 4.3 mM Na₂HPO₄, 1.47 mM KH₂PO₄, pH 7.4, and mixing with 100 mM sodium dodecylsulfate (SDS) in 4.3 mM Na₂HPO₄, 1.47 mM KH₂PO₄, pH 7.4 to yield samples composed of 5

μM αS with 10 mM SDS in 45.7 mM NaCl, 0.9 mM KCl, 4.3 mM Na_2HPO_4 , 1.47 mM KH_2PO_4 , pH 7.4. CD spectra were acquired on a JASCO J-1500 spectrometer in quartz cuvettes with a path length of 1 mm at 25 °C. Spectra were collected over the range of 190-260 nm using a 1 nm data pitch, 2 nm bandwidth, 8 s data integration time and 50 nm/min scanning speed. At each wavelength, spectra were background subtracted for buffer blank and corrected for concentration, path length, and number of residues as described by the following equation, where θ_{sample} and θ_{blank} refer to raw ellipticity values for the sample and buffer blank, respectively, ϵ is the path length of the cuvette, c is the protein concentration, and n is the number of residues.

$$[\theta] = \frac{((\theta_{\text{sample}} - \theta_{\text{blank}}) - (\theta_{\text{sample},260\text{nm}} - \theta_{\text{blank},260\text{nm}}))}{10 \times \epsilon \times c \times n} \times 10^{-3}$$

To determine the effects on helicity, the $[\theta_{222}]$ value acquired for each acetylated αS was normalized by the $[\theta_{222}]$ value of αS WT.

§7.11 Protein aggregation kinetics and percentage incorporation into fibrils

Aggregation of αS monomer seeded by preformed fibrils (PFFs) of WT αS was performed with 100% WT αS or with mixtures of 10% or 25% acetylated αS or αS Gln mutants. The seeding experiments were carried out by agitation at 1400 rpm at 37 °C and monitored by ThT. αS WT monomer in buffer (1x phosphate-buffered saline (PBS), pH 7.4) was prepared as a 40 μM stock solution and a 50 μL aliquot was added to each well of a 96-well half area clear bottom plate (6 replicates per one construct). The plate was sealed with a plastic film and incubated at 37 °C for 30 min before aggregation. PFF seeds were prepared by resuspending fibrils in PBS to make a 4 μM stock solution and freshly sonicating in an

Eppendorf tube in an ice bath (2 min, 1 s ON, 1 s OFF). A 50 μ L aliquot of sonicated seeds was added to monomers in each well (10% seeds). Samples were shaken on an IKA MS3 orbital shaker set to 1400 rpm at 37 °C. At each time point, ThT fluorescence was measured on a Tecan SPARK platereader (excitation: 450 nm, emission: 485 nm, emission bandwidth: 5 nm, integration time: 40 μ s). The extent of aggregation was determined based on normalized fluorescence intensity at 485 nm calculated from the minimum intensity and maximum intensity of each replicate. The data points were fit using Graphpad Prism software with the nonlinear regression model using the following equation:

$$y = Mi + \frac{Ma - Mi}{1 + \left(\frac{T_{1/2}}{x}\right)^z}$$

where M_i and M_a are the minimal and maximum y values, respectively, $T_{1/2}$ is the time at the mid-point of aggregation, and z is a parameter that determines the steepness of the curve. For the plots in Figure 4, Aggregation time was normalized to $T_{1/2}$ of the WT control, performed in parallel, and minimum and maximum fluorescence values were also normalized.

After the final time point, samples were pelleted at maximum speed on a tabletop centrifuge for 90 min. The supernatant was removed, and pellet was resuspended in the original volume of buffer. Samples were supplemented with SDS to a 25 mM final concentration, boiled for 20 min, and chilled on ice. Monomeric samples for calibration were prepared by 2-fold serial dilutions in water. All samples were analyzed by SDS-PAGE (4-15 or 4-20% acrylamide). Gels were stained with Coomassie Brilliant Blue dye. Quantification of the intensity of bands was done using the ImageJ software (National Institutes of Health; Bethesda, MD, USA). Values reported for aggregation kinetics and monomer incorporation are the average and standard error of mean taken from independent replicates.

§7.12 Preparation of synthetic vesicles

Lipid vesicles were prepared by extrusion through porous membranes. A mixture in 50:50 molar ratio of 1-palmitoyl-2-oleoyl-sn-glycero-3-phosphoserine (POPS) and 1-palmitoyl-2-oleoyl-sn-glycero-3-phosphocholine (POPC) were drawn from chloroform stock and dried under nitrogen gas to form a film inside a glass vial. Films were desiccated under vacuum and re-hydrated in 20 mM 3-(*N*-morpholino) propanesulfonic acid (MOPS), 147 mM NaCl, 2.7 mM KCl, pH 7.4. Ten freeze-thaw cycles consisting of cooling in liquid nitrogen for 40 s and warming in a 60 °C water bath for 2 min were performed to aid the formation of uniformly sized vesicles. With syringes, vesicles were then extruded 31 times through stacked 50 nm pore membranes held in place inside an extruder. Vesicles were determined by dynamic light scattering (DLS) to be monodisperse and distributed uniformly around 80 nm in diameter, consistent across different concentrations of all samples. All lipid vesicles were prepared fresh and used within 48 h of extrusion.

§7.13 Fluorescence correlation spectroscopy (FCS)

Fluorescence correlation spectroscopy (FCS) experiments to study the binding of α S-^{Ac}K₄₃C⁴⁸⁸₁₁₄ and α S-^{Ac}K₈₀C⁴⁸⁸₁₁₄, including preparation of synthetic lipid vesicles, collection of FCS data, and data analysis, were carried out as described previously for arginylated α S.³ Eight-well chambered coverglasses (Nunc, Rochester, NY, USA) were prepared by plasma cleaning followed by incubation overnight with polylysine-conjugated polyethylene glycol (PEG-PLL), prepared using a modified Pierce PEGylation protocol (Pierce, Rockford, IL, USA). PEG-PLL coated chambers were rinsed with and stored in Milli-Q

water until use. FCS measurements were performed on a lab-built instrument based on an Olympus IX71 microscope with a continuous emission 488 nm DPSS 50 mW laser (Spectra-Physics; Santa Clara, CA, USA). All measurements were made at 20 °C. The laser power entering the microscope was adjusted to 4.5 μW. Fluorescence emission collected through the objective was separated from the excitation signal through a Z488rdc long pass dichroic filter and an HQ600/200m bandpass filter (Chroma; Bellows Falls, VT, USA). Emission signal was focused onto the aperture of a 50 μm optical fiber. Signal was amplified by an avalanche photodiode (Perkin Elmer; Waltham, MA, USA) coupled to the fiber. A digital autocorrelator (Flex03Q-12, correlator.com; Bridgewater, NJ, USA) was used to collect 10 autocorrelation curves of 10 seconds for each measurement of free protein in buffer without lipids or 30 autocorrelation curves of 30 seconds for each measurement in the presence of lipid vesicles. Fitting was done using lab-written code in MATLAB (The MathWorks; Natick, MA, USA).

To determine the diffusion time of each protein construct, each αS variant labeled with Atto 488 was measured in buffer without lipid. The average of 10 autocorrelation curves was fit to a 1-component autocorrelation function:

$$G(\tau) = \frac{1}{N} \left(\frac{1}{1 + \frac{\tau}{\tau_1}} * \left(\frac{1}{1 + \frac{s^2\tau}{\tau_1}} \right)^{1/2} \right)$$

where $G(\tau)$ is the autocorrelation function, N is the number of molecules in the focal volume, τ_1 is the diffusion time of αS, and s is the radial-to-axial ratio of the excitation volume. The counts per molecule (CPM) for each sample was calculated by dividing the average intensity (Hz) of the measured signal by the number of molecules N . The normalized CPM of each αS was calculated by dividing by the CPM of freely diffusing fluorescent standard Alexa Fluor 488.

§7.14 Vesicle binding affinity

α S constructs labeled with Atto488 were examined in the presence of varying concentrations (0.001 mM to 0.5 mM lipid) of lipid vesicles consisting of 50:50 POPS/POPC. The average of 30 autocorrelation curves was fit to a 2-component equation:

$$G(\tau) = \frac{1}{N} \left(A * \frac{1}{1 + \frac{\tau}{\tau_1}} * \left(\frac{1}{1 + \frac{s^2\tau}{\tau_1}} \right)^{1/2} + Q * (1 - A) * \frac{1}{1 + \frac{\tau}{\tau_2}} * \left(\frac{1}{1 + \frac{s^2\tau}{\tau_2}} \right)^{1/2} \right)$$

where $G(\tau)$ is the autocorrelation function, N is the number of molecules in the focal volume, τ_1 is the characteristic diffusion time of α S, τ_2 is the characteristic diffusion time of the vesicles, s is the radial-to-axial ratio of the excitation volume, Q is the ratio of the brightness of vesicle-bound α S relative to α S, and A is the fraction of free α S. When fitting the autocorrelation curves for α S in the presence of lipid vesicles, the diffusion time of bound and unbound α S were respectively fixed to experimentally determined values. The diffusion time of unbound protein, τ_1 , was determined by measurements of the protein in buffer without lipids. Since bound protein diffuses with the vesicles to which they are bound, the diffusion time of the vesicles, τ_2 , was determined by measurements of the protein in the presence of a concentration of vesicles that gave the maximum diffusion time (0.1 mM lipid). In the binding assay, the fraction of α S bound at each lipid concentration was obtained from the fit to each autocorrelation curve. Averages and standard deviations were calculated from at least 3 independent measurements performed on separate days at each lipid concentration. The resulting binding curve was fit to the following equation, from which the $K_{d,app}$ was determined.

$$A = \frac{B_{max}x}{K_{d,app} + x}$$

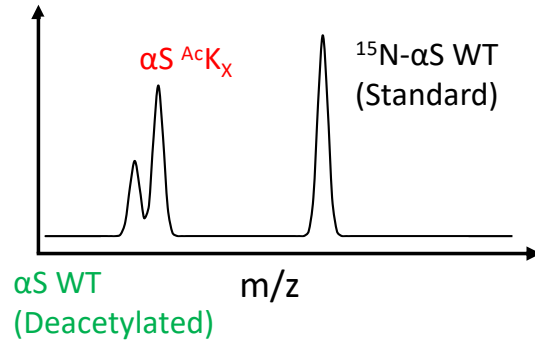
where A is the fraction of α S bound, x is the accessible lipid concentration, B_{\max} is the maximum fraction of α S bound, and $K_{d,app}$ is the apparent dissociation constant.

§7.15 Transmission electron microscopy (TEM)

TEM imaging was carried out on an FEI Tecnai T12 instrument (Hillborough, OR, USA) with an accelerating voltage of 100 kV. Fibril samples were prepared by shaking 100 μ M α S (WT with 25% ^{Ac}K or Gln mutants) at 1500 rpm for 72 hours, then diluted into water at a final concentration of 0.1 mg/mL. A 5 μ L drop of sample was deposited on glow discharged carbon Formvar coated 300-mesh Cu grids and allowed to rest for 1 min at room temperature. 5 μ L of stain (2% w/v uranyl acetate in water) was then applied to the grid. The liquid was wicked off with grid paper, and another 5 μ L of stain was applied and wicked off. Images were collected at magnifications ranging from 11000x to 42000x.

§7.16 HDAC8 deacetylation assay

Acetylated α S substrates (α S $^{Ac}K_X$) and ^{15}N -labeled α S WT were buffer-exchanged into HDAC8 reaction buffer (50 mM Tris, 137 mM NaCl, 2.7 mM KCl, 1 mM $MgCl_2$). Concentrations of each was quantified and deacetylation reaction was setup in triplicate, with final concentrations of HDAC8 8 μ M, 1.25 μ M α S $^{Ac}K_X$, 1.25 μ M ^{15}N - α S WT. The reaction was performed at room temperature for 24 h. MALDI-TOF-MS spectra were collected for each reaction, at 0 h and 24 h timepoints. Peak picking and peak area quantification, via fitting to Gaussian curves, for deacetylated product (^{14}N - α S WT) and the standard (^{15}N - α S WT) were performed on the Bruker flexAnalysis software.



The formula below was used to calculate the increase in %Deacetylated.

$$\Delta\%_{Deacetylated} = \frac{\Delta Peak Area (^{14}N \alpha S_{WT})}{\Delta Peak Area (^{15}N \alpha S_{WT})} = \left(\frac{Peak Area_{t=24} (^{14}N \alpha S_{WT})}{Peak Area_{t=24} (^{15}N \alpha S_{WT})} - \frac{Peak Area_{t=0} (^{14}N \alpha S_{WT})}{Peak Area_{t=0} (^{15}N \alpha S_{WT})} \right) \times 100$$

APPENDIX A: THE EFFECTS OF GLUTAMATE ARGINYLATION ON ALPHA-SYNUCLEIN: STUDYING AN UNUSUAL POST-TRANSLATIONAL MODIFICATION THROUGH SEMI- SYNTHESIS

This chapter is adapted from the published manuscript: Pan, B.; Kamo, N.; **Shimogawa, M.**; Huang, Y.; Kashina, A.; Rhoades, E.; Petersson, E. J., Effects of Glutamate Arginylation on α -Synuclein: Studying an Unusual Post-Translational Modification through Semisynthesis. *Journal of the American Chemical Society* **2020**, 142 (52), 21786-21798. DOI: 10.1021/jacs.0c10054

I performed semi-synthesis of two constructs, alpha-synuclein (α S) with glutamate arginylation at E₄₆, as a label-free version and with a fluorophore attachment.

§A.1 Summary

This work investigated the role of glutamate arginylation, a rarely studied post-translational modification (PTM), in modulating the functional and pathological aspects of alpha-synuclein (α S). To study the effects of glutamate arginylation, a semi-synthetic strategy was developed, integrating peptide synthesis, non-canonical amino acid mutagenesis, and native chemical ligation (NCL) to introduce this modification site-specifically into full-length α S. A protected arginylated glutamate analog and a novel ligation handle were synthesized to enable precise modification at individual or multiple sites. Biophysical characterization of the modified protein revealed that arginylation does not alter α S's native vesicle-binding function, as assessed by fluorescence correlation spectroscopy (FCS). However, aggregation studies demonstrated that arginylation at E₈₃, but not E₄₆, significantly slows fibril formation and reduces monomer incorporation into fibrils in a dose-dependent manner. Modification at both sites further delayed aggregation, further suggesting a potential neuroprotective effect.

§A.2 Relevant Methods

Production of recombinant α S constructs

Unnatural amino acid incorporation via amber codon suppression was used to produce C-terminal fragments for labeling with Atto 488. Plasmid containing the desired α S construct was transformed into *E. coli* pDULE-pXF cells with pre-transformed plasmids encoding propargyl-tyrosine (Ppy or π) synthetase and tRNA. Expression was carried out as above, except cells were grown in M9 minimal media, and π (220 mg/L) was added to the culture at OD ~0.8 with a 10-min incubation prior to inducing expression with IPTG. After purification, the fragment was re-dissolved in 20 mM Tris pH 8 and labeled with Atto 488-azide (**Atto488-N₃**) via copper-catalyzed azide-alkyne cyclization. Catalytic mixture consisting of 2 equiv CuSO₄, 10 equiv Tris(3-hydroxypropyltriazolylmethyl)amine (THPTA), and 20 equiv sodium ascorbate was let sit for 10 min and added to the protein along with 2 equiv fluorophore. Labeled fragments were purified by HPLC over a C4 column. After lyophilization, fragments were redissolved in buffer (2 M guanidinium, 30 mM TCEP, 100 mM methoxyamine) to deprotect pyruvate-derived thiazolidines, and the product was purified by HPLC over a C4 column.

Native chemical ligation (NCL) for singly arginylated α S

Towards ligation between an expressed N-terminal fragment and a middle fragment (referred to as NCL1), the intein of α S fragment-MxeHis₆ was cleaved by stirring with 200 mM 2-mercaptoethane sulfonate sodium salt (MESNa) at 4 °C overnight to generate a thioester.¹ The protein fragment-thioester

was purified by RP-HPLC over a C4 column and lyophilized. To carry out NCL, fragment-MES thioester and partner peptide were both re-dissolved in NCL buffer (6M Gdn•HCl, 200 mM NaH₂PO₄, pH 7) to final concentration 1-3 mM. To the sample was added mercaptophenylacetic acid (MPAA) to 100 mM and TCEP to 50 mM final concentrations. The reaction was incubated at 37 °C with agitation at 500 rpm for several hours, monitored by MALDI-MS, and supplemented with TCEP as necessary. Product was reduced with a few μL of TCEP before purification by RP-HPLC.

For MPAA-mediated ligation between a product of NCL1 and a C-terminal fragment, peptide-acyl-hydrazide was dissolved in low pH NCL buffer (6M Gdn•HCl, 200 mM NaH₂PO₄, pH 3) for a final concentration of 2-3 mM and chilled to -15 °C in an ice-salt bath. Hydrazide to azide conversion² was achieved by adding 10 equiv NaNO₂ and agitating by magnetic stirring for 15 min at -15 °C. 40 equiv MPAA, pre-dissolved in NCL buffer pH 7.0, was added to the mixture, followed by the partner peptide. The reaction was warmed to room temperature, and the pH was adjusted to 6.8-7.0. TCEP was added to 40 mM final concentration, and the reaction was incubated at 37 °C with agitation at 500 rpm. Product formation was monitored by MALDI-MS. To convert cysteines and penicillamines used in ligation to the respective native alanines and valines, the purified NCL product was re-dissolved in pH 7 NCL buffer and incubated with 20 mM radical initiator VA-044, 100 mM glutathione (GSH), and 250 mM TCEP in an argon-purged tube at 37 °C overnight. The desulfurized full-length products were purified by RP-HPLC over a C4 column.

Alternatively, the same ligation was performed using methyl thioglycolate (MTG) as a thioester, which allows for one-pot desulfurization. For MTG-mediated ligation between a product of NCL1 and a C-terminal fragment, purified product of NCL1 was re-dissolved in NCL buffer pH 3, chilled to -15 °C with stirring, converted to thioester by addition of 10 equiv NaNO₂ followed by 100 equiv of MESNa, supplemented with TCEP, and purified by RP-HPLC over a C4 column. The purified intermediate,

bearing C-terminal MES thioester, was dissolved together with its ligation partner in NCL buffer pH 7 to 2 mM final concentration. 100 equiv MTG was added from a stock dilution in NCL buffer pH 7. The reaction was supplemented with TCEP to a 40 mM final concentration, adjusted to pH 6.8-7.0, and incubated at 37 °C with agitation at 500 rpm overnight. To carry out one-pot desulfurization, NCL reaction mixture was diluted with NCL buffer pH 7 so that final protein concentration was 0.4-0.8 mM. The mixture was incubated with 20 mM radical initiator VA-044, 100 mM GSH, and 250 mM TCEP in an argon-purged tube at 37 °C overnight and purified as above.

§A.3 Results

During the synthesis of α S fragments containing E^{Arg}₄₆, there was an interesting finding with copper's role in deprotection, click-labeling, and oxidation. Methoxyamine treatment successfully deprotected thiazolidine-protected α S₅₆₋₁₄₀-C₅₆ π ₁₁₄, but subsequent click labeling using Atto488-azide in the presence of a copper catalytic mixture resulted in an unexpected +16 Da shift in MALDI-MS, which seems to be oxidation of the N-terminal cysteine, as the peptide is unreactive in NCL. To circumvent this, an alternative approach was employed in which thiazolidine-protected α S₅₆₋₁₄₀-C₅₆ π ₁₁₄ underwent simultaneous deprotection and click-labeling under an argon atmosphere, yielding a cleanly labeled product except for residual pyruvate-derived thiazolidines. A final methoxyamine deprotection step produced the fully processed α S₅₆₋₁₄₀-C₅₆ π ⁴⁸⁸₁₁₄ fragment in 41% yield over all steps.

To generate full-length α S-E^{Arg}₄₆, NCL was performed between α S₁₋₃₆-MES and α S₃₇₋₅₅-V*₃₇E^{Arg}₄₆ hydrazide, yielding the α S₁₋₅₅-V*₃₇E^{Arg}₄₆ intermediate in 79%. A second ligation with α S₅₆₋₁₄₀-C₅₆ resulted in the full-length product, which was then desulfurized, yielding α S-E^{Arg}₄₆ in 4.1% overall yield. To improve upon this, an alternative approach using methyl thioglycolate (MTG) instead of 4-

mercaptophenylacetic acid (MPAA) was tested to allow for in situ desulfurization, eliminating an intermediate purification step. While direct use of MTG in hydrazide activation resulted in side reactions, conversion of $\alpha\text{S}_{1-55}\text{-V}^*_{37}\text{E}^{\text{Arg}}_{46}$ hydrazide to a MES thioester before ligation successfully prevented cysteine oxidation and led to a more efficient ligation. The final MTG-mediated approach improved the overall yield of $\alpha\text{S-E}^{\text{Arg}}_{46}$ to 14.4% and $\alpha\text{S-E}^{\text{Arg}}_{46}\pi^{488}_{114}$ to 37.7%, representing a significant increase compared to the MPAA-mediated strategy.

APPENDIX B: CYSTEINE-BASED MIMIC OF ARGINYLATION REPRODUCES NEUROPROTECTIVE EFFECTS OF THE AUTHENTIC POST-TRANSLATIONAL MODIFICATION ON ALPHA-SYNUCLEIN

This chapter is adapted from the previously published manuscript: Pan, B.; **Shimogawa, M.**; Zhao, J.; Rhoades, E.; Kashina, A.; Petersson, E. J. Cysteine-Based Mimic of Arginylation Reproduces Neuroprotective Effects of the Authentic Post-Translational Modification on α -Synuclein. *Journal of the American Chemical Society* **2022**, 144 (17), 7911-7918. DOI: 10.1021/jacs.2c02499.

I performed *in vitro de novo* aggregation experiments, *in vitro* seeding experiments, transmission electron microscopy and proteinase K digestion assay.

§B.1 Summary

This manuscript explores an alternative strategy for incorporating arginylation into alpha-synuclein (α S). Arginylation, a post-translational modification (PTM) involving the enzymatic transfer of arginine to aspartate or glutamate sidechains, has been shown to exhibit neuroprotective effects by modulating α S aggregation. Previous studies have employed native chemical ligation (NCL) to generate arginylated α S, but this approach is labor-intensive and yields are often low, limiting its broader applicability. This manuscript introduces a method for incorporating a mimic of arginylation into α S using bromoacetyl arginine, which reacts with site-specific cysteine mutants, enabling orthogonal labeling such as fluorophore conjugation. We validate this modification by assessing vesicle binding affinity, aggregation kinetics, and monomer incorporation into fibrils, comparing these properties to those of authentically arginylated α S produced via NCL. Additionally, we evaluate the fibril seeding potential of arginylated α S

in cultured neurons. Consistent with authentic arginylation, the mimic modification preserves α S's native function while modulating its aggregation behavior and reducing fibril formation. Both mimic and authentic arginylation suppress α S aggregation in neuronal cells. This manuscript provides further insight into the neuroprotective effects of α S arginylation and establishes a new approach for studying this PTM in proteins that are challenging to modify through NCL.

§B.2 Relevant Methods

Protein aggregation kinetics and percent incorporation into fibrils

Aggregation of α S-C^{Arg}₄₆, α S-C^{Arg}₈₃, and α S-C^{Arg}₄₆C^{Arg}₈₃ was carried out by agitation at 1300 rpm at 37 °C and monitored by Congo Red as described previously for authentically arginylated α S.⁷⁴ Protein samples (100 μ M total concentration in monomer units) in buffer (20 mM Tris, 100 mM NaCl, pH 7.5) were prepared in triplicate in Eppendorf tubes. Samples were shaken in an Ika MS3 orbital shaker set to 1300 rpm at 37 °C. At each time point, a 10 μ L aliquot from each sample was added to 140 μ L Congo Red solution (20 μ M in 20 mM Tris, 100 mM NaCl, pH 7.5) in a clean Eppendorf tube and incubated for 10-15 min. Samples were transferred to 96-well clear bottom plates. Absorbance was measured on a Tecan M1000 platereader using a 230-700 nm range, 1 nm step size, 25 flashes/read. The extent of aggregation was determined based on the ratio of absorbance at 540 nm/480 nm. The data points were fit using Graphpad Prism software with the nonlinear regression model using the following equation:

$$y = Mi + \frac{Ma - Mi}{1 + \left(\frac{T_{1/2}}{x}\right)^z}$$

where M_i and M_a are the minimal and maximum y values, respectively, $T_{1/2}$ is the time at the mid-point of aggregation, and z is a parameter that determines the steepness of the curve.

After the final time point, samples were spun down at maximum speed on a tabletop centrifuge for 90 min. The supernatant was removed, and pellet was resuspended in the original volume of buffer. Samples were supplemented with sodium dodecyl sulfate (SDS) to a 25 mM final concentration, boiled for 20 min, and chilled on ice. Monomeric samples for calibration were prepared by 2-fold serial dilutions in water. All samples were analyzed by SDS-PAGE (4-15 or 4-20% acrylamide). Gels were stained with Coomassie Brilliant Blue dye. Quantification of the intensity of bands was done using the ImageJ software (National Institutes of Health, Bethesda, Maryland). Values reported for aggregation kinetics and monomer incorporation are the average and standard deviation taken from independent triplicates.

In vitro aggregation seeding experiments

Aggregation of α S WT monomer seeded by preformed fibrils (PFFs) of WT or WT with 5% α S- C^{Arg}_{46} , α S- C^{Arg}_{83} , α S- $C^{Arg}_{46}C^{Arg}_{83}$, α S- E^{Arg}_{46} , α S- E^{Arg}_{83} , or α S- $E^{Arg}_{46}E^{Arg}_{83}$ was carried out by agitation at 1400 rpm at 37 °C and monitored by Thioflavin T (ThT). α S WT monomer in buffer (1x phosphate-buffered saline (PBS), pH 7.4) was prepared as 40 μ M stock solution and a 50 μ L aliquot was added to each well of a 96-well half area clear bottom plate (6 replicates per one construct). The plate was sealed with a plastic film and incubated at 37 °C for 30 min before aggregation. PFF seeds were prepared by resuspending fibrils in PBS to make a 4 μ M stock solution and freshly sonicating in an Eppendorf tube in an ice bath (2 min, 1 s ON, 1 s OFF). A 50 μ L aliquot of sonicated seeds was added to monomers in each well (10% seeds). Samples were shaken on an IKA MS3 orbital shaker set to 1400 rpm at 37 °C. At each time point, ThT fluorescence was measured on a Tecan SPARK platereader (excitation: 450 nm, emission: 485 nm,

emission bandwidth: 5 nm, integration time: 40 μ s). The extent of aggregation was determined based on normalized fluorescence intensity at 485 nm calculated from the minimum intensity and maximum intensity of each replicate. Kinetic data were fit using Prism as described above for Congo Red assays. After the final time point, samples were spun down at maximum speed on a tabletop centrifuge for 90 min. Quantification of monomer incorporation to fibrils was performed as described above in the unseeded aggregation assays.

Transmission Electron Microscopy (TEM)

TEM imaging was carried out on an FEI Tecnai T12 instrument with an accelerating voltage of 100 kV. Fibril samples obtained from unseeded aggregations described above were centrifuged and stored at -80 °C as dry pellets, then resuspended in 20 mM Tris, 100 mM NaCl pH 7.5. A 3 μ L drop of sample was deposited on glow discharged carbon Formvar coated 300-mesh Cu grids and allowed to rest for 1 min at room temperature. 3 μ L of stain (2% w/v uranyl acetate in water) was then applied to the grid. The liquid was wicked off with grid paper, and another 3 μ L of stain was applied and wicked off. Images were collected at magnifications ranging from 11000x to 42000x.

Proteinase K Digestion Assay

Proteinase K (P-2308) was obtained from Millipore Sigma and stock solutions were prepared in Dulbecco's PBS. 3 μ g PFFs from the endpoint of unseeded aggregation (WT α S or 5% α S-C^{EArg}₄₆, 5% α S-C^{EArg}₈₃, or 5% α S-C^{EArg}₄₆C^{EArg}₈₃) assays were sonicated in an Eppendorf tube in an ice bath (2 min, 1 s ON, 1 s OFF) and digested with 2 μ g/mL of protease in Dulbecco's PBS. Digestions were performed in a final volume of 20 μ L and incubated at 37 °C for 10, 20, or 30 min. Digestions were stopped with 1 mM

phenylmethylsulfonyl fluoride (PMSF). Reaction samples were then boiled with SDS sample buffer for 15 min and resolved on NuPAGE Novex 12% Bis-Tris gels (Invitrogen). The gels were stained with a Coomassie Brilliant Blue dye solution (Imperial Protein Stain, Thermo Scientific). Experiments were performed in triplicate. Quantification of band intensity was done using ImageJ software. Results were analyzed by two-way ANOVA (α S construct and protease digestion time as factors) and pairwise comparisons were made using the Bonferroni multiple comparison test, both in GraphPad Prism software.

§B.3 Results

Mimic arginylation at either E₄₆ or E₈₃ slowed aggregation, with dual modification at both sites further reducing aggregation rates (Figure 32), consistent with previously reported data for authentic arginylation. Similar to the effects observed with authentic arginylation, α S mimic-arginylated at E₄₆ exhibited slowed aggregation at 10% dosing but did not significantly impact monomer incorporation into fibrils (Figure 32). In contrast, mimic arginylation at E₈₃ reduced fibril incorporation, though this effect was only significant when α S-CE^{Arg}₈₃ was present at 10%, suggesting that the mimic was slightly less potent than authentic arginylation at this site. The doubly modified α S-CE^{Arg}₄₆CE^{Arg}₈₃ construct also displayed decreased fibril incorporation, mirroring the effects observed for authentic arginylation. Overall, with the exception of the E₈₃ monomer incorporation data, the mimic constructs quantitatively reproduced the effects of authentic arginylation in fibril incorporation assays.

In contrast to *de novo* aggregation, where arginylation slowed fibril formation, seeding with α S preformed fibrils (PFFs) significantly increased the rate and extent of fibril incorporation for all arginylation constructs compared to WT PFFs (Figure 33). The similarity between authentic and mimic

arginylated PFF seeds suggests that arginylation affects different stages of the aggregation pathway, potentially influencing nucleation and elongation phases differently. These findings further motivate cell-based PFF seeding studies to determine which effect dominates in a physiological context. Apart from a slight difference between $\alpha\text{S-E}^{\text{Arg}_{46}}$ and $\alpha\text{S-CE}^{\text{Arg}_{46}}$ in their effects on aggregation rate, these results support the validity of the mimic as a functional substitute for authentic arginylation.

To assess whether arginylation affects αS fibril morphology, transmission electron microscopy (TEM) imaging was performed on 5% modified PFFs. No gross morphological differences were observed compared to WT PFFs. To further analyze fibril conformation, proteinase K digestion assays were conducted on 5% mimic-arginylated PFFs (Figure 34). No significant differences in band patterns were observed in the 10–15 kDa range, although differences in digestion kinetics were evident. Arginylation at site 46 significantly accelerated protease cleavage, with most full-length protein digested before the 10-minute time point. Arginylation at site 83 had minimal effects on digestion kinetics, except for a lower relative intensity of band 2. The absence of band 1 for this construct may be due to slight variations in PFF concentration. Dual arginylation accelerated digestion, though not as extensively as $\text{CE}^{\text{Arg}_{46}}$ alone. These differences in proteinase K digestion patterns suggest that arginylation at site 46 results in looser fibril packing.

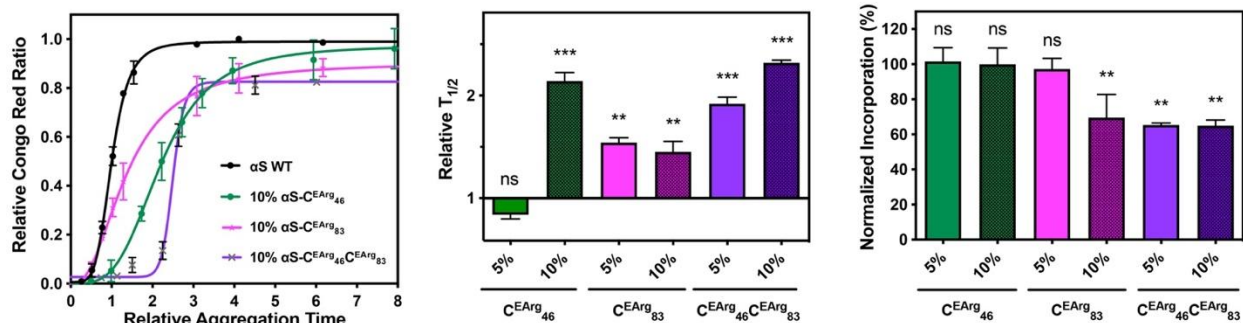


Figure 32. Aggregation kinetics and total monomer incorporation for mimic arginylated α S.

WT monomer starting material was mixed with different percentages of mimic arginylated α S, aggregated by shaking at 37 °C, and monitored by Congo Red. Left: Aggregation curves showing that mimic arginylation at either glutamate 46 or 83 slows aggregation of α S and that the doubly mimic arginylated α S slows aggregation further. Aggregation time shown relative to matched WT control for each trial. Center: Relative time to half completion of aggregation ($T_{1/2}$), normalized to that of WT. Results shown as mean with standard deviation ($n=3$) ** $p < 0.01$; *** $p < 0.001$; ns, not significant. Right: Aggregation end point samples were centrifuged to pellet fibrils for quantification by gel band density, from which percentage incorporation of each α S variant was calculated and normalized to that of WT. Results shown as mean with standard deviation ($n \geq 3$) ** $p < 0.01$; ns, not significant.

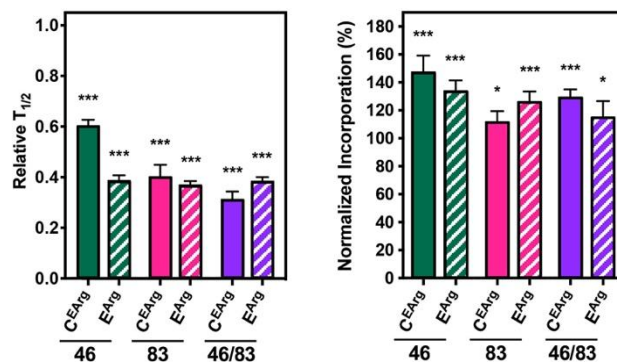


Figure 33. Aggregation kinetics and total monomer incorporation for seeded aggregation assays.

WT monomer starting material was mixed with various PFF seeds, and aggregated by shaking at 37 °C, and monitored by Thioflavin T. Left: Relative time to half completion of aggregation ($T_{1/2}$). Results shown as mean with standard deviation (n=6) **p < 0.01; ***p < 0.001; ns, not significant. Right: Aggregation end point samples were quantified as in Figure 2. Results shown as mean with standard deviation (n=6) *p < 0.05; **p < 0.01; ***p < 0.001.

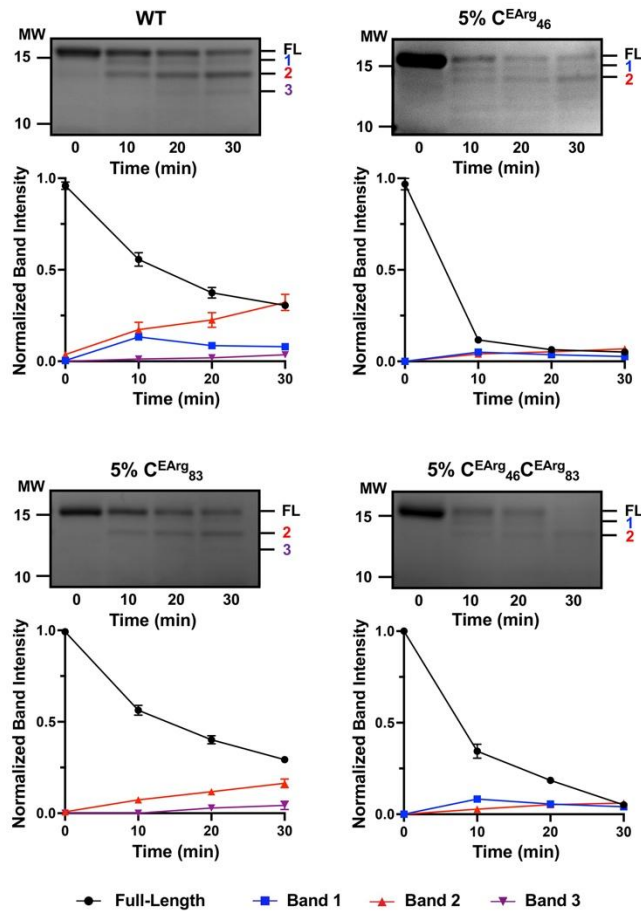


Figure 34. Proteinase K digestion of PFFs with 5% arginylation mimic.

Each type of PFF was mixed with Proteinase K and incubated at 37 °C for 10, 20, or 30 min. Digested reactions were resolved on 12% SDS-PAGE gels stained with Coomassie Brilliant Blue dye. Major bands are labeled on the right (FL: Full-length α S). Molecular weight (MW) marker masses are in kD. Each band intensity was normalized to the intensity of the uncleaved PFFs. Results shown as mean with standard error of the mean from 3 independent digestion experiments.

APPENDIX C: SYNTHESIS OF PEPTIDES AND PROTEINS WITH SITE-SPECIFIC GLUTAMATE ARGINYLATION

This chapter is adapted from the published manuscript: **Shimogawa, M.**; Huang, Y.; Pan, B.; Petersson, E. J. Synthesis of peptides and proteins with site-specific glutamate arginylation. In *Protein Arginylation*, Kashina, A. S. Ed.; Methods in Molecular Biology, Vol. 2620; Springer Nature, 2023.

The synthesis of peptide library is also documented in the following manuscript: MacTaggart, B.; **Shimogawa, M.**; Lougee, M.; Tang, H.-Y.; Petersson, E. J.; Kashina, A. Global analysis of post-translational sidechain arginylation using pan-arginylation antibodies. *Molecular & Cellular Proteomics* **2023**, 100664. DOI: <https://doi.org/10.1016/j.mcpro.2023.100664>

§C.1 Summary

This manuscript describes protocols for the site-specific incorporation of glutamate arginylation (E^{Arg}) into peptides and proteins using solid-phase peptide synthesis (SPPS) and protein semi-synthesis. These methods provide a controlled alternative to enzymatic arginylation, enabling a detailed investigation of the PTM. Applications of this approach include biophysical characterization, cell-based imaging studies, and proteomic profiling of E^{Arg} in human tissue samples.

The described workflow involves the synthesis of an E^{Arg} monomer unit with protecting groups suitable for Fmoc-based SPPS, allowing for the preparation of various peptide constructs. These include antigen peptides for generating E^{Arg} -specific antibodies, peptide libraries for developing a pan- E^{Arg} antibody, photo-crosslinkable peptides for interactome studies, and peptide fragments for use in protein semi-synthesis. The semi-synthetic process further involve recombinant expression and purification of

protein fragments, which are assembled via native chemical ligation (NCL). Additionally, an unnatural amino acid mutagenesis strategy is used to introduce a "click" chemistry handle for site-specific fluorescence labeling, which can be efficiently integrated into the ligation workflow. Finally, *in situ* desulfurization converts thiol-containing residues, such as cysteine to alanine or penicillamine to valine, yielding a fully assembled and modified protein.

Overall, this manuscript presents a versatile and scalable method for incorporating E^{Arg} at defined sites, facilitating a comprehensive study of its biological significance.

§C.2 Relevant Methods

Synthesis of the arginylated peptide library XXXXXE^{Arg}XXXXXC (X: mixture of 19 non-cysteine natural amino acids, methionine is replaced with norleucine to prevent oxidation issues) was performed on the 100 μ mol scale for generation of antibodies recognizing arginylation regardless of the surrounding sequence. A non-arginylated peptide library XXXXXEXXXXXC was synthesized in parallel for generation of negative-control antibodies.

2-chlorotrityl resin was swollen in v1:1 DCM (dichloromethane)/DMF (dimethylformamide) for 30 min. The first amino acid Cys was coupled using 2 equiv Fmoc-Cys(Trt)-OH at a concentration of 0.15 M in DMF and 4 equiv of *N,N*-diisopropylethylamine (DIPEA), reacted for 15 min at room temperature. Unreacted sites were capped with methanol. Fmoc deprotection was performed after stirring in 20v% piperidine/DMF for 5 min, repeated once, and the resin was adjusted to 100 μ mol.

For coupling of X residues, Isokinetic mixture was prepared by combining a mixture of 19 natural amino acids (240 equiv total per residue) at the ratio determined previously⁷⁵ (Table 2) with HOBt (240

equiv per residue). Coupling was carried out for an hour at room temperature, following activation of the amino acids by DIC (240 equiv, 3.716 mL). Fmoc deprotection was performed as described above. Coupling of Fmoc-Glu(Arg(Pbf)OtBu)-OH (2 equiv) was carried out at 37 °C for 1-2 h with shaking at 250 rpm, using 2 equiv of the amino acid in DMF with 1.9 equiv HBTU and 4 equiv DIPEA.

Peptide cleavage from the resin was performed using 30 μ L of Reagent K (82.5% v/v TFA, 5% w/v phenol, 5% v/v water, 5% v/v thioanisole and 2.5% v/v 1,2-ethanedithiol) per mg of resin and agitating for 1.5 h. Cocktail containing cleaved peptide was collected, and peptide was precipitated using at least 10-fold volume of diethyl ether. The crude pellet was dissolved in acetonitrile-water mixture and lyophilized.

Reagent	Equiv	MW (g/mol)	Weight for 1 mmol scale(g)
Fmoc-l-Ala-OH	8.16	311.33	2.5404528
Fmoc-l-Arg(Pbf)-OH	15.6	648.77	10.120812
Fmoc-l-Asn(Trt)-OH	12.48	596.67	7.4464416
Fmoc-l-Asp(tBu)-OH	8.4	411.45	3.45618
Fmoc-l- Gln(Trt)-OH	12.72	610.7	7.768104
Fmoc-l-Glu(tBu)-OH	8.64	425.47	3.6760608
Fmoc-Gly-OH	6.96	297.31	2.0692776
Fmoc-l-His(Trt)-OH	8.4	619.71	5.205564
Fmoc-l-Ile-OH	41.76	353.41	14.7584016

Fmoc-l-Leu- OH	11.76	353.41	4.1561016
Fmoc-l-Lys(Boc)-OH	14.88	468.54	6.9718752
Fmoc- l-Phe-OH	6	387.43	2.32458
Fmoc-l-Pro-OH	10.32	337.37	3.4816584
Fmoc-l-Ser(tBu)-OH	6.72	383.44	2.5767168
Fmoc-l-Thr(tBu)-OH	11.52	397.46	4.5787392
Fmoc-l-Trp(Boc)-OH	9.12	526.58	4.8024096
Fmoc-l- Tyr(tBu)-OH	9.84	459.53	4.5217752
Fmoc-l-Val-OH	27.12	339.39	9.2042568
Fmoc-l-Nle-OH	9.12	353.41	3.2230992
19 amino acids total	240		

Table 2. Components of isokinetic mixture.

§C.3 Results

This study shows successful synthesis of the E^{Arg} monomer unit for Fmoc-based SPPS, followed by peptides for generating E^{Arg}-specific antibodies, peptide libraries for developing a pan-E^{Arg} antibody (Figure 35), photo-crosslinkable peptides for interactome studies, and peptide fragments for use in protein semi-synthesis.

Protein semi-synthesis involved three fragment ligation, where the middle peptide has glutamate arginylation. Protein expression and purification steps were described, to generate the N-terminal fragment with thioester functionalization and C-terminal fragments, either with or without click handle. The ligation part includes two strategies: (i) the use of 4-Mercaptophenylacetic acid (MPAA) as a thiol additive, which allows thioesterification and NCL without purifying the intermediate thioester, thanks to its quenching ability of excess sodium nitrite. The ligation product needs to be purified before desulfurization reaction due to radical quenching ability of MPAA⁴⁷; (ii) the use of methyl thioglycolate (MTG) as a thiol additive, which allows NCL and desulfurization reaction in a one-pot manner, due to its poor ability of radical quenching.

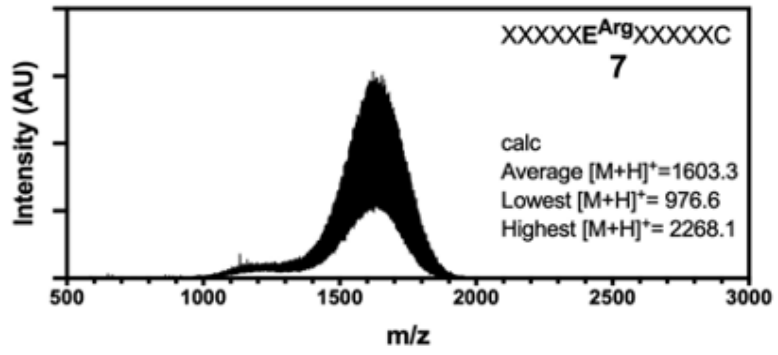


Figure 35. MALDI-MS of product peptide library XXXXXE^{Arg}XXXXXC

APPENDIX D: SEMI-SYNTHETIC COA-ALPHA-SYNUCLEIN CONSTRUCTS TRAP N-TERMINAL ACETYLTRANSFERASE NATB FOR BINDING MECHANISM STUDIES

This chapter is adapted from the published manuscript: Pan, B.; Gardner, S. M.; Schultz, K.; Perez, R. M.; Deng, S.; **Shimogawa, M.**; Sato, K.; Rhoades, E.; Marmorstein, R.; Petersson, E. J. Semi-Synthetic CoA- α -Synuclein Constructs Trap N-Terminal Acetyltransferase NatB for Binding Mechanism Studies. *Journal of the American Chemical Society* **2023**. DOI: 10.1021/jacs.3c03887.

I performed the semi-synthesis of CoA- α -Synuclein (CoA attachment, ligation and desulfurization).

§D.1 Summary

This manuscript investigates the interaction between human N-terminal acetyltransferase B (hNatB) and alpha-synuclein (α S). NatB catalyzes the N-terminal acetylation of α S, which modulates its lipid vesicle binding and amyloid fibril formation. While the molecular details of how NatB recognizes the N-terminus of α S are known, the role of the remainder of the protein in enzyme interaction remains unclear.

To address this, we synthesized a bisubstrate inhibitor of hNatB using native chemical ligation (NCL), consisting of coenzyme A conjugated to full-length α S, with two fluorescent probes incorporated for conformational studies. Using cryo-electron microscopy (cryo-EM), we determined that beyond the first few residues, α S remains largely disordered within the hNatB complex. Single-molecule Förster resonance energy transfer (smFRET) experiments further revealed that α S undergoes a conformational expansion at the C-terminal domain upon binding to hNatB. Computational modeling based on cryo-EM and smFRET data provided insights into how these structural changes impact hNatB's substrate recognition and inhibition mechanisms.

Beyond characterizing α S and hNatB interactions, this study highlights a powerful strategy for investigating challenging structural biology targets by integrating protein semi-synthesis, cryo-EM, smFRET, and computational modeling, expanding the toolkit for studying enzyme-substrate interactions at the molecular level.

§D.2 Relevant methods

The reaction for CoA- α S₁₋₁₈-NHNH₂ with coenzyme A lithium salt at room temperature overnight also afforded the desired product. In this case, the resulting hydrazide was converted to the corresponding thioester for easy purification. Specifically, an aliquot of the lyophilized bromoacetyl- α S₁₋₁₈-NHNH₂ (6.7 mg, 3.3 μ mol) was redissolved in TEAB buffer pH 8 to a final concentration of 3 mM. Two equiv coenzyme A lithium salt was added, and the mixture was allowed to react at room temperature overnight. Product formation was confirmed by MALDI-MS. The alkylated product was roughly purified by RP-HPLC over a C4 column. To a solution of the hydrazide (2.2 mg, 0.72 μ mol) in low pH buffer (6 M guanidinium, 200 mM NaH₂PO₄, pH 3.0) was added 10 equiv NaNO₂ at -15 °C in an ice-salt bath. After 15 min reaction at -15 °C, 100 equiv MESNa was added to the mixture. The pH was adjusted to 7.0 and the reaction was let sit for 30 min at room temperature. The desired thioester was purified by RP-HPLC over a C4 semi-preparative column.

CoA- α S was synthesized through the NCL of CoA- α S₁₋₁₈-MES (0.22 μ mol) and 1.8 equiv α S₁₉₋₁₄₀-C₁₉ (0.40 μ mol). These fragments were dissolved in NCL buffer (0.22 mL, 6 M guanidinium, 200 mM Na₂HPO₄, 100 mM MPAA, 50 mM TCEP, pH 7) and the reaction was incubated at 37 °C. Product formation was monitored by MALDI-MS and analytical HPLC. After completion of the NCL, the pH was

adjusted to 2 and MPAA was extracted with Et₂O thoroughly. The residual Et₂O was removed by argon stream and the pH was adjusted back to 7. To the resulting solution was added desulfurization buffer (0.75 mL, 6 M guanidinium, 200 mM Na₂HPO₄, 500 mM TCEP, 200 mM MESNa, pH 7) and 100 equiv VA-044.

§D.3 Results

A synthesis of CoA- α S using ligation at residues 18/19 based on the route developed for labeled fluorescently labeled CoA- α S produced protein in a slightly higher yield than the original route using ligation at 10/11.

BIBLIOGRAPHY

- 1 Iwai, A. *et al.* The precursor protein of non-A beta component of Alzheimer's disease amyloid is a presynaptic protein of the central nervous system. *Neuron* **14**, 467-475 (1995).
[https://doi.org/10.1016/0896-6273\(95\)90302-x](https://doi.org/10.1016/0896-6273(95)90302-x)
- 2 Benskey, M. J., Perez, R. G. & Manfredsson, F. P. The contribution of alpha synuclein to neuronal survival and function - Implications for Parkinson's disease. *J Neurochem* **137**, 331-359 (2016).
<https://doi.org/10.1111/jnc.13570>
- 3 Emamzadeh, F. N. Alpha-synuclein structure, functions, and interactions. *J Res Med Sci* **21**, 29 (2016). <https://doi.org/10.4103/1735-1995.181989>
- 4 Uversky, V. N. & Fink, A. L. Amino acid determinants of alpha-synuclein aggregation: putting together pieces of the puzzle. *FEBS Lett* **522**, 9-13 (2002). [https://doi.org/10.1016/s0014-5793\(02\)02883-1](https://doi.org/10.1016/s0014-5793(02)02883-1)
- 5 Fauvet, B. *et al.* α -Synuclein in central nervous system and from erythrocytes, mammalian cells, and Escherichia coli exists predominantly as disordered monomer. *J Biol Chem* **287**, 15345-15364 (2012). <https://doi.org/10.1074/jbc.M111.318949>
- 6 Poewe, W. *et al.* Parkinson disease. *Nat Rev Dis Primers* **3**, 17013 (2017).
<https://doi.org/10.1038/nrdp.2017.13>
- 7 Meade, R. M., Fairlie, D. P. & Mason, J. M. Alpha-synuclein structure and Parkinson's disease – lessons and emerging principles. *Molecular Neurodegeneration* **14**, 29 (2019).
<https://doi.org/10.1186/s13024-019-0329-1>

- 8 Ghosh, D., Mehra, S., Sahay, S., Singh, P. K. & Maji, S. K. α -synuclein aggregation and its modulation. *Int J Biol Macromol* **100**, 37-54 (2017).
<https://doi.org/10.1016/j.ijbiomac.2016.10.021>
- 9 Baba, M. *et al.* Aggregation of alpha-synuclein in Lewy bodies of sporadic Parkinson's disease and dementia with Lewy bodies. *Am J Pathol* **152**, 879-884 (1998).
- 10 Goedert, M. Alpha-synuclein and neurodegenerative diseases. *Nat Rev Neurosci* **2**, 492-501 (2001). <https://doi.org/10.1038/35081564>
- 11 Spillantini, M. G. *et al.* Alpha-synuclein in Lewy bodies. *Nature* **388**, 839-840 (1997).
<https://doi.org/10.1038/42166>
- 12 Trexler, A. J. & Rhoades, E. α -Synuclein Binds Large Unilamellar Vesicles as an Extended Helix. *Biochemistry* **48**, 2304-2306 (2009). <https://doi.org/10.1021/bi900114z>
- 13 Ulmer, T. S., Bax, A., Cole, N. B. & Nussbaum, R. L. Structure and dynamics of micelle-bound human alpha-synuclein. *J Biol Chem* **280**, 9595-9603 (2005).
<https://doi.org/10.1074/jbc.M411805200>
- 14 Middleton, E. R. & Rhoades, E. Effects of curvature and composition on α -synuclein binding to lipid vesicles. *Biophys J* **99**, 2279-2288 (2010). <https://doi.org/10.1016/j.bpj.2010.07.056>
- 15 Bartels, T., Choi, J. G. & Selkoe, D. J. α -Synuclein occurs physiologically as a helically folded tetramer that resists aggregation. *Nature* **477**, 107-110 (2011).
<https://doi.org/10.1038/nature10324>
- 16 Wang, W. *et al.* A soluble α -synuclein construct forms a dynamic tetramer. *Proc Natl Acad Sci U S A* **108**, 17797-17802 (2011). <https://doi.org/10.1073/pnas.1113260108>

- 17 Alam, P., Bousset, L., Melki, R. & Otzen, D. E. α -synuclein oligomers and fibrils: a spectrum of species, a spectrum of toxicities. *J Neurochem* **150**, 522-534 (2019).
<https://doi.org/10.1111/jnc.14808>
- 18 Mahul-Mellier, A. L. *et al.* The process of Lewy body formation, rather than simply α -synuclein fibrillization, is one of the major drivers of neurodegeneration. *Proc Natl Acad Sci U S A* **117**, 4971-4982 (2020). <https://doi.org/10.1073/pnas.1913904117>
- 19 Wood, S. J. *et al.* α -synuclein fibrillogenesis is nucleation-dependent. Implications for the pathogenesis of Parkinson's disease. *J Biol Chem* **274**, 19509-19512 (1999).
<https://doi.org/10.1074/jbc.274.28.19509>
- 20 Danzer, K. M., Krebs, S. K., Wolff, M., Birk, G. & Hengerer, B. Seeding induced by α -synuclein oligomers provides evidence for spreading of α -synuclein pathology. *J Neurochem* **111**, 192-203 (2009). <https://doi.org/10.1111/j.1471-4159.2009.06324.x>
- 21 Luk, K. C. *et al.* Exogenous α -synuclein fibrils seed the formation of Lewy body-like intracellular inclusions in cultured cells. *Proceedings of the National Academy of Sciences* **106**, 20051-20056 (2009). <https://doi.org/10.1073/pnas.0908005106>
- 22 Volpicelli-Daley, L. A., Luk, K. C. & Lee, V. M. Addition of exogenous α -synuclein preformed fibrils to primary neuronal cultures to seed recruitment of endogenous α -synuclein to Lewy body and Lewy neurite-like aggregates. *Nat Protoc* **9**, 2135-2146 (2014).
<https://doi.org/10.1038/nprot.2014.143>
- 23 Kordower, J. H., Chu, Y., Hauser, R. A., Freeman, T. B. & Olanow, C. W. Lewy body-like pathology in long-term embryonic nigral transplants in Parkinson's disease. *Nat Med* **14**, 504-506 (2008).
<https://doi.org/10.1038/nm1747>

- 24 Uversky, V. N., Li, J. & Fink, A. L. Evidence for a partially folded intermediate in alpha-synuclein
fibril formation. *J Biol Chem* **276**, 10737-10744 (2001). <https://doi.org/10.1074/jbc.M010907200>
- 25 Gaspar, R. *et al.* Secondary nucleation of monomers on fibril surface dominates α -synuclein
aggregation and provides autocatalytic amyloid amplification. *Q Rev Biophys* **50**, e6 (2017).
<https://doi.org/10.1017/s0033583516000172>
- 26 Knowles, T. P. *et al.* An analytical solution to the kinetics of breakable filament assembly. *Science*
326, 1533-1537 (2009). <https://doi.org/10.1126/science.1178250>
- 27 Shahnawaz, M. *et al.* Discriminating α -synuclein strains in Parkinson's disease and multiple
system atrophy. *Nature* **578**, 273-277 (2020). <https://doi.org/10.1038/s41586-020-1984-7>
- 28 Peng, C. *et al.* Cellular milieu imparts distinct pathological α -synuclein strains in α -
synucleinopathies. *Nature* **557**, 558-563 (2018). <https://doi.org/10.1038/s41586-018-0104-4>
- 29 Danzer, K. M. *et al.* Different species of alpha-synuclein oligomers induce calcium influx and
seeding. *J Neurosci* **27**, 9220-9232 (2007). <https://doi.org/10.1523/jneurosci.2617-07.2007>
- 30 Tuttle, M. D. *et al.* Solid-state NMR structure of a pathogenic fibril of full-length human alpha-
synuclein. *Nature Structural & Molecular Biology* **23**, 409-415 (2016).
<https://doi.org/10.1038/nsmb.3194>
- 31 Li, B. *et al.* Cryo-EM of full-length α -synuclein reveals fibril polymorphs with a common
structural kernel. *Nature Communications* **9**, 3609 (2018). <https://doi.org/10.1038/s41467-018-05971-2>
- 32 Guerrero-Ferreira, R. *et al.* Cryo-EM structure of alpha-synuclein fibrils. *Elife* **7** (2018).
<https://doi.org/10.7554/eLife.36402>
- 33 Schweighauser, M. *et al.* Structures of α -synuclein filaments from multiple system atrophy.
Nature (2020). <https://doi.org/10.1038/s41586-020-2317-6>

- 34 Yang, Y. *et al.* Structures of α -synuclein filaments from human brains with Lewy pathology. *Nature* **610**, 791-795 (2022). <https://doi.org/10.1038/s41586-022-05319-3>
- 35 Zhang, S. *et al.* Post-translational modifications of soluble α -synuclein regulate the amplification of pathological α -synuclein. *Nat Neurosci* **26**, 213-225 (2023). <https://doi.org/10.1038/s41593-022-01239-7>
- 36 Fujiwara, H. *et al.* α -Synuclein is phosphorylated in synucleinopathy lesions. *Nature Cell Biology* **4**, 160-164 (2002). <https://doi.org/10.1038/ncb748>
- 37 Anderson, J. P. *et al.* Phosphorylation of Ser-129 Is the Dominant Pathological Modification of α -Synuclein in Familial and Sporadic Lewy Body Disease*. *Journal of Biological Chemistry* **281**, 29739-29752 (2006). <https://doi.org/https://doi.org/10.1074/jbc.M600933200>
- 38 Paleologou, K. E. *et al.* Phosphorylation at Ser-129 but not the phosphomimics S129E/D inhibits the fibrillation of alpha-synuclein. *Journal of Biological Chemistry* **283**, 16895-16905 (2008). <https://doi.org/10.1074/jbc.M800747200>
- 39 Oueslati, A., Fournier, M. & Lashuel, H. A. in *Progress in Brain Research* Vol. 183 (eds Anders Björklund & M. Angela Cenci) 115-145 (Elsevier, 2010).
- 40 Paleologou, K. E. *et al.* Phosphorylation at S87 is enhanced in synucleinopathies, inhibits alpha-synuclein oligomerization, and influences synuclein-membrane interactions. *J Neurosci* **30**, 3184-3198 (2010). <https://doi.org/10.1523/jneurosci.5922-09.2010>
- 41 Hu, J. *et al.* Phosphorylation and O-GlcNAcylation at the same α -synuclein site generate distinct fibril structures. *Nature Communications* **15**, 2677 (2024). <https://doi.org/10.1038/s41467-024-46898-1>

- 42 Rott, R. *et al.* Monoubiquitylation of alpha-synuclein by seven in absentia homolog (SIAH) promotes its aggregation in dopaminergic cells. *J Biol Chem* **283**, 3316-3328 (2008).
<https://doi.org/10.1074/jbc.M704809200>
- 43 Rott, R. *et al.* α -Synuclein fate is determined by USP9X-regulated monoubiquitination. *Proc Natl Acad Sci U S A* **108**, 18666-18671 (2011). <https://doi.org/10.1073/pnas.1105725108>
- 44 Krumova, P. *et al.* Sumoylation inhibits alpha-synuclein aggregation and toxicity. *J Cell Biol* **194**, 49-60 (2011). <https://doi.org/10.1083/jcb.201010117>
- 45 Vicente Miranda, H. *et al.* Glycation potentiates alpha-synuclein-associated neurodegeneration in synucleinopathies. *Brain* **140**, 1399-1419 (2017). <https://doi.org/10.1093/brain/awx056>
- 46 Levine, P. M. *et al.* alpha-Synuclein O-GlcNAcylation alters aggregation and toxicity, revealing certain residues as potential inhibitors of Parkinson's disease. *Proceedings of the National Academy of Sciences of the United States of America* **116**, 1511-1519 (2019).
<https://doi.org/10.1073/pnas.1808845116>
- 47 Balana, A. T. *et al.* O-GlcNAc forces an α -synuclein amyloid strain with notably diminished seeding and pathology. *Nature Chemical Biology* **20**, 646-655 (2024).
<https://doi.org/10.1038/s41589-024-01551-2>
- 48 Arnesen, T. *et al.* Proteomics analyses reveal the evolutionary conservation and divergence of N-terminal acetyltransferases from yeast and humans. *Proc Natl Acad Sci U S A* **106**, 8157-8162 (2009). <https://doi.org/10.1073/pnas.0901931106>
- 49 Pan, Y., Rhoades, E. & Petersson, E. J. Chemoenzymatic Semisynthesis of Phosphorylated alpha-Synuclein Enables Identification of a Bidirectional Effect on Fibril Formation. *Acs Chemical Biology* **15**, 640-645 (2020). <https://doi.org/10.1021/acscchembio.9b01038>

- 50 Pancoe, S. X. *et al.* Effects of Mutations and Post-Translational Modifications on α -Synuclein In Vitro Aggregation. *J Mol Biol* **434**, 167859 (2022). <https://doi.org/10.1016/j.jmb.2022.167859>
- 51 Maltsev, A. S., Ying, J. & Bax, A. Impact of N-terminal acetylation of α -synuclein on its random coil and lipid binding properties. *Biochemistry* **51**, 5004-5013 (2012).
<https://doi.org/10.1021/bi300642h>
- 52 de la Torre, D. & Chin, J. W. Reprogramming the genetic code. *Nature Reviews Genetics* **22**, 169-184 (2021). <https://doi.org/10.1038/s41576-020-00307-7>
- 53 Conibear, A. C., Watson, E. E., Payne, R. J. & Becker, C. F. W. Native chemical ligation in protein synthesis and semi-synthesis. *Chemical Society Reviews* **47**, 9046-9068 (2018).
<https://doi.org/10.1039/c8cs00573g>
- 54 Khoo, K. K. *et al.* Chemical modification of proteins by insertion of synthetic peptides using tandem protein trans-splicing. *Nat Commun* **11**, 2284 (2020). <https://doi.org/10.1038/s41467-020-16208-6>
- 55 Burton, A. J., Haugbro, M., Parisi, E. & Muir, T. W. Live-cell protein engineering with an ultra-short split intein. *Proc Natl Acad Sci U S A* **117**, 12041-12049 (2020).
<https://doi.org/10.1073/pnas.2003613117>
- 56 Ramirez, J. *et al.* Multivalency drives interactions of alpha-synuclein fibrils with tau. *PLOS ONE* **19**, e0309416 (2024). <https://doi.org/10.1371/journal.pone.0309416>
- 57 Burré, J. *et al.* Alpha-synuclein promotes SNARE-complex assembly in vivo and in vitro. *Science (New York, N.Y.)* **329**, 1663-1667 (2010). <https://doi.org/10.1126/science.1195227>
- 58 Cabin, D. E. *et al.* Synaptic vesicle depletion correlates with attenuated synaptic responses to prolonged repetitive stimulation in mice lacking alpha-synuclein. *J Neurosci* **22**, 8797-8807 (2002). <https://doi.org/10.1523/jneurosci.22-20-08797.2002>

- 59 Baskakov, I. V. From Posttranslational Modifications to Disease Phenotype: A Substrate Selection Hypothesis in Neurodegenerative Diseases. *Int J Mol Sci* **22**, 901 (2021).
<https://doi.org/10.3390/ijms22020901>
- 60 Schaffert, L. N. & Carter, W. G. Do Post-Translational Modifications Influence Protein Aggregation in Neurodegenerative Diseases: A Systematic Review. *Brain Sci.* **10**, 30 (2020).
<https://doi.org/10.3390/brainsci10040232>
- 61 Chen, H., Zhao, Y. F., Chen, Y. X. & Li, Y. M. Exploring the Roles of Post-Translational Modifications in the Pathogenesis of Parkinson's Disease Using Synthetic and Semisynthetic Modified alpha-Synuclein. *ACS Chem. Neurosci.* **10**, 910-921 (2019).
<https://doi.org/10.1021/acchemneuro.8b00447>
- 62 Moon, S. P., Balana, A. T. & Pratt, M. R. Consequences of post-translational modifications on amyloid proteins as revealed by protein semisynthesis. *Current Opinion in Chemical Biology* **64**, 76-89 (2021).
- 63 Pagan, F. L. *et al.* Pharmacokinetics and pharmacodynamics of a single dose Nilotinib in individuals with Parkinson's disease. *Pharmacol Res Perspect* **7**, e00470 (2019).
<https://doi.org/10.1002/prp2.470>
- 64 Ruijter, A. J. M. d., Gennip, A. H. v., Caron, H. N., Kemp, S. & Kuilenburg, A. B. P. v. Histone deacetylases (HDACs): characterization of the classical HDAC family. *Biochemical Journal* **370**, 737-749 (2003). <https://doi.org/10.1042/bj20021321>
- 65 Sauve, A. A., Wolberger, C., Schramm, V. L. & Boeke, J. D. The Biochemistry of Sirtuins. *Annual Review of Biochemistry* **75**, 435-465 (2006).
<https://doi.org/10.1146/annurev.biochem.74.082803.133500>

- 66 Wang, R., Sun, H. Y., Wang, G. H. & Ren, H. G. Imbalance of Lysine Acetylation Contributes to the Pathogenesis of Parkinson's Disease. *Int J Mol Sci* **21**, 22 (2020).
<https://doi.org/10.3390/ijms21197182>
- 67 de Oliveira, R. M. *et al.* The mechanism of sirtuin 2-mediated exacerbation of alpha-synuclein toxicity in models of Parkinson disease. *Plos Biology* **15** (2017).
<https://doi.org/10.1371/journal.pbio.2000374>
- 68 Thompson, R. E. & Muir, T. W. Chemoenzymatic Semisynthesis of Proteins. *Chemical Reviews* **120**, 3051-3126 (2020). <https://doi.org/10.1021/acs.chemrev.9b00450>
- 69 Merrifield, R. Solid phase peptide synthesis. I. The synthesis of tetrapeptide. *Journal of American Chemical Society* **85**, 2149-2154 (1963).
- 70 Zheng, J. S., Tang, S., Qi, Y. K., Wang, Z. P. & Liu, L. Chemical synthesis of proteins using peptide hydrazides as thioester surrogates. *Nat. Protoc.* **8**, 2483-2495 (2013).
<https://doi.org/10.1038/nprot.2013.152>
- 71 Muir, T. W., Sondhi, D. & Cole, P. A. Expressed protein ligation: A general method for protein engineering. *Proc. Natl. Acad. Sci. U. S. A.* **95**, 6705-6710 (1998).
<https://doi.org/10.1073/pnas.95.12.6705>
- 72 Pan, B. *et al.* Effects of Glutamate Arginylation on α -Synuclein: Studying an Unusual Post-Translational Modification through Semisynthesis. *Journal of the American Chemical Society* **142**, 21786-21798 (2020). <https://doi.org/10.1021/jacs.0c10054>
- 73 Xiao, Q., Zhang, F., Nacev, B. A., Liu, J. O. & Pei, D. Protein N-terminal processing: substrate specificity of *Escherichia coli* and human methionine aminopeptidases. *Biochemistry* **49**, 5588-5599 (2010). <https://doi.org/10.1021/bi1005464>

- 74 Liu, J., Chan, K. K. J. & Chan, W. Identification of Protein Thiazolidination as a Novel Molecular Signature for Oxidative Stress and Formaldehyde Exposure. *Chemical Research in Toxicology* **29**, 1865-1871 (2016). <https://doi.org/10.1021/acs.chemrestox.6b00271>
- 75 Haase, C., Rohde, H. & Seitz, O. Native chemical ligation at valine. *Angew. Chem.-Int. Edit.* **47**, 6807-6810 (2008). <https://doi.org/10.1002/anie.200801590>
- 76 Huang, Y. C. *et al.* Synthesis of L- and D-Ubiquitin by One-Pot Ligation and Metal-Free Desulfurization. *Chem.-Eur. J.* **22**, 7623-7628 (2016). <https://doi.org/10.1002/chem.201600101>
- 77 Bryson, D. I. *et al.* Continuous directed evolution of aminoacyl-tRNA synthetases. *Nat Chem Biol* **13**, 1253-1260 (2017). <https://doi.org/10.1038/nchembio.2474>
- 78 Batjargal, S., Walters, C. R. & Petersson, E. J. Inteins as traceless purification tags for unnatural amino acid proteins. *J Am Chem Soc* **137**, 1734-1737 (2015). <https://doi.org/10.1021/ja5103019>
- 79 Pott, M., Schmidt, M. J. & Summerer, D. Evolved Sequence Contexts for Highly Efficient Amber Suppression with Noncanonical Amino Acids. *ACS Chemical Biology* **9**, 2815-2822 (2014). <https://doi.org/10.1021/cb5006273>
- 80 Pan, B. *et al.* Chemoenzymatic Semi-synthesis Enables Efficient Production of Isotopically Labeled alpha-Synuclein with Site-Specific Tyrosine Phosphorylation. *ChemBioChem*, **9** <https://doi.org/10.1002/cbic.202000742>
- 81 Ramirez, J., Pancoe, S. X., Rhoades, E. & Petersson, E. J. The Effects of Lipids on α-Synuclein Aggregation In Vitro. *Biomolecules* **13** (2023).
- 82 Ulmer, T. S., Bax, A., Cole, N. B. & Nussbaum, R. L. Structure and Dynamics of Micelle-bound Human α -Synuclein. *Journal of Biological Chemistry* **280**, 9595-9603 (2005). <https://doi.org/10.1074/jbc.M411805200>

- 83 Zhao, J. *et al.* α -Synuclein arginylation in the human brain. *Translational Neurodegeneration* **11**, 20 (2022). <https://doi.org/10.1186/s40035-022-00295-0>
- 84 Pan, B. *et al.* Cysteine-Based Mimic of Arginylation Reproduces Neuroprotective Effects of the Authentic Post-Translational Modification on α -Synuclein. *Journal of the American Chemical Society* **144**, 7911-7918 (2022). <https://doi.org/10.1021/jacs.2c02499>
- 85 Haney, C. M. *et al.* Comparison of strategies for non-perturbing labeling of α -synuclein to study amyloidogenesis. *Organic & Biomolecular Chemistry* **14**, 1584-1592 (2016). <https://doi.org/10.1039/C5OB02329G>
- 86 Marotta, N. P. *et al.* Alpha-synuclein from patient Lewy bodies exhibits distinct pathological activity that can be propagated in vitro. *Acta Neuropathologica Communications* **9**, 188 (2021). <https://doi.org/10.1186/s40478-021-01288-2>
- 87 Eliezer, D., Kutluay, E., Bussell, R. & Browne, G. Conformational properties of α -synuclein in its free and lipid-associated states¹¹Edited by P. E. Wright. *Journal of Molecular Biology* **307**, 1061-1073 (2001). <https://doi.org/https://doi.org/10.1006/jmbi.2001.4538>
- 88 Bussell, R., Jr. & Eliezer, D. Effects of Parkinson's disease-linked mutations on the structure of lipid-associated alpha-synuclein. *Biochemistry* **43**, 4810-4818 (2004). <https://doi.org/10.1021/bi036135+>
- 89 Bodner, C. R., Dobson, C. M. & Bax, A. Multiple tight phospholipid-binding modes of alpha-synuclein revealed by solution NMR spectroscopy. *J Mol Biol* **390**, 775-790 (2009). <https://doi.org/10.1016/j.jmb.2009.05.066>
- 90 Rhoades, E., Ramlall, T. F., Webb, W. W. & Eliezer, D. Quantification of alpha-synuclein binding to lipid vesicles using fluorescence correlation spectroscopy. *Biophysical Journal* **90**, 4692-4700 (2006). <https://doi.org/10.1529/biophysj.105.079251>

- 91 Georgieva, E. R., Ramlall, T. F., Borbat, P. P., Freed, J. H. & Eliezer, D. The lipid-binding domain of wild type and mutant alpha-synuclein: compactness and interconversion between the broken and extended helix forms. *J Biol Chem* **285**, 28261-28274 (2010).
<https://doi.org/10.1074/jbc.M110.157214>
- 92 Cholak, E. *et al.* Avidity within the N-terminal anchor drives α -synuclein membrane interaction and insertion. *Faseb j* **34**, 7462-7482 (2020). <https://doi.org/10.1096/fj.202000107R>
- 93 Fusco, G. *et al.* Direct observation of the three regions in α -synuclein that determine its membrane-bound behaviour. *Nature Communications* **5**, 3827 (2014).
<https://doi.org/10.1038/ncomms4827>
- 94 Guerrero-Ferreira, R. *et al.* Two new polymorphic structures of human full-length alpha-synuclein fibrils solved by cryo-electron microscopy. *eLife* **8**, e48907 (2019).
<https://doi.org/10.7554/eLife.48907>
- 95 Li, Y. *et al.* Amyloid fibril structure of α -synuclein determined by cryo-electron microscopy. *Cell Research* **28**, 897-903 (2018). <https://doi.org/10.1038/s41422-018-0075-x>
- 96 Tuttle, M. D. *et al.* Solid-state NMR structure of a pathogenic fibril of full-length human α -synuclein. *Nature Structural & Molecular Biology* **23**, 409-415 (2016).
<https://doi.org/10.1038/nsmb.3194>
- 97 Frey, L. *et al.* On the pH-dependence of α -synuclein amyloid polymorphism and the role of secondary nucleation in seed-based amyloid propagation. *eLife* **12**, RP93562 (2024).
<https://doi.org/10.7554/eLife.93562>
- 98 Pan, B., Rhoades, E. & Petersson, E. J. Chemoenzymatic Semisynthesis of Phosphorylated α -Synuclein Enables Identification of a Bidirectional Effect on Fibril Formation. *ACS Chemical Biology* **15**, 640-645 (2020). <https://doi.org/10.1021/acscchembio.9b01038>

- 99 Zhao, K. *et al.* Parkinson's disease-related phosphorylation at Tyr39 rearranges α -synuclein amyloid fibril structure revealed by cryo-EM. *Proceedings of the National Academy of Sciences* **117**, 20305-20315 (2020). <https://doi.org/10.1073/pnas.1922741117>
- 100 Guerrero-Ferreira, R. *et al.* Cryo-EM structure of alpha-synuclein fibrils. *eLife* **7**, e36402 (2018). <https://doi.org/10.7554/eLife.36402>
- 101 Dowling, D. P., Gantt, S. L., Gattis, S. G., Fierke, C. A. & Christianson, D. W. Structural Studies of Human Histone Deacetylase 8 and Its Site-Specific Variants Complexed with Substrate and Inhibitors. *Biochemistry* **47**, 13554-13563 (2008). <https://doi.org/10.1021/bi801610c>
- 102 Decroos, C. *et al.* Compromised Structure and Function of HDAC8 Mutants Identified in Cornelia de Lange Syndrome Spectrum Disorders. *ACS Chemical Biology* **9**, 2157-2164 (2014). <https://doi.org/10.1021/cb5003762>
- 103 Osko, J. D. *et al.* Structural analysis of histone deacetylase 8 mutants associated with Cornelia de Lange Syndrome spectrum disorders. *Journal of Structural Biology* **213**, 107681 (2021). <https://doi.org/https://doi.org/10.1016/j.jsb.2020.107681>
- 104 Vanaja, G. R., Ramulu, H. G. & Kalle, A. M. Overexpressed HDAC8 in cervical cancer cells shows functional redundancy of tubulin deacetylation with HDAC6. *Cell Communication and Signaling* **16**, 20 (2018). <https://doi.org/10.1186/s12964-018-0231-4>
- 105 Outeiro, T. F. *et al.* Sirtuin 2 Inhibitors Rescue α -Synuclein-Mediated Toxicity in Models of Parkinson's Disease. *Science* **317**, 516-519 (2007). <https://doi.org/10.1126/science.1143780>
- 106 Shimogawa, M. *et al.* Investigation of All Disease-Relevant Lysine Acetylation Sites in α -Synuclein Enabled by Non-canonical Amino Acid Mutagenesis. *bioRxiv*, 2025.2001.2021.634178 (2025). <https://doi.org/10.1101/2025.01.21.634178>

- 107 Wang, X. & Hayes, J. J. Acetylation mimics within individual core histone tail domains indicate distinct roles in regulating the stability of higher-order chromatin structure. *Mol Cell Biol* **28**, 227-236 (2008). <https://doi.org/10.1128/mcb.01245-07>
- 108 Li, M., Luo, J., Brooks, C. L. & Gu, W. Acetylation of p53 inhibits its ubiquitination by Mdm2. *J Biol Chem* **277**, 50607-50611 (2002). <https://doi.org/10.1074/jbc.C200578200>
- 109 de Boor, S. *et al.* Small GTP-binding protein Ran is regulated by posttranslational lysine acetylation. *Proceedings of the National Academy of Sciences* **112**, E3679-E3688 (2015). <https://doi.org/10.1073/pnas.1505995112>
- 110 Fatema, N., Li, X., Gan, Q. & Fan, C. Characterizing lysine acetylation of glucokinase. *Protein Sci* **33**, e4845 (2024). <https://doi.org/10.1002/pro.4845>
- 111 Koo, H. J., Lee, H. J. & Im, H. Sequence determinants regulating fibrillation of human alpha-synuclein. *Biochem Biophys Res Commun* **368**, 772-778 (2008). <https://doi.org/10.1016/j.bbrc.2008.01.140>
- 112 Fujimoto, H. *et al.* A possible overestimation of the effect of acetylation on lysine residues in KQ mutant analysis. *J Comput Chem* **33**, 239-246 (2012). <https://doi.org/10.1002/jcc.21956>
- 113 Musselman, C. A. & Kutateladze, T. G. Strategies for Generating Modified Nucleosomes: Applications within Structural Biology Studies. *ACS Chem Biol* **14**, 579-586 (2019). <https://doi.org/10.1021/acscchembio.8b01049>
- 114 Li, F. P. *et al.* A Direct Method for Site-Specific Protein Acetylation. *Angewandte Chemie-International Edition* **50**, 9611-9614 (2011). <https://doi.org/10.1002/anie.201103754>
- 115 Fiore, K. E., Phan, H. A. T., Robkis, D. M., Walters, C. R. & Petersson, E. J. Incorporating thioamides into proteins by native chemical ligation. *Methods Enzymol* **656**, 295-339 (2021). <https://doi.org/10.1016/bs.mie.2021.04.011>

- 116 Venkat, S. *et al.* Genetically encoding thioacetyl-lysine as a non-deacetyltable analog of lysine acetylation in *Escherichia coli*. *FEBS Open Bio* **7**, 1805-1814 (2017).
<https://doi.org/https://doi.org/10.1002/2211-5463.12320>
- 117 Fatkins, D. G., Monnot, A. D. & Zheng, W. N ϵ -Thioacetyl-lysine: A multi-facet functional probe for enzymatic protein lysine N ϵ -deacetylation. *Bioorganic & Medicinal Chemistry Letters* **16**, 3651-3656 (2006). <https://doi.org/https://doi.org/10.1016/j.bmcl.2006.04.075>
- 118 Robkis, D. M., Hoang, E. M., Po, P., Deutsch, C. J. & Petersson, E. J. Side-chain thioamides as fluorescence quenching probes. *Biopolymers* **112**, e23384 (2021).
<https://doi.org/https://doi.org/10.1002/bip.23384>
- 119 Johnson, M., Coulton, A. T., Geeves, M. A. & Mulvihill, D. P. Targeted amino-terminal acetylation of recombinant proteins in *E. coli*. *PLoS One* **5**, e15801 (2010).
<https://doi.org/10.1371/journal.pone.0015801>
- 120 Costello, A. *et al.* Genetic Code Expansion History and Modern Innovations. *Chemical Reviews* **124**, 11962-12005 (2024). <https://doi.org/10.1021/acs.chemrev.4c00275>
- 121 Zhu, P., Gafken, P. R., Mehl, R. A. & Cooley, R. B. A Highly Versatile Expression System for the Production of Multiply Phosphorylated Proteins. *ACS Chemical Biology* **14**, 1564-1572 (2019).
<https://doi.org/10.1021/acscchembio.9b00307>
- 122 Kinoshita, E., Kinoshita-Kikuta, E. & Koike, T. History of Phos-tag technology for phosphoproteomics. *J Proteomics* **252**, 104432 (2022).
<https://doi.org/10.1016/j.jprot.2021.104432>
- 123 Galesic, A. *et al.* Combining non-canonical amino acid mutagenesis and native chemical ligation for multiply modifying proteins: A case study of α -synuclein post-translational modifications. *Methods* **218**, 101-109 (2023). <https://doi.org/10.1016/j.ymeth.2023.08.002>

- 124 Vesely, C. H. *et al.* Accessing isotopically labeled proteins containing genetically encoded phosphoserine for NMR with optimized expression conditions. *Journal of Biological Chemistry* **298** (2022). <https://doi.org/10.1016/j.jbc.2022.102613>
- 125 Pan, B. *et al.* Chemoenzymatic Semi-synthesis Enables Efficient Production of Isotopically Labeled α -Synuclein with Site-Specific Tyrosine Phosphorylation. *Chembiochem* **22**, 1440-1447 (2021). <https://doi.org/10.1002/cbic.202000742>
- 126 Ferrie, J. J. *et al.* Identification of a nanomolar affinity α -synuclein fibril imaging probe by ultra-high throughput in silico screening. *Chem Sci* **11**, 12746-12754 (2020). <https://doi.org/10.1039/d0sc02159h>
- 127 Hsieh, C. J. *et al.* Alpha Synuclein Fibrils Contain Multiple Binding Sites for Small Molecules. *ACS Chem Neurosci* **9**, 2521-2527 (2018). <https://doi.org/10.1021/acscchemneuro.8b00177>
- 128 Zhao, K. *et al.* Parkinson's disease-related phosphorylation at Tyr39 rearranges α -synuclein amyloid fibril structure revealed by cryo-EM. *Proc Natl Acad Sci U S A* **117**, 20305-20315 (2020). <https://doi.org/10.1073/pnas.1922741117>
- 129 Ha, Y. *et al.* Facile “stop codon” method reveals elevated neuronal toxicity by discrete S87p- α -synuclein oligomers. *Biochemical and Biophysical Research Communications* **443**, 1085-1091 (2014). <https://doi.org/https://doi.org/10.1016/j.bbrc.2013.12.099>
- 130 Yan, Y. *et al.* X-linked ubiquitin-specific peptidase 11 increases tauopathy vulnerability in women. *Cell* **185**, 3913-3930.e3919 (2022). <https://doi.org/10.1016/j.cell.2022.09.002>